PONTIFICIA UNIVERSIDAD CATÓLICA DE CHILE
FACULTAD DE CIENCIAS BIOLÓGICAS

"Mechanisms of lipodystrophy in the AGPAT2 deficient mouse"

Thesis presented to Pontificia Universidad Católica de Chile in partial fulfillment of the requirements for the degree of Doctor in Biological Sciences, Mention in Molecular Genetics and Microbiology.

By

Kelly Margarita Cautivo Reyes

Thesis advisor: Víctor A. Cortés Mora, M.D., Ph.D.

April, 2014

ACKNOWLEDGEMENTS

This thesis was carried out in the Department of Nutrition at Pontificia Universidad Catolica de Chile and Department of Molecular Genetics at University of Texas Southwestern during the years 2011-2013. At the end of this period, I would like to offer my heartfelt thanks to my funding source, the National Commission for Science and Technology (CONICYT), and all the people who contributed in some way to the work described in this thesis.

First, I sincerely thank Professors Victor Cortes and Jay Horton, for accepting me into their labs, giving me intellectual freedom in my work, and demanding a high quality of work in my entire endeavor. To all lab members, facility staff and friends in each lab I was doing my research, thank you for welcoming and helping me. Special thanks to Pablo Tapia, Eugenia Morselli, Veronica Quinones and Norma Anderson. I would also like to express my sincere gratitude to Dr. Jose Luis Santos, who generously gave me free access to his lab equipment and supplies in the hardest moment of my thesis. Furthermore, special thanks to my thesis committee, for their time, thoughtful review and valuable suggestions.

Additionally, I want to acknowledge my dear family for their continuous love and for always believing in me. Special thanks to my mom and sister Camila, who took care of my cats during my stay in the USA. I want to also extend my gratitude to my love, Carlos, who encouraged me to always finish this project along with enriching my life in every way imaginable and always inspiring me to be my best self.

Lastly, I want to dedicate this work to my family and my dear “Cabezon”, who passed away just before I defended.

TABLE OF CONTENTS

ABBREVIATIONS

AdV	:	Adenovirus
AGPAT2	:	1-acylglycerol-3-phosphate-O-acyltransferase 2
aP2-1c Tg	:	aP2–SREBP-1c transgenic mouse
AT	:	Adipose tissue
ATGL	:	Adipose triglyceride lipase
BAT	:	Brown adipose tissue
BSA	:	Bovine serum albumin
Bscl2	:	Berardinelli-Seip congenital lipodystrophy 2
CDK	:	Cyclin-dependent kinase
C/EBP	:	CCAAT/enhancer binding protein
cDNA	:	complementary deoxyribonucleic acid
CGL	:	Congenital generalized lipodistrophy
CIDE	:	Cell death-inducing DNA fragmentation factor 45-like effector
CREB	:	cAMP response element-binding
DGAT	:	Diacylglycerol acyltransferase
DMEM	:	Dulbecco's Modified Eagle Medium
EdU	:	5-ethynyl-2′-deoxyuridine
ER	:	Endoplasmic reticulum
ERK	:	Extracellular signal-regulated kinase
FABP4	:	Fatty acid binding protein-4

Fld	:	Fatty liver dystrophy
G3P	:	Glycerol-3-phosphate
GPAT	:	Glycerol phosphate acyltransferase
HSL	:	Hormone sensitive lipase
IBMX	:	3-isobutyl-1-methylxanthine
iBAT	:	interscapular BAT
IL-6	:	Interleukin-6
IR	:	Insulin receptor
LD	:	Lipid droplet
LPA	:	Lysophosphatidic acid
MAPK	:	Mitogen-activated protein kinase
MCE	:	Mitotic clonal expansion
MDMC	:	Muscle-derived multipotent cells
MEF	:	Mouse embryonic fibroblast
MGAT	:	Monoacyglycerol acyltransferase
mRNA	:	Messenger ribonucleic acid
MRI	:	Magnetic resonance imaging
MSC	:	Mesenchimal stem cells
NF-κB	:	Nuclear factor kappa-light-chain-enhancer of activated B cells.
ORO	:	Oil red-O
PA	:	Phosphatidic acid
PAP	:	Phosphatidate phosphatase

PAT	:	Perilipin, Adipophilin, TIP47
PBS	:	Phosphate buffered saline
PC	:	Phosphatidylcholine
PI3K	:	Phosphoinositide 3-kinase
PPARγ	:	Peroxisome proliferator-activated receptor gamma
PREF-1	:	Preadipocyte factor-1
RB	:	Retinoblastoma
RXR	:	Retinoid X receptor
SREBP-1c	:	Sterol regulatory element-binding protein-1c
TBS	:	Tris-buffered saline
TG	:	Triacylglycerol
TNFα	:	Tumor necrosis factor-alpha
TUNEL	:	Terminal deoxynucleotidyl transferase dUTP nick end labeling
WAT	:	White adipose tissue

ABSTRACT

1-acylglycerol-3-phosphate O-acyltransferase-2 (AGPAT2) is an enzyme expressed at high levels in the adipose tissue. It catalyzes the conversion of lysophosphatidic acid (LPA) to phosphatidic acid (PA), which is an important reaction in the triglyceride and glycerophospholipid biosynthesis pathways. Inactivating mutations of the *AGPAT2* gene cause a pathological and severe absence of adipose tissue mass, a condition known as congenital generalized lipodystrophy, both in humans and mice. The mechanisms by which AGPAT2 deficiency causes lipodystrophy remains poorly understood. In this work, I hypothesized that the lack of AGPAT2 impairs the differentiation process that converts adipose precursor cells (preadipocytes) into mature adipocytes, thus precluding the formation and expansion of mature adipose tissue in the *Agpat2*$^{-/-}$ mice. To test this hypothesis, I used a combined *in vitro* and *in vivo* approach. Mouse embryonic fibroblast (MEF) adipogenesis studies revealed that adipogenic differentiation is impaired at multiple levels in the *Agpat2*$^{-/-}$ MEFs. First, activation of adipogenic differentiation in *Agpat2*$^{-/-}$ MEFs results in exaggerated cell death at the mitotic clonal expansion phase (34 % vs. 6 % in wild type MEFs). This leads to a significantly reduced proportion of cells that progress to more advanced adipogenesis stages and correlates with significantly decreased activation of insulin signaling pathway. Second, the progression of transcriptional events that regulate adipogenesis, including the induction of key transcription factors c/EBPs and PPARγ, is impaired in *Agpat2*$^{-/-}$ MEFs. Third, adipogenically differentiated *Agpat2*$^{-/-}$ MEFs are significantly smaller and have lower total neutral lipid content and smaller intracellular lipid droplets (LDs) than wild type MEFs. Furthermore, LDs distribution is disorganized

with multiple lipid-free intracellular aggregates of Perilipin, a protein exclusively found on the surface of LDs in wild type cells.

Analysis of late-stage fetuses and newborn mice unexpectedly revealed normal adipose tissue mass and histological structure in the *Agpat2*$^{-/-}$ mice. However, as soon as the second day after birth, adipose tissue lipid loaded cells are rapidly replaced by infiltrating macrophages and TUNEL-positive apoptotic cells in the *Agpat2*$^{-/-}$ mice. Finally, six days after birth virtually no adipose tissue is detectable in these mice, defining a fully established lipodystrophic syndrome.

As a whole, the findings in this thesis demonstrate that AGPAT2 is absolutely required for adipocyte and adipose tissue survival, growth and differentiation *in vitro* and in postnatal mice, respectively. The implications of these findings in human adipose biology are discussed.

RESUMEN

1-acilglicerol-3-fosfato O-aciltransferasa-2 (AGPAT2) es una enzima que normalmente se expresa en altos niveles en el tejido adiposo y cataliza la conversión de ácido lisofosfatídico (LPA) a ácido fosfatídico (PA), un paso fundamental en la biosíntesis de triglicéridos y glicerofosfolípidos. Mutaciones que inactivan el gen *AGPAT2* causan reducción severa del tejido adiposo, tanto en seres humanos como en ratones, generando una condición patológica conocida como lipodistrofia generalizada. Los mecanismos por los cuales la deficiencia de AGPAT2 causa lipodistrofia son desconocidos. La hipótesis de este trabajo es que la falta de AGPAT2 altera el proceso de diferenciación que convierte a las células precursoras adiposas (preadipocitos) en adipocitos maduros, impidiendo, por lo tanto, la formación y expansión de tejido adiposo en los ratones *Agpat2*$^{-/-}$. Para probar esta hipótesis se utilizó un enfoque experimental combinado, *in vitro* e *in vivo*. Estudios de adipogénesis *in vitro* con fibroblastos de embriones de ratón (FERs) reveló que la diferenciación adipogénica es anormal en múltiples niveles en los FERs *Agpat2*$^{-/-}$. En primer lugar, la inducción adipogénica resultó en una alta proporción de FERs *Agpat2*$^{-/-}$ que mueren durante el proceso de expansión clonal mitótica (34 % frente a 6 % en los controles). Esto se tradujo en una proporción significativamente menor de células que progresaron a fases adipogénicas avanzadas y se correlacionó con una reducida activación de la vía de señalización de insulina. En segundo lugar, los FERs *Agpat2*$^{-/-}$ que lograron diferenciarse presentaron menor tamaño celular, menor contenido de lípidos neutros y gotas lipídicas pequeñas y desorganizadas, las cuales contienen una menor cantidad de Perilipina

asociada a su superficie. Además, se observó presencia de múltiples agregados intracelulares de Perilipina no asociada a gotas lipídicas.

El análisis de fetos en la última etapa de desarrollo intra uterino y de ratones recién nacidos reveló, inesperadamente, que tanto la masa total de tejido adiposo como su estructura tisular fue normal en estas etapas del desarrollo en ratones *Agpat2*$^{-/-}$. Sin embargo, al segundo día después del nacimiento el tejido adiposo de los ratones *Agpat2*$^{-/-}$ fue rapidamente reemplazado por una elevada proporción de adipocitos en proceso de muerte celular, seguido por una masiva respuesta inflamatoria mediada por macrófagos. Finalmente, al sexto día después del nacimiento, el tejido adiposo fue indetectable en estos ratones, estableciendo un generalizado sindrome lipodistrofico.

En resumen, los hallazgos de esta tesis demuestran que AGPAT2 es absolutamente necesaria para la supervivencia, el crecimiento y la diferenciación de los FER, así como para el crecimiento y viabilidad del tejido adiposo en la vida postnatal del ratón.

1. INTRODUCTION

Adipose tissue (AT) is necessary for normal energy balance and metabolic regulation. It functions as a safe storage place for metabolic energy in times of positive energy balance, and as a supplier of this energy in times of negative balance. In addition, AT is an endocrine organ secreting bioactive molecules playing key roles in whole body metabolism, food intake, energy expenditure, inflammation and reproduction; functions that are all essential for the evolution and survival of the species. To fulfill these roles, AT has the ability to expand itself through the formation of new specialized fat-storage cells called adipocytes, which can either overfill and grow by synthesis and storing of large amounts of triglycerides or shrink themselves by a finely tuned process of intracellular lipolysis that releases free fatty acids and glycerol into the circulation.

In mammals, the development of AT starts late in fetal life and its largest physiological expansion occurs early after birth, as a consequence of massive energy loading from the maternal milk. Here, AT growth is regulated by a number of factors that influence the differentiation of committed preadipocytes into mature adipocytes. This process is called adipogenesis and involves the coordinated activation of transcriptional and post transcriptional processes that allow the extracellular fatty acids uptake, their esterification into neutral lipids (lipogenesis) and the biogenesis of specialized fat-storing organelles called lipid droplets (LDs).

The clinical presentation of subjects with severe and generalized reduction of AT, a condition called generalized lipodystrophy, illustrates the key roles that AT plays in the regulation of the whole body homeostasis. These patients frequently develop severe

metabolic complications such as insulin resistance, diabetes mellitus, hypertriglyceridemia, and hepatic steatosis (1) that closely recapitulate those observed in severly obese individuals. The underlying mechanisms for this medical paradox, i.e. that the pathological extremes of the body adiposity share identical metabolic complications, still remain unknown. However, strong experimental evidence suggest that in both, lipodystrophy and obesity, abnormal endocrine functioning as well as impaired remodelling of the AT result in severe systemic insulin resistance.

AGPAT2 gene, wich encodes 1-acylglycerol-3-phosphate-O-acyltransferase 2 protein, was identified in 2002 as the first locus causally linked with congenital forms of generalized lipodystrophy (CGL) in humans. Functionally, AGPAT2 catalyzes the conversion of lysophsophatidic acid (LPA) to phosphatidic acid (PA) in the *de novo* glycerolipids biosynthesis pathway. However, how does AGPAT2 absence results in AT deficiency is not known yet. Given the critical role of AGPAT2 in triglycerides (TGs) formation, the most direct question is whether the lack of AGPAT2 results in mature but TG-depleted adipocytes, or does it affect the adipogenesis itself.

To address this fundamental question, I have studied the first animal model of a human lipodystrophy, the AGPAT2 deficient mouse, which fully recapitulates the anatomical, physiological and molecular abnormalities of human CGL syndrome (2). My working hypothesis is that AGPAT2 is required for normal development of the adipose tissue because its deficiency inhibit the adipogenesis, preventing the formation of mature adipocytes. Therefore, the general aims of this thesis were to evaluate whether the lack of adipose tissue in the AGPAT2 deficient mice is caused by impaired adipogenesis and to determine the molecular mechanisms underlying their lipodystrophic phenotype.

The following sections describe the main general biological features of the AT and sumarize the current knowledge of adipocyte differentiation program and the physiological and pathophysiological roles of AGPAT2.

1.1 General aspects of adipose tissue biology.

Fat depots are found across metazoan species (3). Nemotods accumulate lipids in the intestinal epithelium, sharks do it in the liver and drosophila in a specialized organ called fat body. However, true AT is only found in boney fish such as carps (*Cyprinus carpio*) and higher animals, in coincidence with the secretion of leptin, the first described adipokine (i.e. adipose-derived hormone).

AT is essential for body energy homeostasis and insulin sensitivity (4, 5). It is composed by parenchymal lipid-loaded cells called adipocytes which are supported in a framework of collagen fibers and other extracellular matrix (EMC) proteins. Non-adipose stromal cellular elements, including preadipocytes, fibroblasts, blood vessels, nerves and immune cells, also contribute to the AT homeostasis (4, 6). In fact, each one of these non-adipose cells contribute to the AT remodeling in response to physiological requirements and pathological challenges during the adult life (7).

Based on morphological criteria, two types of AT have been classically recognized: white adipose tissue (WAT) and brown adipose tissue (BAT) **(Figure 1)**. Althought both AT classes are involved in energy balance, they are functionally different assuming opposite roles in the body energetics. Recent advances have shown that WAT and BAT have also a quite dissimilar developmental origin.

1.1.1 White adipose tissue.

WAT is the most abundant type of AT in adult mammals, being found in the subcutaneous connective tissue (subcutaneous WAT), surrounding visceral organs (visceral WAT) as well as in many other areas such as the bone marrow, between skeletal muscle fascicles, and in the connective tissue of orbits, palms and soles (3, 6) **(Figure 1)**. Interestingly, despite histological similarities, subcutaneous and visceral WAT are thought to have distinct biological properties and specific metabolic functions (8-10).

WAT adipocytes are characterized by a single-large lipid vesicule called lipid droplet (LD) that occupies >90% of the cell volume and can reach up to 100 µm or more in diameter. In these cells, the nucleus and other organelles are flattened and displaced to cell's periphery forming a thin rim around the unilocular LD **(Figure 2)** (11). Extracellular space is richly supplied with blood vessels, nerve fibers and immune cells.

Functionally, WAT is currently understood as a metabolic and endocrine organ **(Figure 3)**. It is the prime site for the body lipids storage, capable of accumulating large amounts of energy and buffering long-term fluctuations in calorie intake representing a major evolutionary adaptation to starvation in vertebrates (12). In fact, upon proper endocrine and nutritional signaling, large amounts of fatty acids are released from WAT to fulfill energy requirements of peripheral tissues during fasting: 1 kg of normal WAT contains 37 MJ, equivalent to approximately 6 days's supply for an individual spending 6 MJ/day (13). In addition, several other lipid species including cholesterol, retinol and prostanoids are also stored and released from WAT.

As an endocrine organ, WAT participate in the regulation of a number of other, non-nutritional functions, such as fertility/reproduction, offspring growth, sexual/mating selection, and inflammation **(Figure 3)** (14). By secreting a variety of active factors, collectively called adipokines, WAT integrates body energy balance with feeding behavior, basal metabolic rate, insulin sensitivity, inflammation, angiogenesis and vascular function (15). The growing list of adipokines includes: leptin, adiponectin, adipsin, resistin, RBP4, TNFα and visfatin, among others. Interestingly, almost all these adipokines are dysregulated in obesity and lipodystrophy and this could be relevant for the metabolic dysregulation of these conditions (16). Because leptin, as well as other adipokines, are only synthesized and secreted by fully differentiated adipocytes, these can be operationally used as adipogenic markers and indicators of WAT mass.

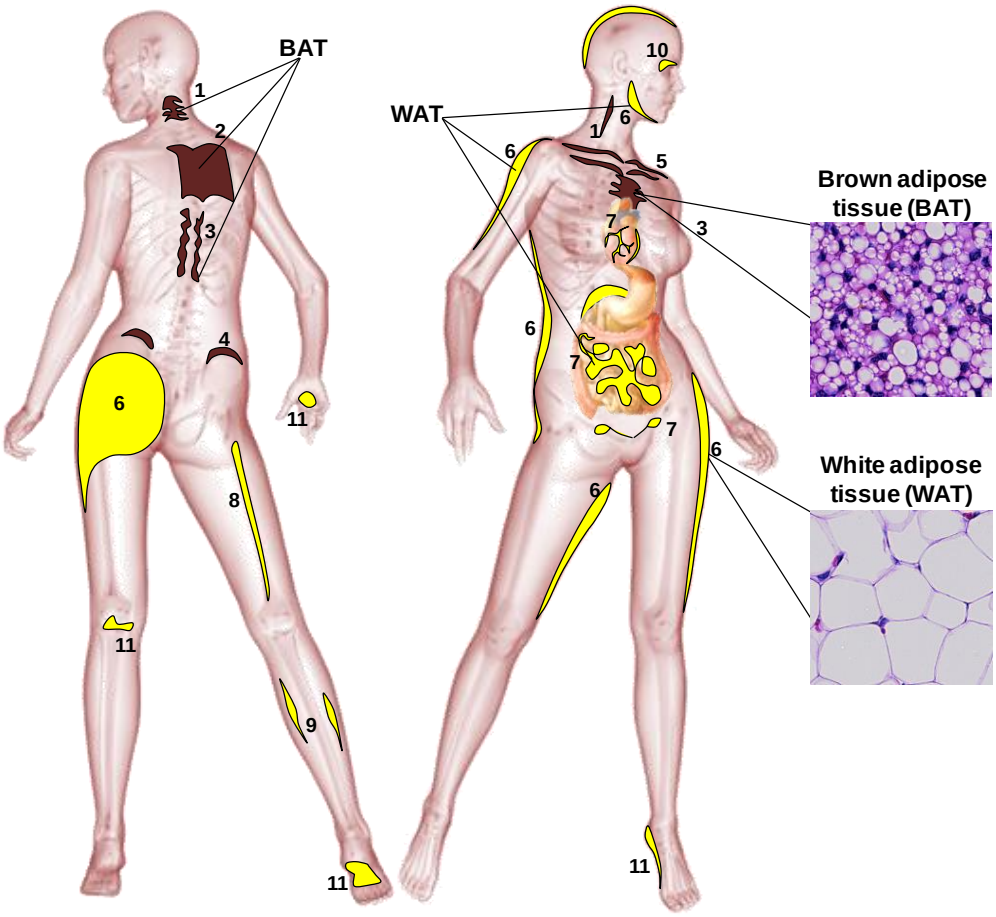

Figure 1: Classification and anatomical distribution of the adipose tissue (AT) in the adult human body. Adipose depots from BAT and WAT are represented in brown and yellow color, respectively. Numbers indicate different adipose compartments. **1:** cervical AT, **2:** interscapular AT, **3:** paravertebral AT, **4:** suprarenal AT, **5:** supraclavicular AT, **6:** subcutaneous AT, **7:** visceral AT (omental, mesenteric, retroperitoneal, gonadal and pericardial), **8:** bone marrow AT, **9:** intramuscular AT. **10:** retro-orbital AT, **11:** structural-impact bearing AT.

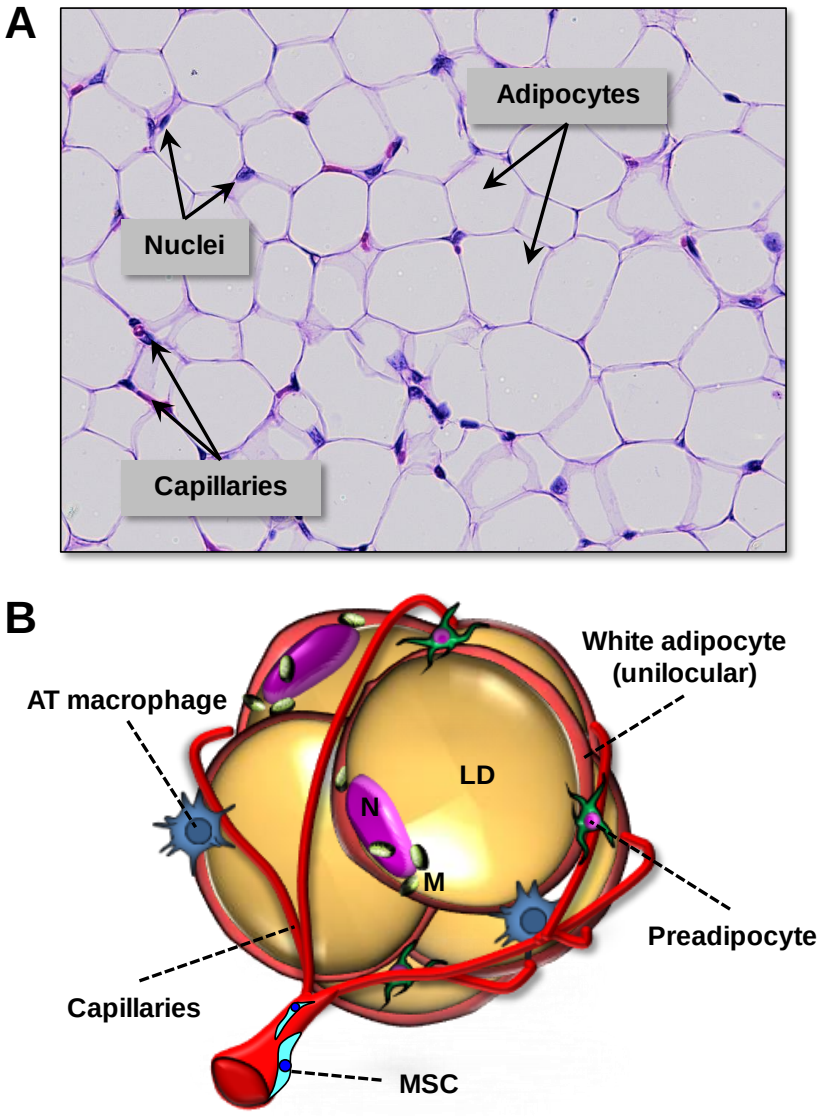

Figure 2: White adipose tissue (WAT) composition. (A) Light photomicrography of mouse white adipose tissue section stained with Hematoxylin and Eosin. Picture shows large globular cells corresponding to white adipocytes. The white space in each cell corresponds to a lipid droplet. The surrounding eosin-stained material represents the cytoplasm of the adjoining cells and some intervening connective tissue. Capillaries are observed between adipocytes. **(B)** Artistic representation illustrating a healthy WAT organization. AT: adipose tissue, LD: lipid droplet, N: nucleus, M: mitochondria, MSC: mesenchymal stem cell.

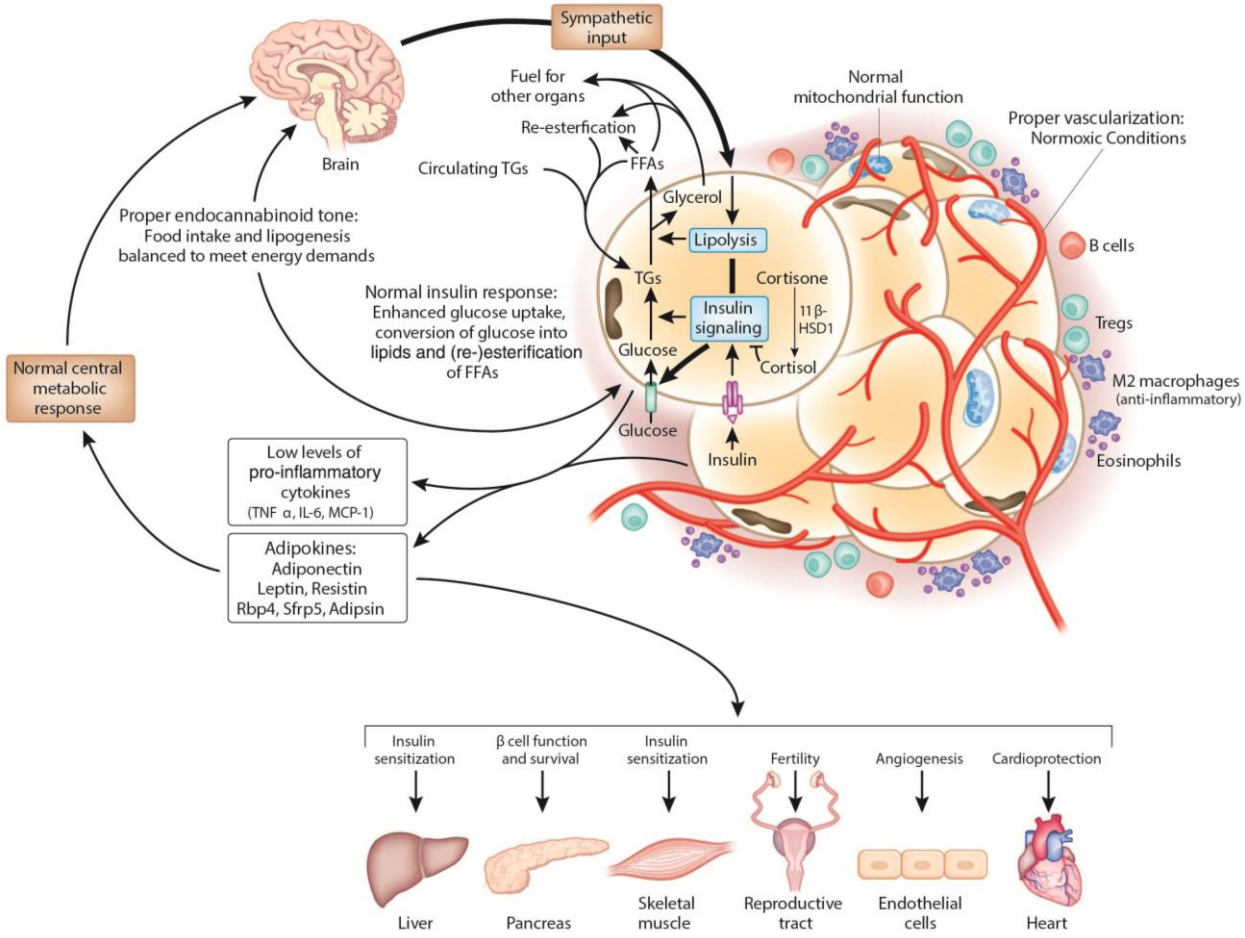

Figure 3: Metabolic and endocrine functions of WAT. Adipocytes interact with other metabolically active tissues through the release of adipokines as well as pro-inflammatory cytokines that are expressed at low levels in a healthy adipocyte. These factors ensure proper metabolic responses of key targets, such as liver, skeletal muscle, β cells of the pancreas, cardiac myocytes and endothelium. Fertility is also critically influenced by adipose tissue. Moderate levels of leptin effectively communicate with hypothalamic centers in the brain, resulting in proper regulation of food intake and energy expenditure. Abbreviations: TNFα: tumor necrosis factor alpha; IL-6: interleukin 6; MCP-1: monocyte chemoattractant protein-1; Rbp4: retinol binding protein 4; Sfrp5: secreted frizzled-related protein 5; 11β HSD1: 11β-hydroxysteroid dehydrogenase type 1. *(Figure reproduced from Metabolic Syndrome ePoster, Nature Medicine 2011(Vol. 17, No. 7))*

1.1.2 Brown adipose tissue.

In human fetuses and newborns, BAT is a prominent tissue in axillar, cervical, perirenal, and periadrenal regions. Its mass rapidly decreases with aging and is normally undetectable in adults. However, this traditionally concept has been challenged by very recent [18F]-2-fluoro-D-2-deoxy-D-glucose (FDG) positron emission tomography (PET scan) studies that have disclosed metabolically active BAT in healthy humans (17-19). Notably, this FDG detectable BAT is lower in obese subjects and it can be activated by cold exposure in healty humans, correlating with increased resting energy expenditure, reduced body weight (20, 21) and improved insulin sensitivity and glucose homeostasis (22). These findings are driving new efforts to develop anti-obesity therapies based on BAT activation (23).

BAT is composed by multilocular adipocytes, with several-small LDs and large and numerous mitochondria **(Figure 4)**. Evolutionary, BAT is newer than WAT (3) and is the prime site for non-shivering thermogenesis, a process essential for cold adaptation in mammals. For this, BAT uses the chemical energy of fatty acids and glucose to produce heat by uncoupling mitochondrial oxidative phosphorylation from ATP synthesis. Uncoupling protein 1 (UCP1, thermogenin), a 32 KDa member of the mitochondrial anion carrier proteins, is responsible for this energy dissipation by decreasing the proton gradient across the internal mitochondrial membrane of BAT. Since UCP1 is exclusively expressed in BAT, it is an accepted *bona fide* marker for brown adipocytes (24).

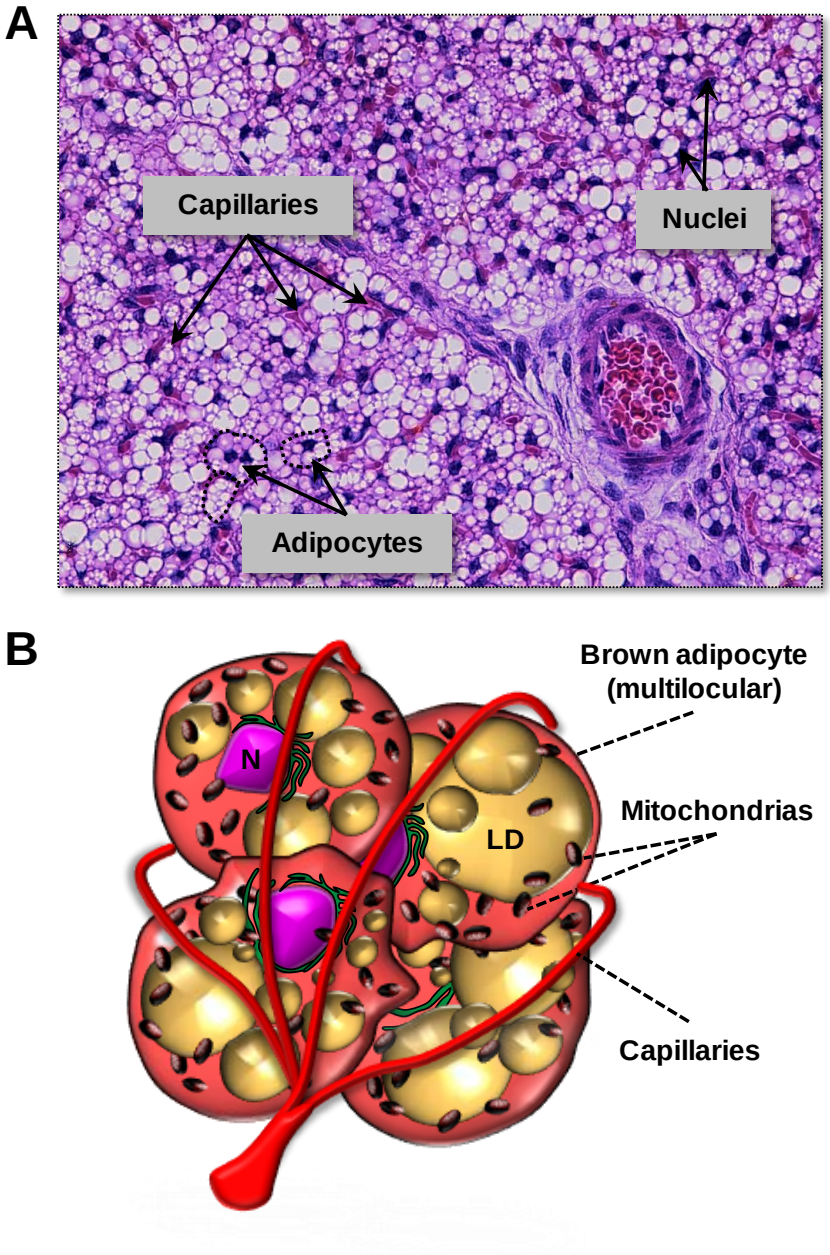

Figure 4: Brown adipose tissue (BAT) composition. (A) Light photomicrography of brown adipose tissue (BAT) section stained with Hematoxylin and Eosin. Picture shows cells closely packed with numerous LDs which are smaller than the large single droplet in a white adipocyte. BAT is highly vascularized with blood vessels. **(B)** Artistic representation illustrating the BAT organization. AT: adipose tissue, LD: lipid droplet, N: nucleus.

1.2 Adipose tissue development and growth.

In spite of the functional and morphological differences between white and brown adipocytes, both share a common transcriptional program for the first steps of differentiation. This differentiation process is known as adipogenesis (25-27).

The transcriptional control of adipogenesis has been described in detail in recent years. However, much of this knowledge has come from the study of established cultured pre-adipocyte cell lines such as the 3T3-L1 or 3T3-F442A, or precursor cells harvested from animals, such as mouse embryonic fibroblasts (MEFs) or mouse mesenchymal stem cells (28). Based on these *in vitro* models, adipogenesis is now understood as a multi-stage process that involves the sequential expression or repression of a number of transcription factors, co-activators, co-repressors and cell-cycle regulatory molecules, all of which integrate in a complex network of molecular interactions **(Figure 5)** (29). This process can be organized in two major stages: 1) commitement/determination and 2) terminal differentiation.

In vivo, WAT commitement begins late in the gestation and involves the determination of pluripotent mesenchimal stem cells to adipocyte lineage, giving rise to specific adipocyte precursor cells, known as preadipocytes. Terminal differentiation step, which leads to the transformation of preadipocytes into fully mature functional adipocytes, starts soon after birth in response to various nutrient and neuroendocrine stimuli (4). Under this process, maturing preadipocytes acquire all the required machinery for lipid transport, synthesis and storage, become sensitive to a number of hormones, including insulin, and

neurotransmitters, and start the secretion of adipocyte-specific proteins, including adipokines and immunomodulatory cytokines. WAT expansion is, thus, a postnatal phenomenon that depends on both hyperplastic and hypertrophic mechanisms (30). By contrast, BAT differentiates and grows mostly *in utero*, being fully differentiated at the time of birth, possibly to maintain body temperature right after delivery.

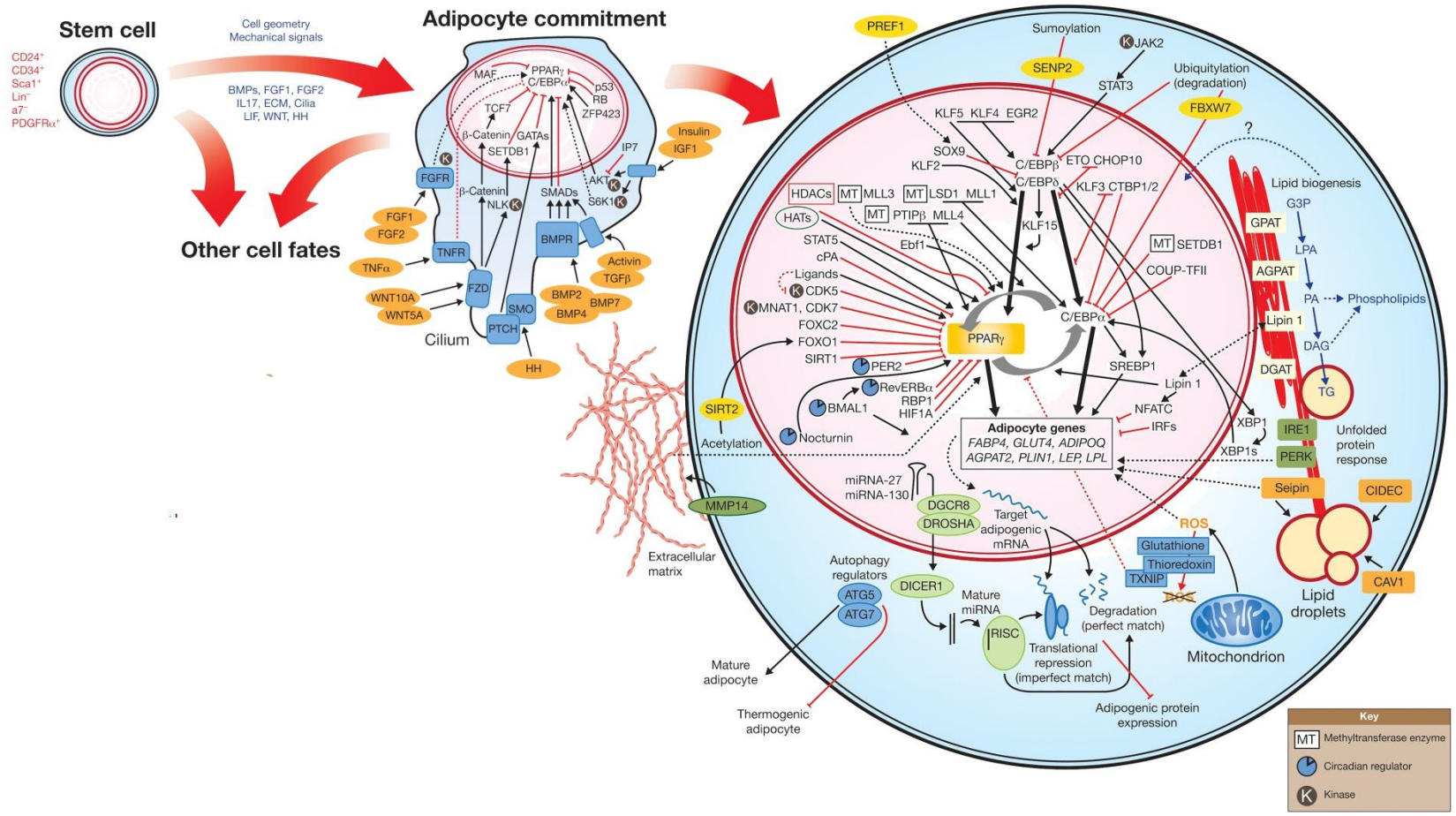

Figure 5: Molecular pathways and signals controlling the formation of adipocytes from precursor stem cells (adipogenesis). This illustration show the transition of precursor stem cells into mature lipid-laden adipocytes, and the numerous molecules, pathways and signals required to accomplish this *(Figure reproduced from Journal of Cell Science 2011 (124, pp. 2681-2686))*

1.2.1 Early adipogenesis: commitment of adipocyte precursor cells.

Preadipocytes are derived from pluripotent mesenchimal stem cells (MSCs) that reside in the vascular stroma of the adipose tissue as well as in the bone marrow (31) **(Figure 6)**. Little is known about the mechanisms that regulate commitment of MSC to preadipocytes *in vivo*, however, recent *in vitro* adipogenesis and mouse models studies have revealed several factors and signaling pathways involved in early adipogenesis (27). Bone morphogenic proteins (BMP) -2 and -4, and Wnt pathway inhibition, via ubiquitination and degradation of β-catenin, have been involved in the commitment of MSCs to preadipocytes (4, 27, 32). After initial cell fate determination, extracellular factors such as extracellular matrix (ECM) proteins, mechanical stress, cell-to-cell interaction and cellular shape changes through RhoHO GTPase-RhoHO-associated kinase (ROCK) signaling, seem to be required for preadipocytes to fully differentiate into mature adipocytes (4). Importantly, although committed preadipocytes are restricted to differentiate into adipocytes, *in vitro* studies have shown that they fail to spontaneously undergo terminal differentiation in the absence of sustained adipogenic stimulation.

Cellular and molecular identity of *in vivo* preadipocytes hasn´t been elucidated yet, although many advances have been done in this field during the last decade. Morphologically, committed adipocytes have spindly fibroblastic phenotype and express a wide set of molecular markers. Among them, Pref-1, also referred as Dlk1, is the only widely accepted marker for the undifferentiated preadipocytes. This protein is highly expressed in white and brown preadipocytes, it is markedly down-regulated upon

differentiation and is absent in mature adipocytes (33, 34). However, Pref-1 is also expressed in mesenchymal stem cells commited to non-adipose cell types, such as chondrocytes and osteoblasts (34), being, therefore, a not truly specific preadipocyte marker.

Recently, two different laboratories using cell-sorting and *in vivo* cell lineage tracking strategies, have succesfully identified and isolated a group of mural cells in the capillary of the adipose vasculature with elevated adipogenic potential *in vitro* and the capacity of reconstituting WAT in lipodystrophic mice (35, 36). Unfortunately, the cell surface markers utilized in these studies (Sca-1, CD24, and CD34), also lack of specificity for preadipocytes. However, these approaches illustrate new strategies for localizing and isolating committed and functionally relevant preadipocytes populations *in vivo*.

More recently, Spiegelman's laboratory identified Zfp423, a multi-zinc finger transcriptional regulator essential for preadipocytes commitment, which could be operationally used as highly specific preadipocytes marker *in vivo* (37).

1.2.2 Late adipogenesis: terminal differentiation.

Terminal adipogenic differentiation involves a complex network of transcriptional events and signaling pathways that allow preadipocytes to acquire the full mature adipocyte phenotype (4). This stage has been extensively studied and characterized *in vitro*, however, the physiological relevance of many of these findings remains to be elucidated (25). Based on these *in vitro* models, terminal adipogenesis involves the sequential expression and repression of a number of transcription factors, co-activators, co-repressors and cell cycle regulatory molecules. Among those, CCAAT/enhancer-binding protein-α (C/EBPα), C/EBPβ and C/EBPδ and peroxisome-proliferator associated receptor gamma (PPARγ) are key drivers of this transcriptional cascade, both *in vitro* and *in vivo* (25, 38) **(Figure 6)**.

In cultured preadipocytes, one of the first events after adipogenic induction is the phosporylation of cyclic AMP response element-binding protein (CREB) and re-entry in the cell cycle. This leads to a mitotic clonal expansion (MCE) phase of approximately two mitotic rounds and the concomitant transcriptional induction of C/EBPβ **(Figure 7)**. Upon adipogenic stimuli, C/EBPβ is phosphorylated by glycogen synthase kinase (GSK)-3β and binds to specific DNA responsive elements to increase the transcriptional activity of its target genes (39-41). As preadipocytes progress through the cell cycle, the abundance of the cyclin-dependent kinase inhibitor p27KIP is decreased, facilitating the activation of cyclin-dependent kinase 4 (cdk4) which in complex with D-type cyclins, phosphorylates retinoblastoma (Rb) resulting in the release of E2F1, a crucial transcriptional regulator of the cell cycle. This, in turn, induces PPARγ transcription during clonal expansion *in vitro*

(42-44). After MCE, expression of C/EBPα and PPARγ is fully induced and expression of C/EBPβ begins to decline.

C/EBP-α and PPAR-γ are considered crucial determinants of adipocyte fate. Indeed, PPARγ transcriptionally activates C/EBPα encoding gene and vice versa, creating a positive-feedback loop that induces their own expression along with activating many downstream adipogenic target genes, including those encoding for glucose transporter 4 (GLUT4), fatty-acid-binding protein (FABP) 4, (also known as adipocyte protein 2, aP2), lipoprotein lipase (LPL), perilipin family of LD associated proteins, and the secreted factors adiponectin and leptin whose expression defines the mature adipocyte (25, 38, 45, 46).

Interestingly, in spite of the dual rol of C/EBPα and PPARγ in driving terminal adipogenic process, elegant studies have shown that ectopic PPARγ expression can completely rescue adipogenesis in C/EBPα-deficient MEFs (47). By contrast, C/EBPα overexpression is ineffective in rescuing adipogenesis in the absence of PPARγ (45). Moreover, ectopic expression and ligand activation of PPARγ in nonadipogenic fibroblasts also promotes their conversion into lipid-filled cells and induces a full program of adipogenic gene expression (48). These findings have established to PPARγ as the master regulator of adipogenesis.

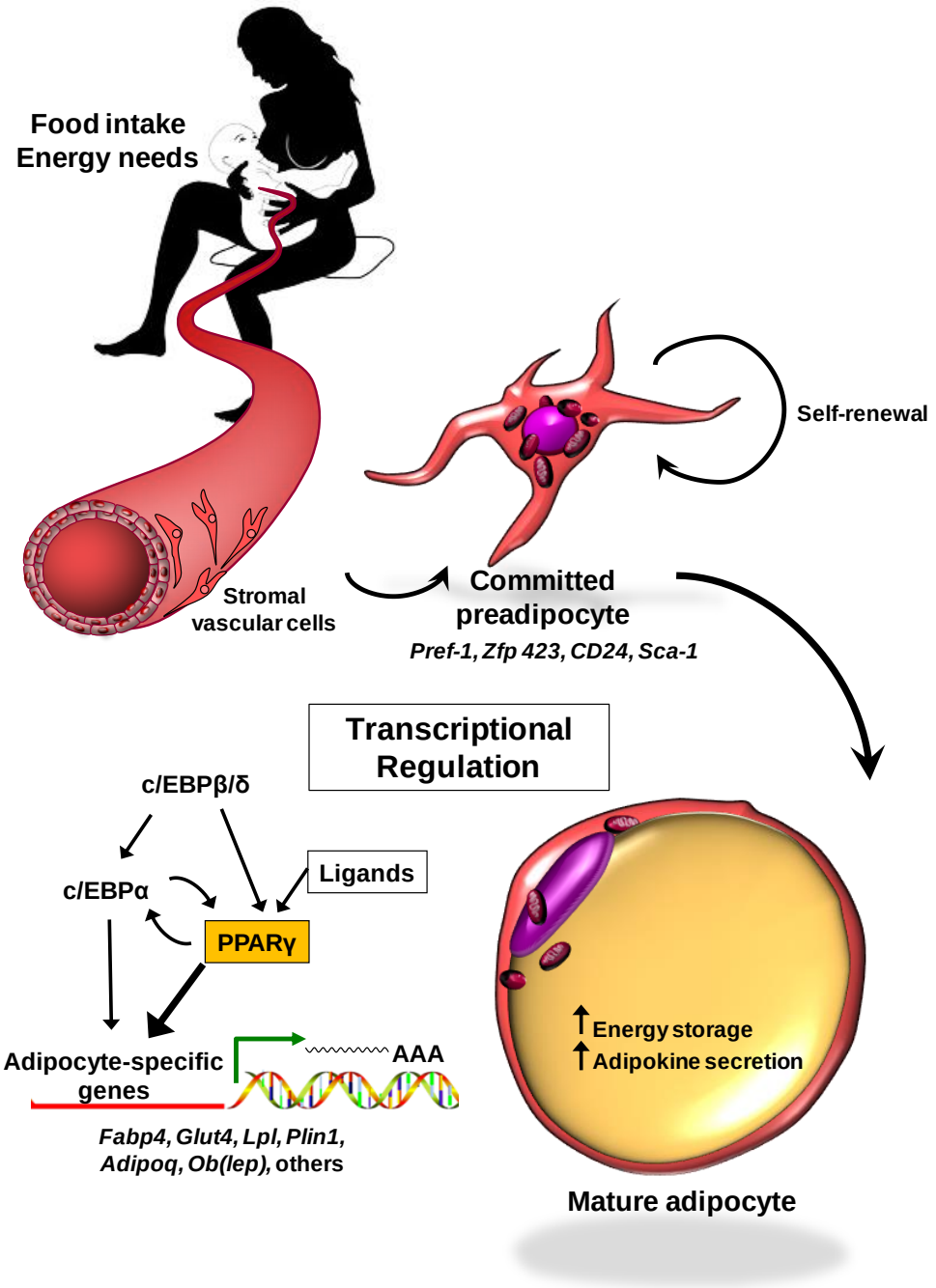

Figure 6: The gene circuitry that regulates the differentiation of predipocyte towards mature adipocytes. Nutritional signals such as food intake induce that committed preadipocytes in the stromal vascular fraction (progenitor niche) enter into the adipogenic differentiation program leading to the functional adipocyte development commanded by the PPARγ transcriptional regulation.

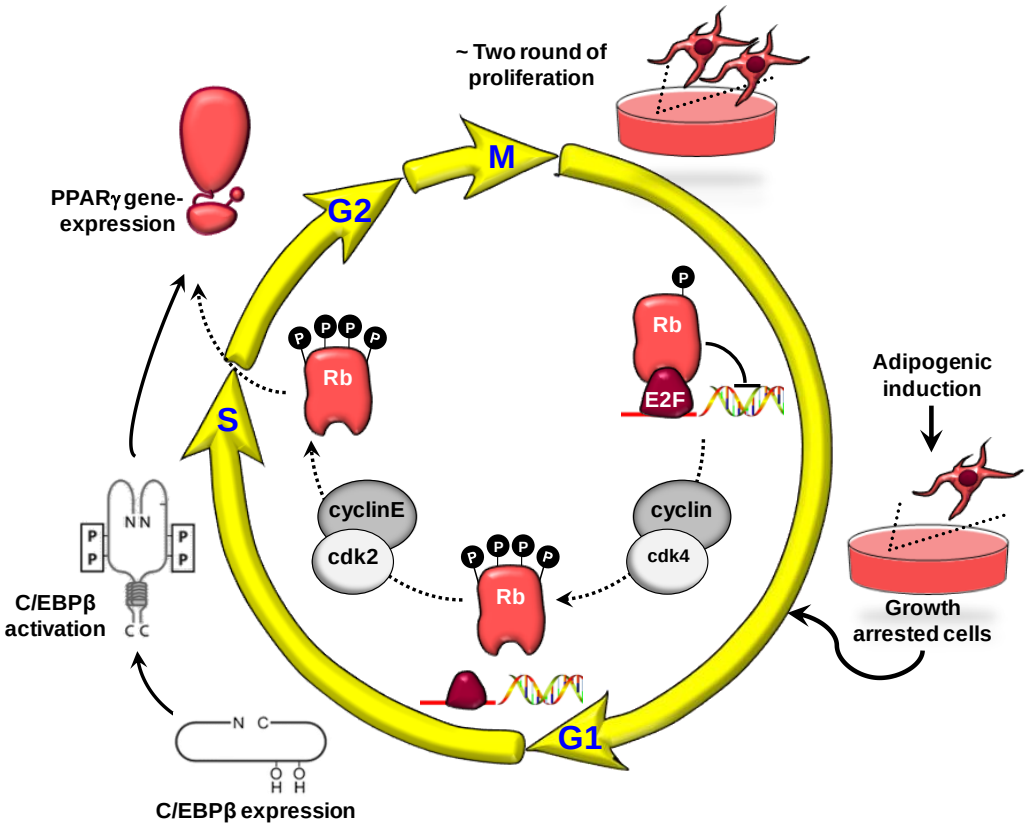

Figure 7: Schematic representation of the preadipocytes mitotic clonal expansion (MCE). Adipogenic induction in growth-arrested preadipocytes initiates MCE before expression of genes that give rise to the adipocyte phenotype. Activated cyclin D/Cdk4 complexes carry out phosphorylation of pRb and subsequent liberation of E2F transcription factors. E2F promotes the transcription of multiple cell cycle regulatory proteins necessary for preadipocytes proliferation, including cyclin E. Cyclin E/Cdk2 complexes activity allow G1/S phase transition.

1.2.3 PPARγ is the master regulator of adipogenesis.

PPARγ belongs to the heterodimeric nuclear receptors superfamily and is the pharmacologic target of thiazolidinediones (TZD), a group of clinically available insulin sensitizers (49). Structurally, it possess well defined transactivation, DNA binding and dimerization domains. After ligand activation, PPARγ heterodimerizes with retinoid X receptors (RXRs) and binds to PPAR gamma response elements (50) on the regulatory regions of its target genes. Consensus PRE sequence consists of two direct repeats of the hexamer 'AGGTCA' separated by a single nucleotide (this is called a 'DR-1' sequence) **(Figure 8)**. Surprisingly, despite the important role of PPARγ in adipogenesis, only few genes have been validated as direct PPARγ targets in adipocytes.

Alternative use of the first exon of *PPARgamma* gene gives rise to two major protein isoforms, PPARγ1 and PPARγ2 (51). Both isoforms are strongly induced during preadipocyte differentiation and remain highly expressed in mature adipocytes. However, tissue expression analysis has revealed that whereas PPARγ1 is present in many cell types, PPARγ2 is almost restricted to WAT and BAT, being regarded as a mature specific adipocyte marker (52, 53).

Multiple lipid metabolites such as modified fatty acids, selected species of lysophosphatidic acid (LPA), fatty acids, eicosanoids and oxidized phospholipids have been proposed to activate PPARγ as physiologic ligands (50, 54-57), however, a true endogenous PPARγ ligand still remains elusive.

PPARγ is both necessary and sufficient for adipogenesis and, to date, no factor has been identified that can rescue adipogenesis in the absence of PPARγ. Actually, most

proadipogenic factors seem to function at least in part by stimulating PPARγ expression or activity (45, 48, 58, 59).

The importance of PPARγ for adipocyte development and function *in vivo* has been demonstrated by a number of genetically modified models. Global PPARγ knockout mice die during early embryogenesis (E9.5) owing to placental and cardiac malformations and dysfunction, however, viable PPARγ knockout mice recovered through tetraploid complementation develop a striking absence of all types of adipose tissue (60). In addition, the two reported adipose-specific PPARγ knockout mice (aP2-Cre/PPARγ$^{lox/lox}$) exhibit marked reduction adipocytes mass (>70-80%) and morphologic defects of both WAT and BAT (61, 62). Moreover, PPARγ hypomorphic mice and PPARγ2 knockout mice have also reduced adipose mass throughout life (63, 64). Remarkably, human partial lipodistrophies have been associated with several missense mutations in PPARγ (65-70). In fact, the mouse model carrying the homozygous dominant negative P467L human mutation in the ligand-binding domain of PPARγ dies *in utero* whereas the heterozygous mice (Pparg$^{P465L/+}$) has normal amount of total adipose but grossly abnormal fat distribution with selective reduction of interscapular BAT and visceral (mesenteric, gonadal, and retroperitoneal) WAT, and increased subcutaneous (inguinal) WAT mass (71). Together these observations provide direct evidence that PPARγ is indispensable for normal adipogenesis *in vivo*.

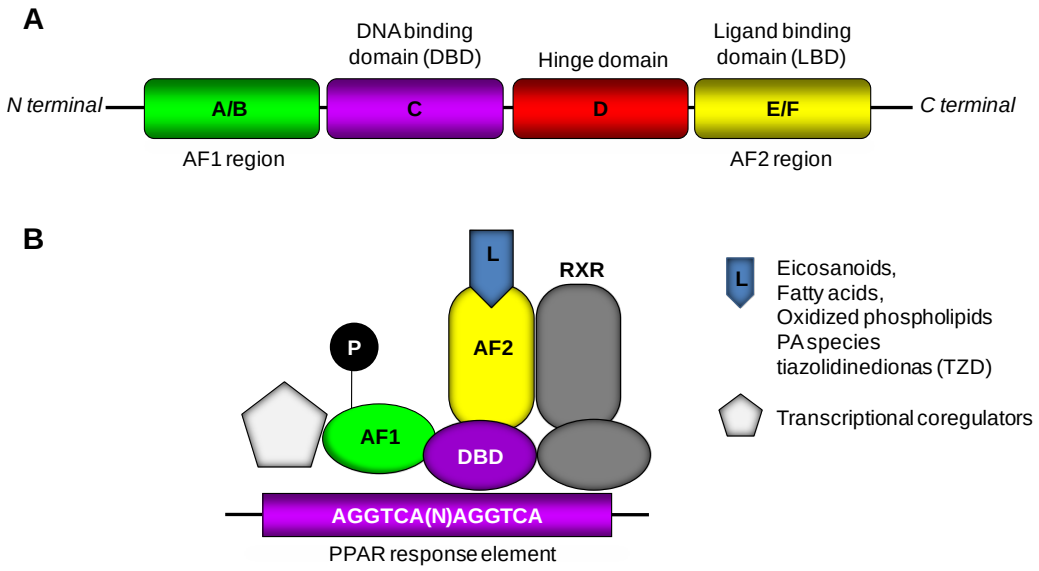

Figure 8: Schematic structure of PPARγ protein. (A) Like other members of the nuclear hormone receptor family, PPARγ is composed of four separate functional domains: the N-terminal A/B domain containing a ligand independent activation function 1 (AF-1); the C domain containing zinc finger DNA binding motif that binds to PPAR response elements (PPRE) in target genes; the hinge region; and the C-terminal ligand binding domain (LBD) containing the ligand dependent activation function 2 (AF-2). **(B)** Schematic structure of the PPARγ-RXRα heterodimer on DNA reveals that PPARγ interacts with RXR through the ligand binding domain as well as the DNA binding domain. In addition the structure also demonstrates that the LDB binds various polyunsaturated fatty acids, fatty acids derivate and synthetic ligands.

1.3 Lipid storage and lipid droplet biogenesis.

One of the fundamental results of adipogenesis is the generation of professional lipid acumulating cells. In fact, while most cell types have the capacity to accumulate lipids in small intracellular lipid droplets (LDs, also referred in the literature as to lipid bodies, fat bodies, oil bodies, spherosomes or adiposomes), usually ranging from 100 to 200 nm (72), the white adipocyte, is the only cell that can store massive amounts of lipids (mainly triglycerides, TGs) in a single and unilocular LD, which can physiologically reach up to 100 μm in diameter (73-75).

LDs are cytoplasmic organelles largely ignored by cell biologists during most of XX century, mainly because of the well established idea that they were mere, almost inert, lipid storage sites. The global epidemic of obesity and metabolic diseases, however, has fueled a new area research, that among other discoveries has revealed that LDs are indeed, highly dynamic and complex structures, intrinsically connected with many crucial processes such as cellular proliferation, metabolism, remodeling, signaling, detoxification and death (72, 75).

Structurally, LDs consist of a hydrophobic core made of neutral lipids (mainly TGs, cholesteryl and retinyl esters) and surrounded by a monolayer of phospholipids and specific associated proteins **(Figure 9)**. The most abundant LD proteins include members of Perilipin (Plin1-5) and Cell death-inducing DFF45-like effector (cidea, cidec/FSP27 and cideb) families, lipases such as Adipose triglyceride lipase (ATGL), Hormone sensitive lipase (HSL) and Monoacylglycerol lipase (MGL) and various membrane-trafficking

proteins (74, 76-81). Many other proteins have been identified by proteomic analysis but their roles in LDs biology remain unclear (79, 80)

Notably, in spite of its apparent simplicity, many crucial aspects of LDs biology still remain unknown. According to the prevailing model, lipid droplets originate from subdomains of the endoplasmic reticulum (ER) lipid bilayer as a lens of neutral lipid that after reaching a critical volume buds off to form a discrete nascent droplet within the cytoplasm (76, 78) **(Figure 10)**. However, how this process is initiated and regulated and how it is linked to the cellular metabolism of lipids remains to be disclosed. It is logical to predict that adipogenesis, lipid metabolism, and LD biogenesis are all interconnected processes that require each other for normal adipocyte formation. Concordantly, even though most of TGs-biosynthetic enzymes are localized in the endoplasmic reticulum (ER), after lipogenic activation at least some of them, such as diacylglycerol acyl transferase (DGAT) 2, localize in ER subdomains close to the LD (82) or even result embedded on the LD´s surface, such as glycerolphosphate acyl transferase 4 (GPAT-4) (83).

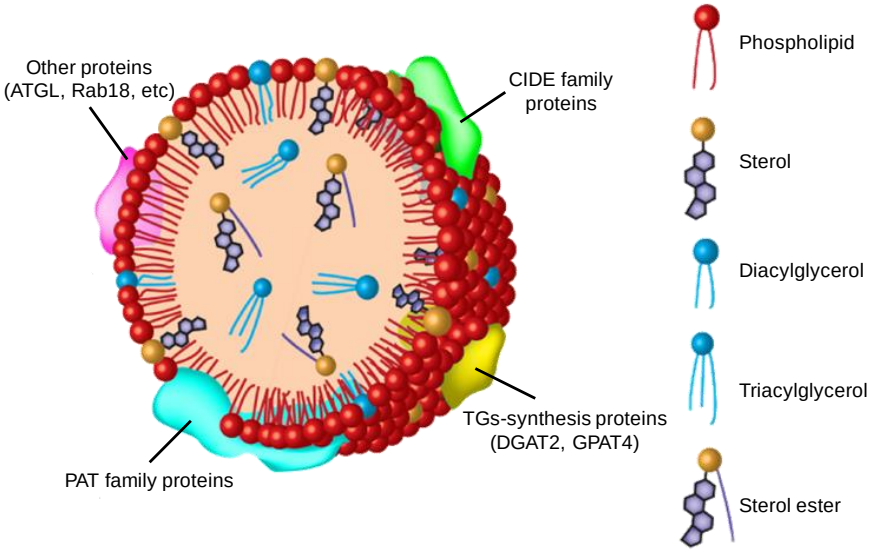

Figure 9: Structure of a Lipid Droplet (LD). The LD has a monolayer of polar lipids (phospholipids and sterols) at its surface and a core of nonpolar lipids (sterol esters, retinyl esters and triacylglycerols). A growing number of proteins have been identified on the surface of the droplet. These proteins include members of the PAT family (perilipin-1, ADRP/adipophilin, Tip47 and related proteins), CIDE family (CIDEA, CIDEC/FSP27) TG-synthesis enzymes (DGAT2, GPAT4) and other functional proteins *(Figure modified from Journal of Cell Science 2009 (122, pp. 749-752)).*

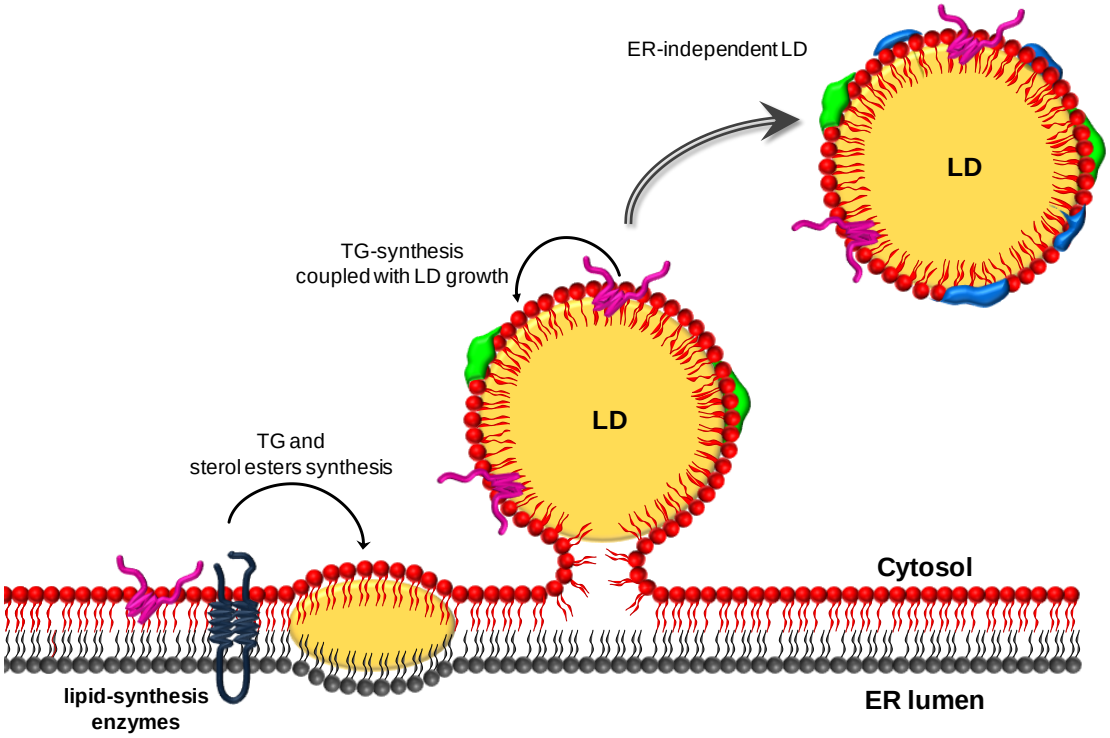

Figure 10: Model of LD biogenesis by ER budding. In the most widely accepted model, neutral lipids are synthesized by neutral lipid-synthesizing enzymes in the ER and bulge from the outer leaflet of the ER membrane driving a "budding". The mature LD is then thought to bud from the ER membrane to form an independent organelle that is bounded by a limiting monolayer of phospholipids and LD-associated proteins.

1.4 Intersection of TG synthesis, LD formation and adipogenesis.

Triglycerides are the primary form of energy storage in adipocytes, and alterations in TG biosynthesis can lead to pathological changes in the AT such as obsesity and lipodistrophy.

There are two major pathways for TG synthesis: the glycerol phosphate pathway and the monoacylglycerol pathway. The latter one is functional almost exclusively in the small intestine to generate TGs from dietary monoacylglycerol and free fatty acids. In contrast, the glycerol phosphate pathway is considered the main TG biosynthetic pathway in most cells types, including the adipocytes. Glycerol-3-phosphate (G3P) is the initial substrate in this pathway and the fatty-acyl groups that are sequentially incorporated to the glycerol backbone, are either derived from the hydrolysis of dietary TGs found in circulating chylomicrons or from the *de novo* lipogenetic activity in AT (84). When the pool of intracellular fatty acids increases, they are conjugated with CoA, forming fatty acyl-CoAs. These are used by a group of enzymes (glycerol-3-phosphate acyltransferases (GPATs), AGPATs, phosphatidic acid phosphatases (PAPs) and diacylglycerol (DAG) acyltransferases (DGATs) to synthesize TGs and intermediary products, such as PA and DAG, as well as for glycerophospholipid biosynthesis **(Figure 11)** (85). Developing adipocytes must couple glycerolipids synthesis and LDs biogenesis in order to safely store this growing lipid load and avoid cellular lipotoxicity.

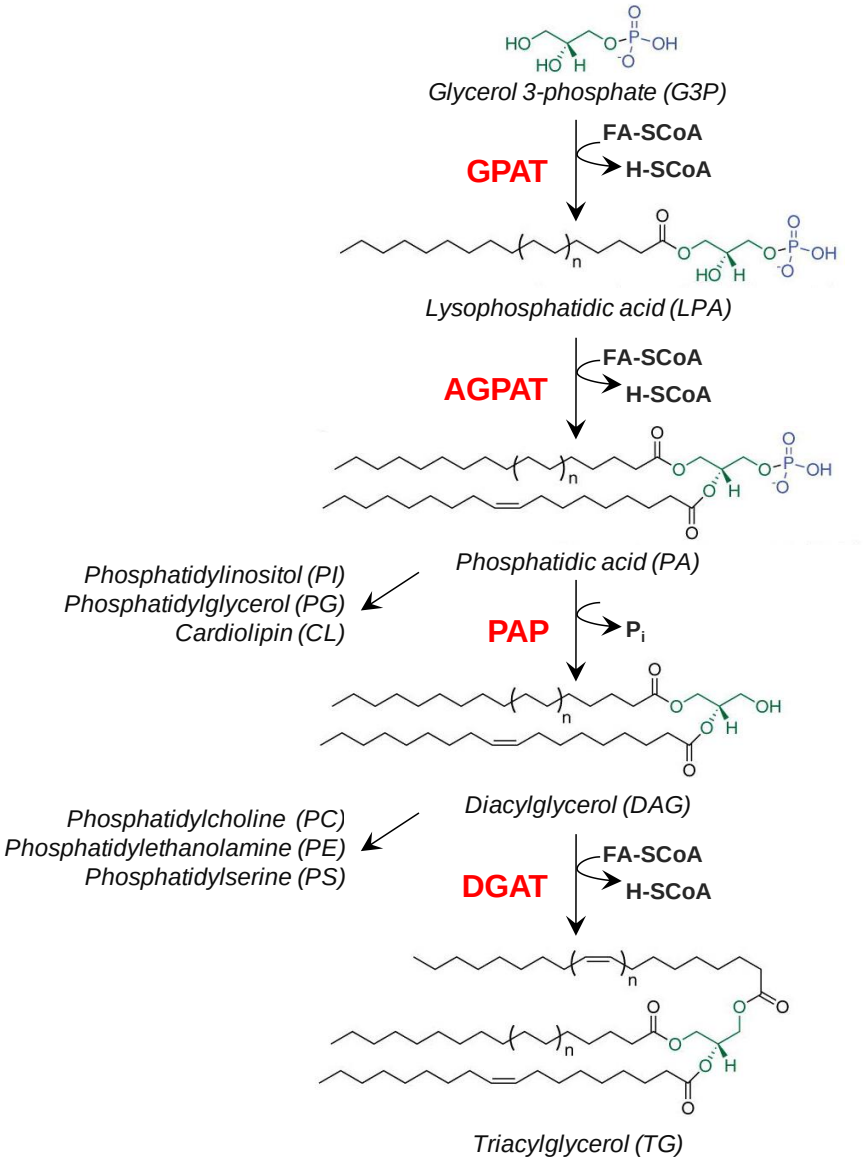

Figure 11: Overview of glycerol phosphate pathway that accounts for triacylglycerol (TG) and glycerophospholipid synthesis. GPAT, glycerol-3-phosphate acyltransferase; AGPAT, 1-acylglycerol-3-phosphate acyltransferase; PAP, phosphatidate phosphatase; DGAT, diacylglycerol acyltransferase; FA, fatty acid; H-SCoA, Coenzyme A; Pi, phosphate inorganic.

All the enzymes involved in the TG synthesis are located in the ER membrane. As mentioned in section 1.3, it is thought that the neutral lipids produced in the ER are progressively accumulated between the two leaflets of the ER membrane, forming a lipid lens that eventually buds off the ER, forming a LD. In this model, the phospholipid monolayer delimiting the LDs is derived exclusively from the outer leaflet of the ER membrane. In nearly all cells, the LD monolayer contains mainly phospholipids and smaller amounts of free cholesterol. This phospholipid composition is very similar to the one in the ER membrane, only with minor differences, such as a slightly increased lysophosphatidylcholine (Lyso-PC) content and small variations in the fatty acid composition (86). PC and phosphatidylethanolamine (PE) are the most abundant phospholipids, constituting more than 90% of total LD phospholipids. Besides PC and PE, small amounts of phosphatidylserine (PS), phosphatidic acid (PA) and phosphatidylinositol (PI) can be found (87). However, in spite of having these clues on the LD lipid composition, little is known on how the synthesis of glycerolipids is regulated during LDs biogenesis and growth and how these lipids are vectorized to the different compartments of the growing LD.

In particular, remain puzzling how such highly hydrophobic neutral lipids can translocate from the ER to growing LDs, especially since components for a potential transfer mechanism have not been described yet. Recent studies have shown that DGAT2, catalyzing the final step of TG synthesis, localizes to LDs, thereby suggesting that TG lipids might be locally synthesized on the LDs (87, 88). Nevertheless, it still not known how TGs are transferred to the LD core and whether only the reaction catalyzed by

DGAT2, or maybe more steps of the TG synthesis pathway, occur directly on the LD surface or on surrounding specialized membrane domains.

Notably, loss of function mutations in genes encoding *de novo* TG synthesis enzymes are associated with adipose tissue alterations commoly characterized by adipose tissue loss and/or atrophy (lipodistrophies) in mice. Other lipodystrophy-related genes encode LD associated proteins involved in LD formation and regulation while others genesenconde proteins that regulate directlly the adipogenesis.. Therefore, a central question regarding to the pathophysiology of lipodystrophy is whether this phenotype results from mature but TGs depleted adipocytes or affects adipogenesis itself.

To address this question we need back to the TG-synthesis. The rate limiting step of TGs pathway is the first acylation of G3P backbone, catalyzed by GPATs (89). Notably, although GPAT deficient mice have reduced TGs in all studied tissues, including adipose, they are not lipodystrophic, indicating that TGs synthesis, although required for adipocyte growth, is not essential for adipocyte differentiation. Similarly, AGPAT1 and AGPAT6/GPAT4 knockout mice have reduced subcutaneous adiposity but they are not lipodystrophic since significant adipose depots are still found elsewhere. Concordantly, *Agpat6/Gpat4*$^{-/-}$ MEFs fully differentiate into adipocyte-like cells in culture, indicating preservation of adipogenic potential (90). In contrast, AGPAT2 deficiency in humans and mice cause severe generalized lipodystrophy and insulin resistance, being the only TG-synthesis enzyme whose absence is associated with severe lipodystrophy in humans and mice (2, 84, 91). Fatty liver dystrophic (Fld) mice harbor a spontaneous inactivating mutation in Lpin1, the gene encoding for LIPIN1, the main PAP of adipocytes, which catalyzes the dephosphorylation of phosphatidic acid (PA) to generate diacylglycerol

(DAG) **(Figure 11)**, This mouse model develops congenital generalized lipodystrophy and insulin resistance (92). Moreover, LIPIN1 is also present in the cell nucleus and has transcriptional regulatory roles that are independent of its PAP enzymatic activity. Adipogenic studies with Fld MEFs have revelead that LIPIN1 is required for normal C/EBPα and PPARγ expression and full mature adipocyte differentiation (93). This is possibly the result of impaired PPAR recruitment on regulatory regions of PPAR target genes (94). DGAT2 deficiency is not compatible with postnatal life in mice, however, newborn *Dgat2*$^{-/-}$ mice have almost 90 % of TG reduction in carcasess. By contrast, DGAT1 deficient mice only have 50 % reduction in adiposity (95). Notably, whereas single *Dgat1* or *Dgat2* gene deletion does not preclude TGs synthesis and LDs formation in adipogenically induced MEFs, double *Dgat1*$^{-/-}$;*Dgat2*$^{-/-}$ MEFs completely fails to accumulate intracellular TGs (93). However, although *Dgat1*$^{-/-}$;*Dgat2*$^{-/-}$ MEFs are severely depleted of TGs, they seem to be, otherwise, fully capable of acquiring another mature adipocyte charactersitics, including normal expression of PPARγ, C/EBPs and secretion of high molecular weight adiponectin (93), indicating that, at least in this model, TG accumulation is not absolutely required for adipogenicn differentiation *in vitro*.

1.5 Lipodystrophies: key syndromes to understand the development of the adipose tissue.

Lipodystrophies are a heterogeneous group of disorders characterized by lipoatrophy, i.e. loss of WAT, with or without partial or segmental lipohypertrophy, i.e. increase of adipose mass in restricted areas of the body. The clinical consequences of lipodystrophy usually exceed the mechanical or cosmetic implications of abnormal WAT mass or distribution. In fact, severe reductions of WAT associate with various metabolic manifestations, likely as a result of insulin resistance. Genetic forms of lipodystrophy are infrequent (1 per 1 million people of general population) and include congenital generalized and familial partial lipodystrophies (96). Acquired lipodystrophies are more common and also include generalized and partial forms (97, 98). Among them, partial lipodystrophy developed by HIV-infected patients upon highly active anti-retroviral therapy (HAART) is currently, the most common form of acquired lipodistrophies and, is becoming a growing public health problem mainly because its associated metabolic complications (99).

1.5.1 Clinical features and molecular basis of CGL.

CGL or Berardinelli-Seip syndrome is an autosomal recessive disorder first reported in Brazil by Berardinelli almost 60 years ago (97). Since then, over 1000 patients have been reported in the literature. Patients with CGL are recognized at birth or soon thereafter, and are characterized by a near-total lack of WAT in subcutaneous, intra-abdominal, intra-thoracic and bone marrow depots **(Figure 12)**. Early metabolic consequences of adipose tissue loss are hyperphagia (increased appetite and food intake), severe hyperinsulinaemia,

hypertriglyceridemia, hepatic steatosis, acromegaloid features and organomegaly. Affected women usually develop oligoamenorrhea and polycystic ovary syndrome (100, 101). Diabetes mellitus usually starts after puberty.

Noteworthy, all CGL associated genes encode for proteins involved in TG synthesis, LDs formation or fatty acid intracellular trafficking: 1) *AGAPT2* gene encodes, as mentioned in section 1.4, an ezyme involved in the biosynthesis of triglycerides and glycerophospholipids and its mutations account for ~50% of all CGL described cases (102). 2) *BSCL2* gene encodes Seipin, an ER protein of unknown function but absolutely required for LD biogenesis. 3) *CAV1* gene encodes Caveolin-1, an essential organizer of plasma membrane caveolae, with strong fatty acid binding activity and also localized on adipocytes' LD surface (103-105). 4) *PTRF* gene encodes Cavin 1, a caveolin-1 binding protein also essential for caveolae formation (106-108).

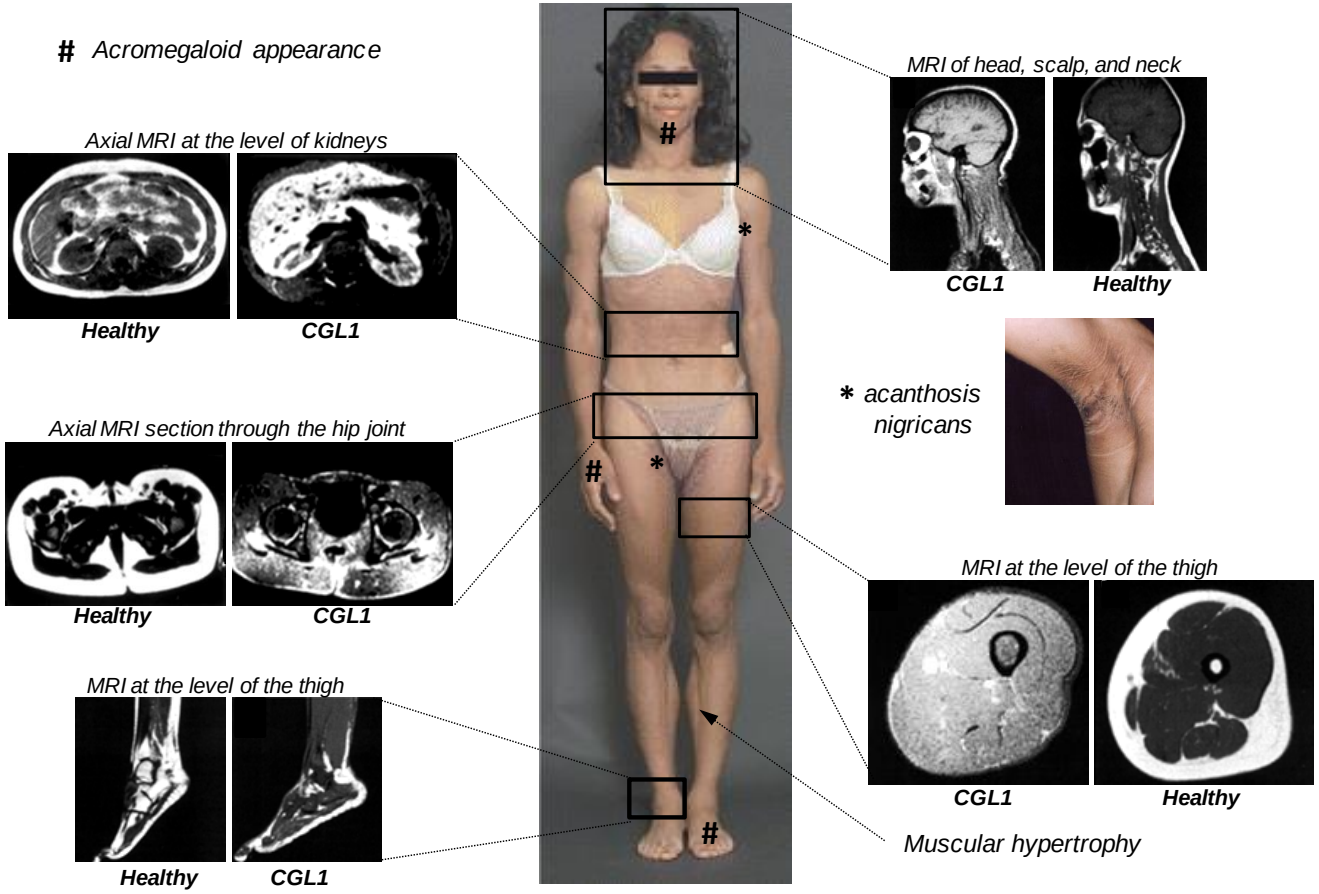

Figure 12: Whole-body MRI of a female patient with CGL1. MRI reveals extreme paucity of subcutaneous adipose tissue in CGL patient compared with normal healthy patient. In these images body fat is contrasted in white color. *(Figure composed out of data obtained from The Journal of Clinical Endocrinology & Metabolism 2003; 88, pp:5433–5437 and Annual Review of Medicine 2006; 57, pp:297–311)*

1.6 Molecular characteristic and function of AGPAT2.

AGPAT2 protein, also called lysophophatidic acid (LPA) acyltransferase (LPAAT)-β, belongs to a family of enzymes catalyzing the *sn*-2 acylation of G3P backbone, in the *de novo* glycerolipid synthesis pathway (see section 1.4). Specifically, AGPATs convert LPA into phosphatidic acid (PA), a key step in the synthesis of TGs and phospholipids **(Figure 11)**. In humans and mice, *AGPAT2* gene encodes a ~31 KDa protein with four predicted transmembrane domains. *In vitro* studies with tagged overexpressed versions of AGPAT2 have shown it mainly in the ER (109).

AGPAT family is composed by 11 members each encoded by a distinct gene. These isoforms display specific patterns of tissue expression and differential substrate preference. Notably, only AGPAT2 has been implicated in CGL, suggesting that this isoform has very specific roles in AT biology. In fact, AGPAT2 is the main AGPAT isoform found in mature WAT; although the transcriptional mechanisms regulating its expression remain unknown (110). Intriguingly, i*n vitro* enzymatic assays have shown that substrate preferences of both AGPAT2 and AGPAT1 are very similar either for acyl-CoAs and LPAs, with oleyl-CoA and oleyl-LPA being the preferred substrates (109). Thus, tissue and time specific expression of AGPAT2 could determine the composition of structural and regulatory glycerolipids in preadipocytes (111).

1.7 Possible mechanisms of lipodystrophy in the *Agpat2*$^{-/-}$ mice.

To advance in the understanding of the physiological role of AGPAT2 our colleagues at University of Texas Southwestern Medical Center (UTSW) developed the first *Agpat2*$^{-/-}$ mouse (2). Like in humans, *Agpat2* deficiency in mice results in generalized lipodystrophy, severe insulin resistance, diabetes and hepatic steatosis. Strikingly, *Agpat2*$^{-/-}$ mice also have total deficiency of BAT. The mechanisms of lipodystrophy in AGPAT2 deficient mice and humans, however, still are elusive.

The simplest hypothesis for the WAT lack in AGPAT2 deficient humans and mice is that the absence of AGPAT2 prevents the formation of TGs, resulting in "empty adipocytes". Nevertheless, gene deletion of upstream or downstream enzymes in the glycerolipid synthesis pathway, such as GPATs, DGATs, although severely decreasing TGs synthesis rate, do not cause generalized lipodystrophy, suggesting that AGPAT2 activity has additional regulatory roles beyond the sole TGs biosynthesis. Furthermore, studies in *Agpat2*$^{-/-}$ livers show increased expression of lipogenic genes and enhanced *de novo* fatty acid and triglyceride biosynthesis (2), indicating that other AGPAT isoforms can compensate AGPAT2 deficiency in terms of TGs generation.

Alternatively, AGPAT2 could regulate adipogenesis by the modulation of cellular level of critical signaling phospholipids. Indeed, a possible regulatory role for AGPAT2 on PPARγ activation could be through the modulation of the intracellular levels of LPA and PA. *In vitro* competition binding assays and PPRE-luciferase reporter expression in RAW264.7 monocytes, have revealed that LPA can bind and activate PPARγ (50). However, it has also been shown that LPA downregulates PPAR expression and impairs

adipogenesis (112). Albeit contradictory, these findings suggest that AGPAT2 enzymatic activity could modulate adipogenic differentiation through the fine tuning of specific LPA and PA moities and consequently, regulate the transcriptional activity of PPARγ.

Concordantly, treatment of 3T3-F442A preadipocytes with growing concentrations of PA but not DAG, attenuates the induction of PPARγ in a dose-dependent manner (113). More recently, cyclic phosphatidic acid (cPA) was shown to directly bind and inhibit PPARγ, owing to the stabilization of PPARγ association with transcriptional co-repressor nuclear receptor co-repressor 2 (NCOR2, also referred as SMRT) (114).

Finally, siRNA induced knockdown of AGPAT2 expression in OP9 cells results in increased levels of total PA (115) whereas its knockdown in 3T3-L1 cells results in increased levels of different LPA and cyclic PA species few days after adipogenic induction, and this was associated with failed full adipocyte maturation (116).

Taken together, the currently available information strongly suggest that AGPAT2 deficiency can inhibit adipogenesis in a PPARγ-dependent manner.

2. HYPOTHESIS AND AIMS

2.1 Hypothesis

"The deficiency of AGPAT2 inhibits the adipogenesis preventing the formation of mature adipocytes.

2.2 General Aims

1. To determine whether the deficiency of AGPAT2 inhibits the adipogenic differentiation of *Agpat2*$^{-/-}$ mouse embryonic fibroblasts (MEFs).
2. To evaluate whether there is development of adipose tissue during the fetal and neonatal life of *Agpat2*$^{-/-}$ mice.

2.3 Specifics aims

To study the process of adipogenic differentiation in vitro, mouse embryonic fibroblast (MEFs) isolated from Agpat2$^{+/+}$ *and Agpat2*$^{-/-}$ *embryos were first generated and characterized. Then, these primary cell cultures were the basic tool to pursue the following specific aims:*

1. To induce adipogenic differentiation in cultured *Agpat2*$^{+/+}$ and *Agpat2*$^{-/-}$ MEFs and to evaluate the formation of lipid droplets-loaded cells and the expression of adipocyte-specific markers at mRNA and protein level.

2. To characterize the expression of C/EBP-α,-β,-δ and PPARγ at mRNA and protein levels in cultured *Agpat2*$^{+/+}$ and *Agpat2*$^{-/-}$ MEFs at different time points of adipogenic differentiation.
3. To induce PPARγ2 overexpression in cultured *Agpat2*$^{-/-}$ MEFs and to evaluate whether adipogenic differentiation might be rescued.

To study if late embryos and newborn Agpat2$^{-/-}$ *mice lack of preadipocytes and/or adipose tissue, we mated Agpat2*$^{+/-}$ *females and males to generate Agpat2*$^{+/+}$ *and Agpat2*$^{-/-}$ *littermates. Those animals were used to perform the following specific aims:*

1. To evaluate the presence, distribution, morphology and molecular features of adipose tissue in late embryos (E18.5) and newborns (0, 2, 4 and 6 days old) *Agpat2*$^{-/-}$ mice.
2. To evaluate the existance of preadipocytes in adipose depots from adipose tissue of late embryos (E18.5) and newborns *Agpat2*$^{-/-}$ mice.

3. MATERIALS AND METHODS

3.1 MATERIALS

3.1.1 Genotyping Reagents

PCR Lysis Reagent (Viagen), 20mg/ml Proteinase K Solution (Viagen), TaKaRa Ex Taq™ Polymerase and dNTP mixture (Takara Biotechnology), Soriano buffer, DMSO (Sigma), Sterile Nuclease free water (Fisher Scientific), LE Quick Dissolve Agarose (GeneMate).

3.1.2 Cell Culture Reagents

Fetal bovine serum, DMEM/F-12 (Dulbecco's Modified Eagle Medium/Nutrient Mixture F-12), DMEM High Glucose (Gibco), 200 mM L-Glutamine (Gibco), 100X MEM Non-Essential Amino Acids (Gibco), 100X Penicillin-Streptomycin-Glutamine (Gibco), 2-Mercaptoethanol (Sigma), 0.25% Trypsin-EDTA (Gibco).

3.1.3 Cloning and Transfection Reagents

Phusion® High-Fidelity DNA Polymerase (New England Biolabs), pENTR™/D-TOPO® Cloning Kit with One Shot® TOP10 Chemically Competent *E. coli* (Invitrogen), pAd/CMV/V5-DEST™ Gateway® Vector Kit (Invitrogen), LR Clonase II (Invitrogen), Proteinase K (Invitrogen), Restriction enzymes: PacI, Not I, Asc I (New England Biolabs), FuGENE®6 Transfection Reagent, QIAquick® Gel Extraction Kit (Qiagen), High Pure Plasmid Isolation Kit (Roche), Genopure Plasmid Maxi Kit (Roche),

Phenol:Chloroform:Isoamyl Alcohol (Sigma), HEK 293A cell line (Invitrogen), Cesium Chloride (Fisher Scientific)

3.1.4 Specifics chemicals and commercial kits

3-Isobutyl-1-methylxanthine (IBMX, Sigma), Dexamethasone (Sigma), Insulin from bovine pancreas (Sigma), Rosiglitazone potassium salt (Cayman), Propidium Iodide (Sigma), Ribonuclease A (Sigma), Optimal Cutting Temperature (O.C.T) Compound (Tissue-Tek), 32% Paraformaldehyde Solution (Electron Microscopy Sciences), Mayer's Hematoxyllin Solution (Sigma) 0.5% Oil Red O Solution (Sigma), BODIPY® 493/503 (Molecular Probes), ProLong® Gold Antifade Reagent with DAPI (Molecular Probes), Click-iT® EdU Alexa Fluor® 488 Flow Cytometry Assay Kit (Molecular Probes), Precision Plus Kaleidoscope Protein Standard (BioRad), Restore™ Super Signal® West Pico Reagents (Pierce), Ponceau S Solution (Sigma), Plus Western Blot Stripping Buffer, 30% Acrylamide/Bis Solution 37.5:1 (Bio-Rad), Complete Mini EDTA-free Protease Inhibitor Cocktail Tablets (Roche), Phos-STOP phosphatase Inhibitor Cocktail Tablets (Roche), TaqMan Reverse Transcription Reagents (Applied Biosystem), Power SYBR® Green PCR Master Mix (Applied Biosystem), DNAse treatment (Ambion), RNA STAT-60 (Tel-Test, Inc).

3.1.5 Antibodies

Unconjugated antibodies

- Akt (pan) (Clone C67E7) Rabbit mAb (Cell Signalling)
- ATGL (Clone 30A4) Rabbit mAb (Cell Signalling)
- β-Actin (Clone 13E5) Rabbit mAb (Cell Signalling)

- C/EBPα (Clone D56F10) XP® Rabbit mAb (Cell Signalling)
- C/EBPδ Antibody (Cell Signalling)
- CDK2 (Clone 78B2) Rabbit mAb. (Cell Signalling)
- CDK4 (Clone DCS156) Mouse mAb (Cell Signalling)
- CREB (Clone 48H2) Rabbit mAb (Cell Signalling)
- Cyclin E1 (Clone HE12) Mouse mAb (Cell Signalling)
- DLK-1 (Clone 3A10) Mouse mAb (Abcam)
- FABP4 (Clone D25B3) XP® Rabbit mAb (Cell Signalling)
- GSK-3β (Clone D5C5Z) XP® Rabbit mAb (Cell Signalling)
- HSL Antibody (Cell Signalling)
- IGF-I Receptor β (Clone D23H3) XP® Rabbit mAb (Cell Signalling)
- Insulin Receptor β (Clone 4B8) Rabbit mAb (Cell Signalling)
- IRS-2 Antibody (Cell Signalling)
- IRS-1 (Clone D23G12) Rabbit mAb (Cell Signalling)
- Mac-2 (Galectin-3) (Clone M3/38) Rat mAb (Cedarlane)
- p44/42 MAPK (Erk1/2) (Clone 137F5) Rabbit mAb (Cell Signalling)
- Perilipin (Clone D1D8) XP® Rabbit mAb (Cell Signalling)
- Phospho-Akt (Ser473) (Clone D9E) XP® Rabbit mAb (Cell Signalling)
- Phospho-Akt (Thr308) (Clone D25E6) XP® Rabbit mAb (Cell Signalling)
- Phospho-C/EBPbeta (Thr235) Antibody (Cell Signalling)
- Phospho-CREB (Ser133) (Clone 87G3) Rabbit mAb (Cell Signalling)
- Phospho-GSK-3β (Ser9) (Clone D85E12) XP® Rabbit mAb (Cell Signalling)

- Phospho-p44/42 MAPK (Erk1/2) (Thr202/Tyr204) (Clone D13.14.4E) Rabbit mAb (Cell Signalling)
- Phospho-p90RSK (Ser380) (Clone 9D9) Rabbit mAb (Cell Signalling)
- Phospho-S6 Ribosomal Protein (Ser235/236) (Clone D57.2.2E) Rabbit mAb (Cell Signalling)
- Phospho-Rb (Ser807/811) (Clone D20B12) XP® Rabbit mAb (Cell Signalling)
- PPARγ (Clone 81B8) Rabbit mAb (Cell Signalling)
- Retinoblastome (D20) Rabbit mAb (Cell Signalling)
- RSK1/RSK2/RSK3 (Clone 32D7) Rabbit mAb (Cell Signalling)
- S6 Ribosomal Protein (Clone 5G10) Rabbit mAb (Cell Signalling)
- Seipin (L-16) Goat mAb (Santa Cruz)

Conjugated Secondary Antibodies

- Alexa Fluor® 488 Donkey Anti-Goat IgG (H+L) Antibody (Molecular Probes)
- Alexa Fluor® 488 Donkey Anti-Rat IgG (H+L) Antibody (Molecular Probes)
- Alexa Fluor® 488 Donkey Anti-Mouse IgG (H+L) Antibody (Molecular Probes)
- Alexa Fluor® 488 Goat Anti-Rabbit IgG (H+L) Antibody, highly cross-adsorbed (Molecular Probes)
- Alexa Fluor® 594 Donkey Anti-Rabbit IgG (H+L) Antibody (Molecular Probes)
- Donkey anti-goat IgG-HRP (Santa Cruz)
- Goat anti-rabbit IgG-HRP (Cell Signalling)
- Horse anti-mouse IgG-HRP (Cell Signalling)

3.2 METHODOLOGY

Mice handling and genotyping.

Agpat2$^{-/-}$ mice were developed at the University of Texas Southwestern Medical Center (UTSW) and formally transferred to Pontificia Universidad Católica de Chile, School of Medicine, under interinstitutional material transfer agreement (MTA). Inactivation of *Agpat2* gene was performed with a gene replacement vector strategy that deleted ~8.5 Kb portion of the proximal promoter and exons 1-4 of *Agpat2* and inserted a neomycin resistance cassette (*NEO*) *in situ* (2). The colony was maintained by heterozygous mice breeding and the resulting offspring was genotyped by PCR with the following primers SI75 (5'-GATTGGGAAGACAATAGCAGGCATGC-3') targeting the 5' end of *NEO* cassette, A8 (5'-AAAGCTGTGCCAGGGTGGGT-3') targeting *Agpat2* promoter region, and A15 (5'-CGGCTAGGTAAGCAGTTTGA-3') targeting *Agpat2* deleted region. The PCR program was: 1. Initial denaturation (1 cycle): 93°C, 1 min; 2. Amplification (40 cycles): 93°C, 30 seg; 60°C, 1 min; 65°C, 3 min; 3. Final extension (1 cycle): 65°C, 10 min. The wild-type allele produced a PCR product of 782 bp, and the deleted allele a product of 614 bp. All the mice used in this thesis were housed in colony cages under controlled environmental temperature and a 12-h light/12-h dark schedule. Animals were fed a regular mouse chow diet (10% of kilocalories from fat) under an *ad libitum* regimen. All experiments involving mice were approved by the Pontificia Universidad Católica de Chile, School of Medicine, Animal Ethics Committee and the Institutional Animal Care and Use Committee of UTSW.

Mouse embryonic fibroblasts (MEFs) generation and culture.

Primary cultures of MEF were prepared from E13.5 *Agpat2*$^{-/-}$ embryos or their wild-type littermates originated by *Agpat2*$^{+/-}$ progenitors. Pregnant females were sacrificed with isoflurane overdose at 13.5 d.p.c., their abdominal wall was wiped with a 70% ethanol solution and the embryos were removed by medial laparotomy and hysterectomy in less than 1 minute. Embryos were individually placed in plates with ice cold sterile phosphate buffer solution (PBS) and killed by decapitation with surgical scissors. Maternal tissues, placental membranes and visceral organs were removed and the resulting carcasses were washed with PBS and finely minced with scissors. This material was digested with 0.25% trypsin/1 mM EDTA for 3 hours at 4°C, and centrifuged for 5 minutes at 400 x g. The resulting pellet was resuspended in culture medium (High glucose DMEM supplemented with 10% heat-inactivated fetal bovine serum (FBS), 2mM L-glutamine, 0.1 mM nonessential amino acids, 100 µg/ml penicillin/streptomycin and 0.1 mM 2-β-mercaptoethanol) and seeded onto 150 mm plates. Cells were cultured at 37°C until they reached 100% confluence. MEFs were frozen in liquid nitrogen at passage 2 in aliquots of 10^6 cells/vial. All differentiation experiments were carried out with MEFs at passage 3.

MEFs adipogenic differentiation.

10^5 MEFs/cm^2 (at passages 3) were seeded in 12-well plates and cultured in standard culture medium (DMEM with 4.5 g/L glucose, supplemented with 10% heat-inactivated FBS, 2 mM L-glutamine, 0.1 mM nonessential amino acids, 100 µg/ml penicillin/streptomycin and 0.1 mM 2-β-mercaptoethanol). Two days after cultures reached

100% confluence, standard medium was removed and replaced with adipogenic induction medium (DMEM-F12 4.5 g/L glucose, supplemented with 10% FBS, 2 mM L-glutamine, 0.1 mM nonessential amino acids, 100µg/ml penicillin/streptomycin and 0.1mM 2-β-mercaptoethanol, 1 µM dexamethasone, 0.5 mM 3-isobutyl-1-methylxanthine (IBMX), 10 µg/ml insulin and incubated at 37%, 5% CO_2 for three days. After induction, MEFs were incubated in adipogenic differentiation medium (DMEM-F12 high glucose supplemented with 10% FBS, 2 mM L-glutamine, 0.1 mM nonessential amino acids, 100 µg/ml penicillin/streptomycin and 0.1 mM 2-β-mercaptoethanol, 10 µg/ml insulin and 10 µM rosiglitazone for 2 days. In the following days, medium was renewed every 2 days by adipogenic maintenance medium (DMEM-F12 high glucose supplemented with 10% FBS, 2 mM L-glutamine, 0.1 mM nonessential amino acids, 100µg/ml penicillin/streptomycin and 0.1 mM 2-β-mercaptoethanol and 10 µg/ml insulin).

Oil-red-O staining.

To visualize neutral lipids, Oil red O (ORO) staining was performed in differentiating MEFs. For this, culture medium was removed and cells were carefully washed once in PBS and fixed with freshly prepared 4% paraformaldehyde (PFA)/PBS for 30 min at room temperature. Cells were washed three times with PBS and stained with Oil Red O solution (six parts of 0.6% Oil red O dye in isopropyl alcohol and four parts water) for 30 minutes at room temperature. Then, ORO solution was removed and cells were washed three times with PBS and counterstained with hematoxylin for 1 minute. Photomicrographies were obtained with a digital camera coupled to a phase contrast optical

microscope. In some experiments, relative ORO content was quantified by spectrometry. For this purpose, ORO stained cells were washed three times with distiller water and incubated with 100% isopropanol on a rocker plate for 15 minutes. Next, optical density (OD) was quantified at a wavelength of 520 nm. To stain mouse histological slides, E18.5 embryos and neonatal mice (between 12 hours to 6 days old) were sacrificed by decapitation, washed with ice-cold PBS and fixed in 4% PFA/PBS. To preserve tissues' lipid content, samples were incubated in a 10 to 18% sucrose/PBS gradient. The tissues were embedded in Optimal Cutting Temperature (OCT) compound and frozen in liquid nitrogen. Sections of 7 µm were obtained from OCT tissue-blocks and stained with ORO following the same procedure described for PFA fixed cells.

Western blot analysis.

Whole protein extracts were prepared from MEFs and mouse tissues by homogenization in ice cold RIPA buffer containing 50 mM Tris (pH 8.0), 180 mM NaCl, 1% NP-40, 1% sodium deoxycholic acid, 0.1 mM EGTA and 0.1% sodium dodecyl sulfate (SDS) supplemented with protease and phosphatase inhibitor cocktails (Roche) and 1 mM phenylmethylsulfonyl fluoride (PMSF). Lysates were sonicated on ice and centrifuged for 15 min at 14,000 × g at 4°C to remove unsoluble debris. Protein concentration was determined by bicinchoninic acid (BCA) assay (Pierce) according to manufacturer's instructions. Western blotting was performed by denaturing 50 µg of total proteins at 95 °C for 3 minutes in Laemmli's sample buffer (62.5 mM Tris, pH 6.8, 2% SDS, 25% glycerol, 0.01% bromophenol blue, and 5% β-mercaptoethanol). Samples were subjected to SDS-

polyacrylamide gel electrophoresis and resolved at 120 V. Then, proteins were visualized with Red Ponceau, rinsed and electrotransferred for 10 minutes at 2.5 A onto nitrocellulose membrane using a Bio-Rad Trans-blot Turbo Transfer System. Membranes were blocked with 5% bovine serum albumin (BSA)/0.1% Tween 20 in tris phosphate buffer (TBS-T) for 2 hours at room temperature. Next, membranes were incubated overnight at 4 °C with primary antibodies diluted in 5% BSA/TBS-T solution. Rabbit antibodies against PPARγ, C/EBPα, C/EBPβ, C/EBPγ, Perilipin-1, HSL, total Akt, phospho-Akt (Thr308), phospho-Rb (Ser807/811), total Rb, p44/42 MAPK (Erk1/2), CDK2; CDK4, Cyclin E1 and PathScan® Multiplex Western Cocktail kit, were all purchased in Cell Signalling. Goat anti Seipin antibody was obtained from Santa Cruz. After incubation with primary antibodies, membranes were washed with TBS-T and incubated with to anti-rabbit IgG, anti-mouse IgG, or anti-goat IgG secondary antibodies, all conjugated with horseradish peroxidase in 5% BSA/TBS-T for 1 hour at room temperature. Blots were visualized by chemiluminescence detection using Super Signal® West Pico Reagents (Pierce) and exposure to X-ray films.

RT-PCR analysis.

Total RNA from cultured cells or mouse tissues was extracted with Trizol extraction kit (Invitrogen), according to manufacturer's instructions. For real-time PCR analysis, 2 µg of total RNA was reverse transcribed using the High Capacity cDNA Reverse Transcription Kit (Applied Biosystems). Real time quantitative PCR was performed on ABI Prism® 7900 HT thermalcycler (Applied Biosystems) using SYBR® Green PCR Master Mix (Applied

Biosystems) and 125 nM primers. Thermal cycling program included an initial denaturation with 50 °C for 2 minutes and 95 °C for 10 minutes, followed by 40 cycles two step amplification (95 °C for 15 seconds; 60 °C for 1 minute). Relative concentration of individual mRNAs was determined after normalization to a reference gene (Cyclophylin) and expressed as fold-change relative to non-differentiated *Agpat2*$^{+/+}$ MEFs using the ΔΔCt method.

Triglycerides quantification

Total triglycerides from differentiating MEFs were extracted and measured using Triglyceride Colorimetric Assay Kit (Cayman Chemicals) according to manufacturer's instructions. This method is based in the enzymatic hydrolysis of the triglycerides by lipoprotein lipase to glycerol and free fatty acids. Glycerol is then phosphorylated to glycerol-3-phosphate (G3P) by glycerol kinase, and this product is then oxidized by glycerol phosphate oxidase to dihydroxyacetone phosphate and hydrogen peroxide (H_2O_2). Peroxidase catalyzes the redox-coupled reaction of H_2O_2 with 4-aminoantipyrine (4-AAP) and N-Ethyl-N-(3-sulfopropyl)-m-anisidine (ESPA), producing a brilliant purple solution that is measured at 540 nm. To extract total glicerophopholipids from tissues, frozen samples were homogenized with 2ml of ice-cold Tris-HCl 20 mM containing protease inhibitors. Then, 0.8 parts homogenized tissue were vigorously mixed with 1 part $CHCl_3$ and 2 parts 0.1N HCl:CH_3OH. Next, 1 part $CHCl_3$ was added to the mix, shaked well and then, centrifuged at 600 x g for 10 minutes at 4 °C. Lower phase was carefully removed and washed with a small volume of 1M KCl.

Total phosphatidic acid quantification.

Total phosphatidic acid was measured in differenting MEFs using a fluorimetric assay (Cayman Chemicals). The method involves the hydrolysis of PA, as well as any LPA that is present, to glycerol-3-phosphate (G3P), which is then oxidized by glycerol-3-phosphate oxidase to generate H_2O_2. In the presence of peroxidase, H_2O_2 reacted with 10-acetyl-3,7-dihydroxyphenoxazine (ADHP) to produce the highly fluorescent compound resorufin, which was then measured using a fluorometer. Culture medium was removed and cells were carefully washed with TBS, harvested in 500 µl of cold pH 7.4 TBS and then sonicated on ice. Total proteins were quantified with BCA kit (Pierce) in a aliquote of the sample. To extract cell lipids, 1.5 ml of methanol, 2.25 ml of 1 M NaCl and 2.5 ml of chloroform were added to the sonicated pellet and then vigorously vortexed. The samples were centrifuged for 10 minutes at 1,500 x g at 4 °C to separate aqueous and organic phases. The upper aqueous phase was removed and discarded and the lower chloroform phase was washed twice with 2 ml preequilibrated upper phase by centrifuging at 1,500 x g for 10 minutes at 4 °C. After the last washing step, chloroform phase was transferred to a 12 x 75-mm glass tube, dried up under a gentle stream of nitrogen and resuspended in 500 µl of 1% Triton X-100. To perform the assay, 10 µl of extracted lipids were diluted and added in triplicate to wells. The reaction was initiated with the addition of 40 µl of lipase to every well and incubation at 37 °C for one hour in darkness. Fluorescence was masured by adding 50 µl of detection solution (containing the ADHP, G3P oxidase and horseradish peroxidase) to each reaction and incubated for 30 minutes at room temperature and protected from light. Reaction was measured by excitation wavelength of 530-540 nm and

an emission wavelength of 585-595 nm. Total PA concentration of the samples was calculated using a equation obtained from the linear regression of the standard curve (ranging from 0 to 125 µM PA). Cellular PA concentration was normalized to protein content of the sample and expressed as nmol PA/mg protein.

Generation of recombinant adenovirus

PPARγ2 and LacZ adenoviruses were generated with the ViraPower adenoviral expression system (Invitrogen). The coding sequence for PPARγ2 was amplified with Phusion high fidelity DNA polymerase (Finnzymes) starting from a mouse liver cDNA library. The PCR product of PPARγ2 was gel-purified and cloned into pENTR/D-TOPO vector (Invitrogen) following manufacturer's instructions. The orientation and the sequence of the inserted cDNAs were confirmed by restriction digestion and direct sequencing analysis. Recombinant adenoviral vectors were generated by Clonase II mediated recombination between PPARγ2-pENTR/D-TOPO or LacZ- pENTR/D-TOPO and pAd/CMV/V5-DEST vector (Invitrogen) following manufacturer's instructions. The resulting recombinant pAD/CMV/V5-DEST plasmids were analyzed by restriction digestion and direct sequencing. To generate recombinant adenoviral infecting particles, 1 µg of PacI digested PPARγ2-pAD/CMV/V5-DEST or LacZ-pAD/CMV/V5-DEST were transfected into 293A cells with FuGENE 6 reagent (Roche Diagnostics), according to the manufacturer's instructions. Transfected cells showed cytopathic signs of infection after 7 to 10 days. Infected cells were broken by 3 cycles of freezing and thawing and then centrifugated at 10,000 x g. Supernatants were used to propagate the adenovirus in 293A

cells. Finally, recombinant adenoviral particles were purified in CsCl gradients and quantified by OD at 260 nm. For infecting MEFs, 6 x 10^9 purified adenoviral particles were used for 60 mm dishes.

Indirect Immunofluorescence assays

For immunofluorescence staining of differentiated MEFs, cells were previously grown onto sterile glass coverslips and 2-days after they reach 100% confluence, adipogenic differentiation was induced as described above. At the indicated days, culture medium was aspirated and coverslips were washed twice with cold PBS, fixed for 30 minutes with 4% paraformaldehyde at room temperature, treated for 15 minutes with permeabilization buffer (0.3% Triton X-100, 3% BSA in PBS) and blocked with 3% BSA in PBS for 1 hour at room temperature. Next, primary antibodies (diluted in blocking buffer) were applied on each coverslip and incubated overnight at 4 °C in a humidified chamber. The following primary antibodies and concentrations were used: rabbit anti-Perilipin1 (1:200, Cell Signalling), goat anti-Seipin (1:100, Santa Cruz), rabbit anti-FABP4 (1:300, Cell Signalling), rabbit anti-ATGL (1:300, Cell Signalling), and rabbit anti-PPARγ (1:100, Cell Signalling). Coverslips were then washed three times in PBS and incubated with Alexa Fluor® 488, or 594, goat anti-rabbit IgG (H+L) and Alexa Fluor®488 donkey anti-goat IgG (H+L) (Molecular Probes). All the secondary antibodies were diluted 1:300 in blocking buffer and incubated for 1 hour at room temperature. F-actin was stained with rhodamine phalloidin (1:30 in PBS, Molecular Probes) for 30 minutes at room temperature. Finally, coverslips were washed, soaked on a fiber-free paper sheet and mounted on a slide

containing ProLong® Gold Antifade Reagent with 4′,6′-diamidino-2-phenylindole (DAPI) (Molecular Probes). The edges were sealed with regular transparent nail polish and dried up for 3 minutes. Images were visualized and captured with Nikon Eclipse C2si Confocal Spectral Imaging System (Nikon Inc., Tokyo, Japan)

For Perilipin-1 and Mac2 immunofluorescence staining in BAT and WAT sections, samples were previously embedded in paraffin following standard methods and cut into 5 µm sections. Slices were deparaffinized with xylene and rehydrated by graded ethanol. Antigen unmasking was carried out by heating slices in 10 mM sodium citrate buffer (pH 6.0) at 95–99°C for 10 minutes. Slices were cooled down to room temperature for 20 minutes and rinsed with H_2O and PBS. For PREF-1 detection, transverse sections of thoracic region of OCT-embedded whole embryos and newborn mice were used. All samples were blocked with 5 % goat serum in PBS-T for 1 hour and incubated overnight at 4 °C. Primary antibodies were diluted in blocking buffer as indicated: rabbit anti-Perilipin-1 (1:200, Cell Signalling), rat anti-Mac2 (1:200, Cedarlane) and mouse anti-DLK/Pref1 (1:50, Abcam). For immunofluorescence detection, slices were incubated for 1 hour with diluted Alexa Fluor® 488 goat anti-rabbit IgG, Alexa Fluor® 594 goat anti-rat IgG or Alexa Fluor® 488 goat anti-mouse IgG (Molecular Probes). After, slices were rinsed with PBS-T and mounted with ProLong® Gold Antifade Reagent with 4′,6′-diamidino-2-phenylindole (DAPI) (Molecular Probes). Images were captured with a Leica SP5 Tandem Scanner Spectral 2-photon confocal microscope (Leica Microsystems, Inc., Buffalo Grove, IL). Optical sections were obtained by confocal scanning microscopy. Image processing was performed with Bitplane Imaris software v. 7.3.1 (Andor Technology PLC, Belfast, N. Ireland).

Histological analysis

For microscopic anatomy analysis of interscapular BAT (iBAT), WAT and skin of *Agpat2*$^{-/-}$ and *Agpat2*$^{+/+}$ mice, interscapular region was surgically excised from the upper back of E18.5, P0.5, P2.5, P4.5 and P6.5 animals and fixed in 4% PFA/PBS. All tissues were embedded in paraffin, cut into 5 µm sections, mounted on positively charged glass slides (Superfrost Plus, Fisher Scientific, Pittsburgh, PA), and stained with hematoxylin and eosin (HE) for histopathologic examination using standard procedures.

Terminal deoxynucleotidyl transferase dUTP nick end labeling (TUNEL) staining.

For detection of apoptotic cells, TUNEL staining was performed according to manufacturer's recommendations. Briefly, 5 µm tissue sections were fixed in 4% formaldehyde-PBS solution, washed in PBS and treated with proteinase K (20 µg/ml). Next, slices were rinsed by immersion in PBS and treated with 100 µl equilibration buffer. Finally, slices were washed and incubated with 50 µl of TUNEL reaction solution (45 µl equilibration buffer, 5 µl nucleotide mix, 1 µl rTdT enzyme) for 1 hour at 37°C. The reaction was stopped by adding saline-sodium citrate buffer. Nuclei were couterstained with 1 µg/ml propidium iodide and rinsed in PBS for 5 minutes. Images were captured with a Leica SP5 Tandem Scanner Spectral 2-photon confocal microscope (Leica Microsystems, Inc., Buffalo Grove, IL).

Cell proliferation assay.

MEFs proliferation after adipogenic induction was evaluated with Click-iT® EdU Flow Cytometry Assay (Molecular Probes). EdU (5-ethynul-2'-deoxyurudine) is a thymidine nucleoside analog that is incorporated in the DNA during DNA synthesis. Detection system is based on a click reaction that consists in a copper catalyzed covalent reaction between an azide and an alkali. In this assay, Edu contains an alkyne group, while the fluorescent dye contains a reactive azide. For this experiment, two-days 100% confluent cultured MEFs were induced to differentiate as described in section 3.3 and 10 µM EdU were simultaneously added to the culture medium. MEFs were harvested in 1% BSA in PBS at 0, 6, 12 and 24 hours post-induction and immediately fixed with 100 µl of Click-iT® fixative solution for 15 minutes at room temperature. Cells were then washed and permeabilized with 100 µl of 1X Saponin buffer by 30 min. For detecting incorporated EdU, each sample was incubated by 30 minutes with 500 µl of Click-iT® reaction cocktail containing Alexa Fluor 488 azide and $CuSO_4$. After two washing steps with PBS, cells were stained with Hoechst 33342 for 30 minutes and immediately analyzed in a FACSAria III flow cytometer (Becton Dickinson).

Flow cytometry cell cycle analysis.

Cell cycle progression was quantified by flow cytometry after propidium iodide (PI) staining. MEFs were harvested at different times after adipogenic induction, washed once with cold PBS supplemented with 5 mM EDTA and fixed in ice-cold 70% ethanol upon gentle vortexing to avoid cell clumping. Cells were stored at -20 °C for 12 hours. Next, cell

were washed twice with cold 0.1% Tween 20/PBS, centrifugated at 400 x g for 6 minutes at 4 °C, resuspended in 500 µl of freshly made PI solution (0.1% v/v Triton X-100, 50 µg/ml PI, 50 µg/ml RNase A) and transferred to 12 x 75 mm polystyrene tubes. After incubation at room temperature for 30 minutes, cell suspensions were immediately analyzed on a BD FACScan flow cytometer and CellQuest software. PI fluorescence was evaluated on a linear scale and pulse width analysis was used to excluded cell doublets and aggregates from the analysis. The number of cells in each region of the cell cycle was expressed as a percentage of the total number of cells present.

Statistical analysis.

GraphPad Prism 5.00 (GraphPad, La Jolla, CA) was used for plotting and statistical analyses. Unpaired, two-sided Student's t test was used to detect statistical significance of the differences observed in two-group experiments. One-way ANOVA was used to compare three or more groups in some experiments. P values of 0.05(*), 0.01(**), and 0.001(***) were considered to assign statistical significance to the observed differences.

4. RESULTS

4.1 Cultured *Agpat2*$^{-/-}$ mouse embryonic fibroblasts (MEFs) have impaired adipogenesis.

4.1.1 Induction of adipogenic differentiation of Agpat2$^{-/-}$ MEFs results in fewer neutral lipid-loaded cells, lower expression of adipocyte gene markers and smaller lipids droplets.

To determine whether AGPAT2 influence adipogenesis, we first studied the ability of *Agpat2*$^{-/-}$ MEFs to differentiate into adipocyte-like cells. For this, we prepared MEFs from 13.5 d.p.c. *Agpat2*$^{+/+}$ and *Agapt2*$^{-/-}$ embryos. All experiments were performed at passage 3 and no differences in the cell morphology and growth were detected between *Agpat2*$^{+/+}$ and *Agpat2*$^{-/-}$ before adipogenic induction (data not shown). To evaluate that MEFs from both genotypes had equivalent cellular composition and that eventual differences in their adipogenic response do not depend on heterogeneous content of mesenchimal precursors, the expression of mesenchimal cell surface markers was analyzed by flow citometry. As shown in **Figure 13**, both *Agpat2*$^{+/+}$ and *Agpat2*$^{-/-}$ MEFs have high levels of Sca1, CD29 and CD44 proteins and largely lack CD45 and CD11b, confirming that MEFs of both genotypes exhibit comparable mesenchymal phenotype.

Two days after confluency (day 0), MEFs were induced to differentiate into adipocyte-like cells by incubation with adipogenic induction medium containing 0.5 mM IBMX, 1 µM dexamethasone, 10 µg/ml insulin. Three days later, induction medium was replaced by fresh medium containing 10 µM rosiglitazone and 10 µg/ml insulin. After day 5, culture medium was replaced every 2 days with complete medium supplemented only

with 10 µg/mL insulin **(Figure 14A)**. The progression of adipogenic differentiation was monitored by contrast phase microscopy and terminal adipocyte differentiation was evaluated at day 15 post-induction. As revealed by Oil Red O staining and immunofluorescent analysis of perilipin-1 protein **(Figure 14B)** adipogenic induction of *Agpat2*$^{+/+}$ MEFs resulted in a robust accumulation of neutral lipids in large perilipin-1 coated LDs. In sharp contrast, adipogenic induction of *Agpat2*$^{-/-}$ MEFs resulted in significantly fewer lipid-loaded cells (~20%) when compared with *Agpat2*$^{+/+}$ cells **(Figure 14C)**. Furthermore, the adipocyte-like cells that arose from induced *Agapt2*$^{-/-}$ MEFs were smaller than those found in *Agpat2*$^{+/+}$ cultures and had more numerous and smaller LDs **(Figure 14B)**. Notably, while perilipin-1 was detected surrounding these small lipid droplets in induced *Agpat2*$^{-/-}$ MEFs, it was also frequently found in multiple lipid-free aggregates **(Figure 14B)**. In agreement with Oil red O accumulation, biochemical determination of total triglycerides (TGs) revealed that adipogenic induction of cultured *Agpat2*$^{-/-}$ MEFs resulted in lower total TGs build up in comparison with differentiated *Agpat2*$^{+/+}$ cells **(Figure 14D)**.

As mentioned before (section 1.3), AGPAT2 converts LPA to PA in the glycerolipid synthesis pathway **(Figure 11).** Therefore, to evaluate if AGPAT2 deletion results in abnormal content of these lipid molecules, we biochemically determined the concentration of total PA in adipogenically induced MEFs. Unexpectedly, differentiated *Agpat2*$^{-/-}$ MEFs had higher content of total PA (PA+LPA) than *Agpat2*$^{+/+}$ cells at day 15 **(Figure 14E)**, indicating that these phospholipid species are quantitatively abnormal in absence of AGPAT2.

To determine the specificity of these findings, we compared the adipogenic defects of *Agpat2*$^{-/-}$ MEFs with those of another murine model of congenital generalized lipodistrophy, the aP2-SREBP-1c transgenic mouse (aP2-1c Tg). In these, the lipogenic transcription factor SREBP-1c is forcedly expressed in the AT under the transcriptional control of aP2 promoter and, by unknown mechanisms, this results in severe lipodystrophy. As shown in the **Figure 14F**, aP2-1c Tg MEFs undergo normal differentiaton after adipogenic induction, in marked contrast with *Agpat2*$^{-/-}$ MEFs. This suggests that lipodistrophy in the aP2-1c Tg mice is likely caused by deffects downstream adipogenesis, whereas in *Agpat2*$^{-/-}$ mice it results from a faulty adipogenic differentiation itself.

To complement the characterization of differentiating *Agpat2*$^{-/-}$ MEFs, we evaluated the expression of adipocyte-specific markers at mRNA and protein level. As shown in **Figure 15**, differentiated cultures of *Agpat2*$^{-/-}$ MEFs also showed decreased mRNA levels of all adipocyte-specific markers tested at day 15 post-adipogenic induction. However, since total number of cells undergoing adipocyte differentiation was significantly lower in *Agpat2*$^{-/-}$ compared with *Agpat2*$^{+/+}$ MEFs **(Figure 14C)**, the reduced levels of adipocyte markers could be the mere result of a lower proportion of differentiating cells in *Agpat2*$^{-/-}$ cultures. To evaluate this possibility, confocal immunofluorescence analysis of individual cells was performed. Interestingly, confocal quantification of fluorescence intensity revealed that adipogenically induced *Agpat2*$^{-/-}$ MEFs have equivalent or even higher levels of classic adipocyte markers in comparison to *Agpat2*$^{+/+}$ cells **(Figure 16)**. In fact, FABP4 levels in LDs-containing *Agpat2*$^{-/-}$ MEFs were ~5-fold higher than in LDs-containing *Agpat2*$^{+/+}$ cells at day 15 of adipogenic differentiation **(Figure 16A, Graph)**. Moreover, FABP4 subcellular distribution was largely different between MEFs of these two

genotypes. In *Agpat2*$^{+/+}$ cells, FABP4 protein was completely restricted to the cell´s periphery, whereas it was predominantly disseminated through the cell in differentiated *Agapt2*$^{-/-}$ MEFs **(Figure 16A)**. Similarly, ATGL, a lipolytic enzyme with abundant cytoplasmatic and LD localization, was observed at higher levels in differentiated *Agapt2*$^{-/-}$ cells with numerous intracellular, possibly cytoplasmic, aggregates **(Figure 16B)**.

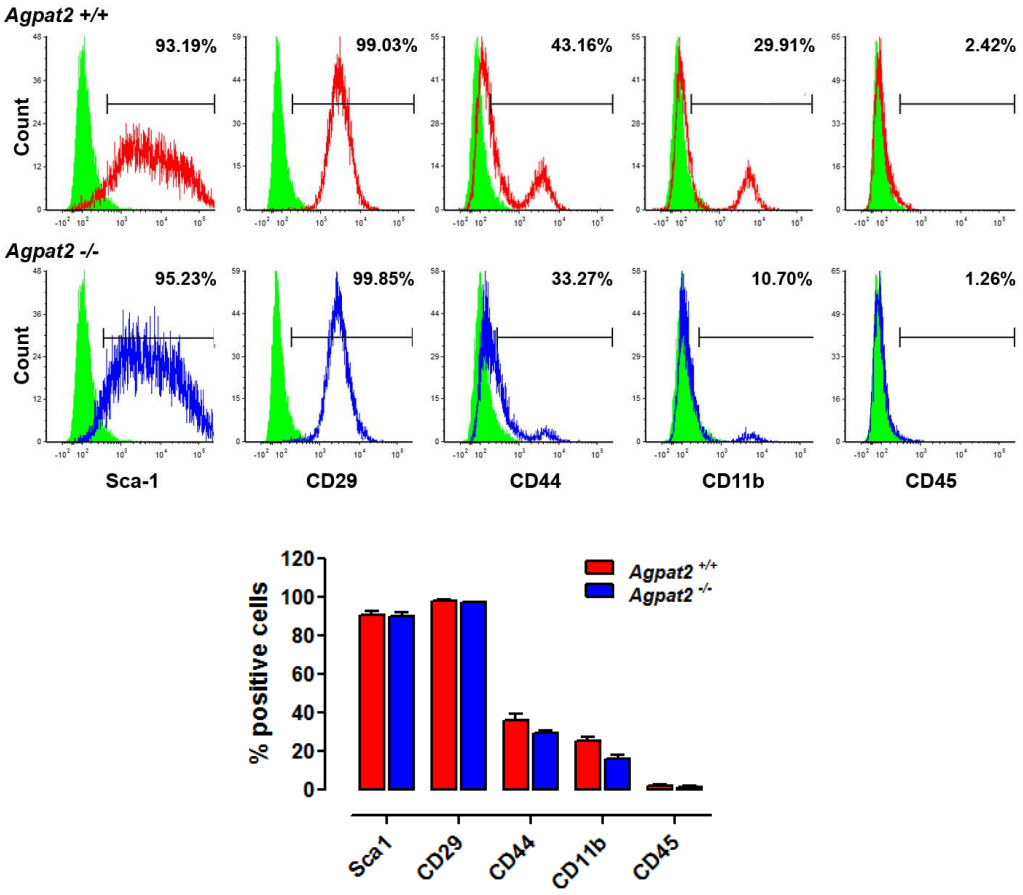

Figure 13: Mouse embryonic fibroblasts (MEFs) characterization. MEF were established by trypsin/EDTA digestion from E13.5 embryos carcasses. After 3 passages, MEF of both genotypes were harvested and stained with specific antibodies. FACS analysis (red and blue histograms) revealed that wild type and *Agpat2*$^{-/-}$ MEF harbored same surface markers characteristic of the mesenchymal stem cells: positive labeling for Sca-1, CD29, CD44 and CD11b, and negative for CD45 (Green histograms correspond to IgG Isotype controls).

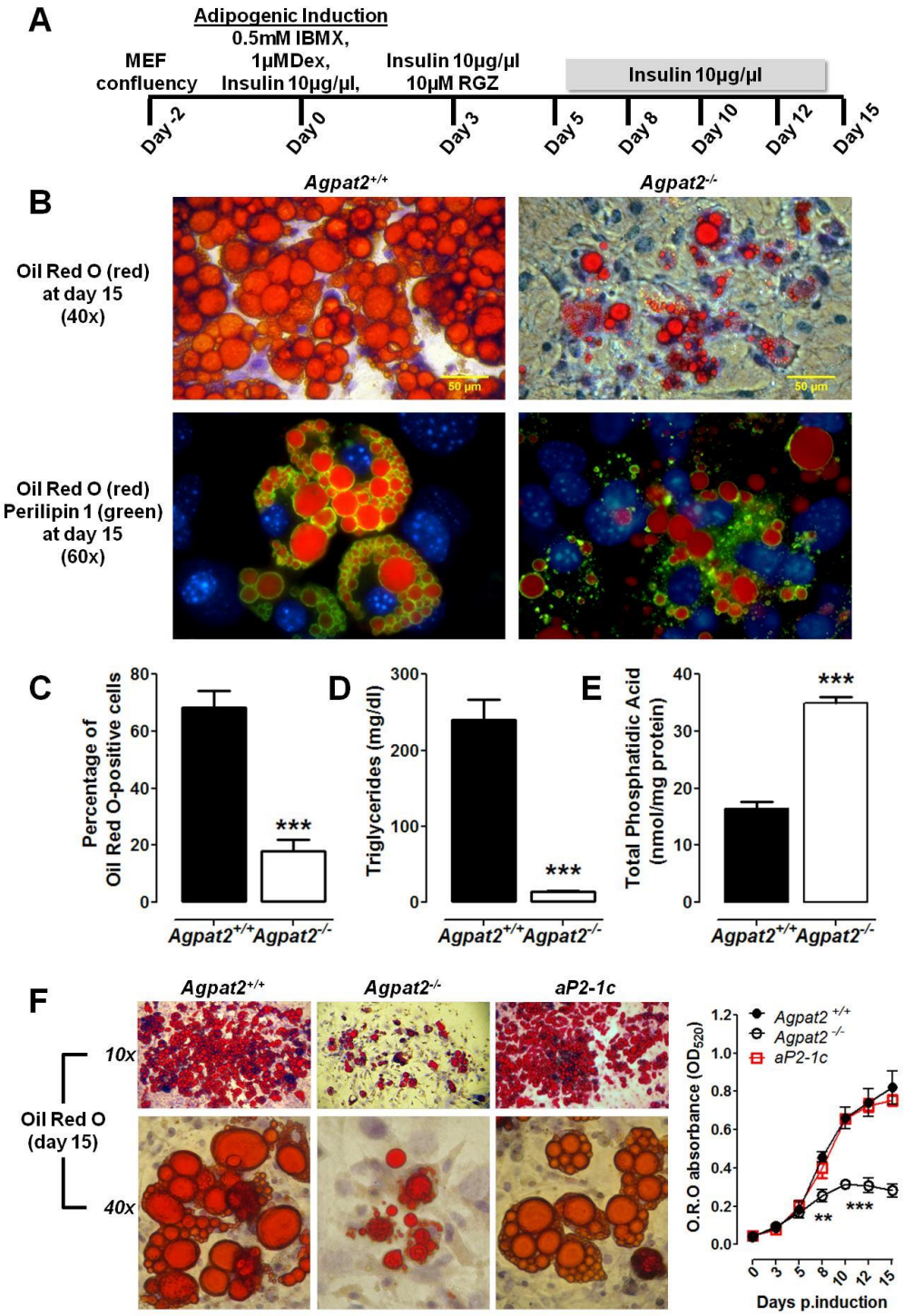
A
Adipogenic Induction
0.5mM IBMX,
1μMDex,
Insulin 10μg/μl,
MEF
confluency
Insulin 10μg/μl
10μM RGZ
Insulin 10μg/μl
Day -2
Day 0
Day 3
Day 5
Day 8
Day 10
Day 12
Day 15
B
Agpat2+/+
Agpat2-/-
Oil Red O (red)
at day 15
(40x)
50 μm
Oil Red O (red)
Perilipin 1 (green)
at day 15
(60x)
C
Percentage of
Oil Red O-positive cells
***
D
Triglycerides (mg/dl)
***
E
Total Phosphatidic Acid
(nmol/mg protein)
***
Agpat2+/+Agpat2-/-
F
Agpat2+/+
Agpat2-/-
aP2-1c
10x
40x
Oil Red O
(day 15)
O.R.O absorbance (OD520)
Agpat2 +/+
Agpat2 -/-
aP2-1c
**
***
Days p.induction

Figure 14. Adipogenic differentiation of *Agpat2*$^{-/-}$ MEFs results in significantly fewer and abnormal neutral lipids-laden cells with smaller LDs, lower total content of TGs and higher levels of PA after 15 days of differentiation. (A) Schematic time-line of the adipogenic differentiation protocol used on primary cultures of *Agpat2*$^{+/+}$ and *Agpat2*$^{-/-}$ MEFs. **(B, top panel)** Representative images (N > 6) from 15 days differentiated MEFs stained with the neutral lipid dye Oil red O (ORO) and hematoxylin, show a marked reduction of neutral lipid-loaded cells in *Agpat2*$^{-/-}$ cultures in comparison with wild-type controls. **(B, bottom panel)** Confocal analysis of Perilipin-1 (green) and LDs (red) shows lipid-free aggregates of Perilipin-1 as well as abnormal LD organization and size in the *Agpat2*$^{-/-}$ MEFs. Nuclei counterstained with DAPI (blue). **(C)** Graph shows the grade of adipogenic differentiation expressed as percentage of ORO and Perilipin-1 stained cells. **(D-E)** Graphs show total cellular triglycerides **(D)**, and total cellular PA+LPA concentrations **(E)** quantified by colorimetric and fluorimetric methods, respectively. **(F)** MEFs from aP2-SREBP-1c transgenic mice (aP2-1c) were prepared and differentiated to adipocytes, in parallel with wild-type and *Agpat2*$^{-/-}$ MEFs. After 15 days of differentiation, plates were stained with ORO such as in B. ORO was extracted with isopropanol at different time-points of the differentiation protocol and the amount of lipid accumulation was quantified by optical absorbance (560 nm). Data shown are to means ± standard deviations of three independent experiments with N>6. ***($p<0.001$) and **($p<0.01$) denote significant difference compared to differentiated *Agpat2*$^{+/+}$ MEFs.

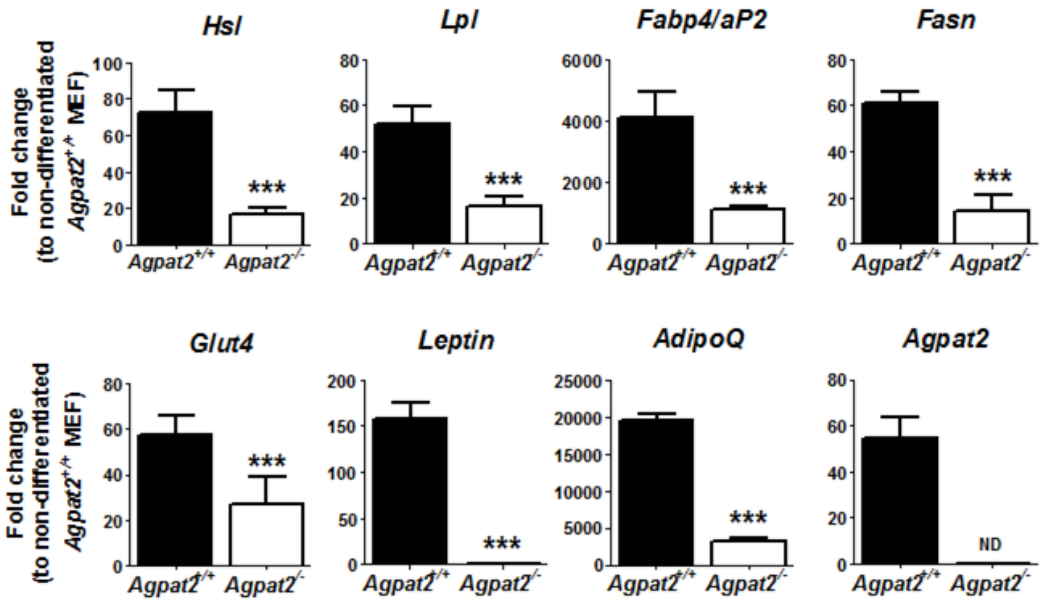

Figure 15. Decreased total expression of adipocyte-specific mRNAs in *Agpat2*$^{-/-}$ MEFs after 15 days of adipogenic differentiation. mRNA levels of hormone sensitive lipase (Hsl), Lipoprotein lipase (Lpl), fatty acid binding protein 4 (Fabp4, also called aP2), fatty acid synthase (Fasn), glucose transporter-4 (GLUT4), diacylglycerol acyltransferase-1 (DGAT1), Leptin, Adiponectin (AdipoQ) and 1-acylglycerol-3-phosphate O-acyltransferase 2 (Agpat2) were quantified by qPCR. Gene expression was normalized to Cyclophilin levels and presented as fold-change relative to non-differentiated *Agpat2*$^{+/+}$ MEFs. Data correspond to the means ± standard deviations of three independent experiments (N>6). ***($p<0.001$) and **($p<0.01$) denote statistically significant difference compared to differentiated *Agpat2*$^{+/+}$ MEFs after 15 days of differentiation. ND = transcript not detected.

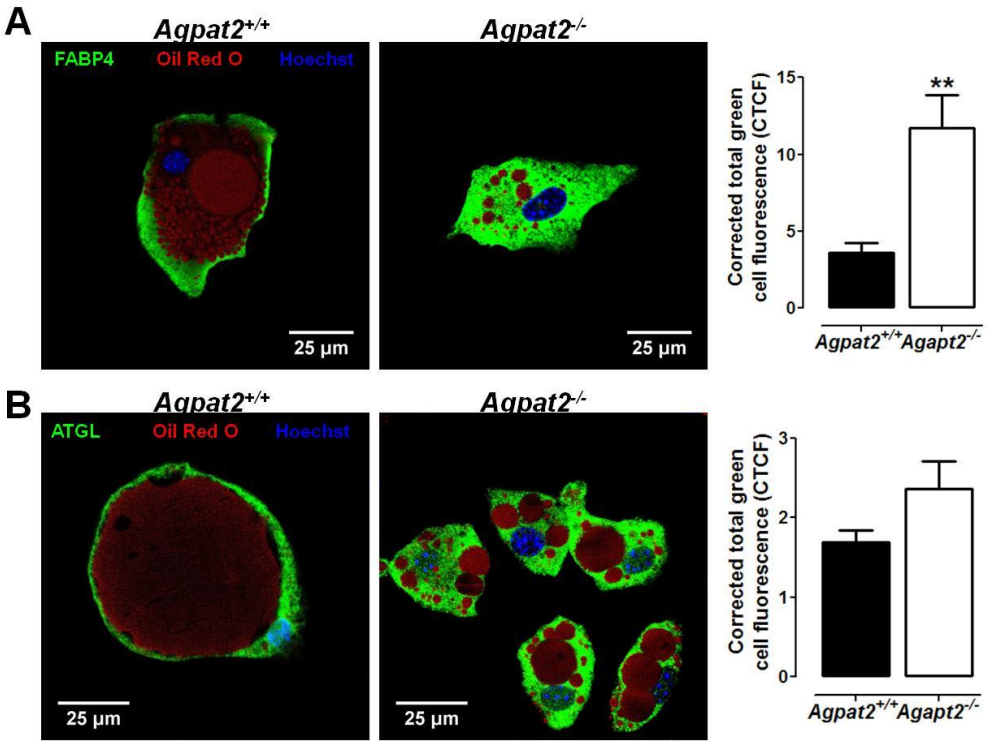

Figure 16. Abnormalities in intracellular distribution of several mature adipocyte-specific proteins are observed upon adipogenic differentiation in *Agpat2*$^{-/-}$ MEFs. The cellular expression of the endogenous FABP4 **(A)**, ATGL **(B)** was determined by indirect immunofluorescence (green) and confocal analysis. LDs were visualized with Oil-Red-O (ORO) staining. Nuclei were counterstained with DAPI. Merged images are shown on panels. Bar graphs on the left show the corrected total cell fluorescence (CTFC) of the corresponding protein levels in single cells (N = 20 for each group) in three independent experiments. **($p<0.01$) denote statistically significant difference.

4.1.2 Smaller LDs in differentiated *Agpat2*$^{-/-}$ MEFs are associated with abnormal expression of LD-related proteins.

The abnormal LDs morphology in differentiating *Agapt2*$^{-/-}$ MEFs, led us to investigate if this phenotype is the result of a decreased or aberrant expression of LD-associated proteins. As shown in **Figure 17A**, at day 15 post adipogenic induction, differentiating *Agpat2*$^{-/-}$ MEFs had numerous smaller LDs and this correlated with lower mRNA levels of LD-coating proteins Perilipin-1, CIDEA, CIDEC and DGAT2 in total differentiated cultures of these cells **(Figure 17B)**. Also, mRNA levels of Seipin, an ER-protein necessary for LD formation and mutated in cases of congenital generalized lipodystrophy type II (CGL-2), were significantly lower in *Agapt2*$^{-/-}$ MEFs **(Figure 17C)**.

Immunofluorescence double staining of Seipin and Perilipin-1 in single cells revelead that Perilipin-1 protein was, indeed, not reduced in lipid loaded *Agpat2*$^{-/-}$ cells **(Figure 18)**, but it showed a frankly aberrant intracelullar distribution. In fact, the strongest fluorescence signal was consistently associated with intracellular lipid-free aggregates that were diffusely and unevenly distributed inside *Agpat2*$^{-/-}$ cells **(Figure 18, arrows)**. This observation was similar for ATGL protein. Seipin was distributed at the endoplasmic reticulum (ER) and also co-localized with Perilipin-1 at ER-LD junctions in differentiated *Agpat2*$^{+/+}$ MEFs **(Fig. 18, arrowheads)**. In contrast, Seipin was completely undetected in *Agpat2*$^{-/-}$ lipid-loaded cells **(Figure 18, right panel).**

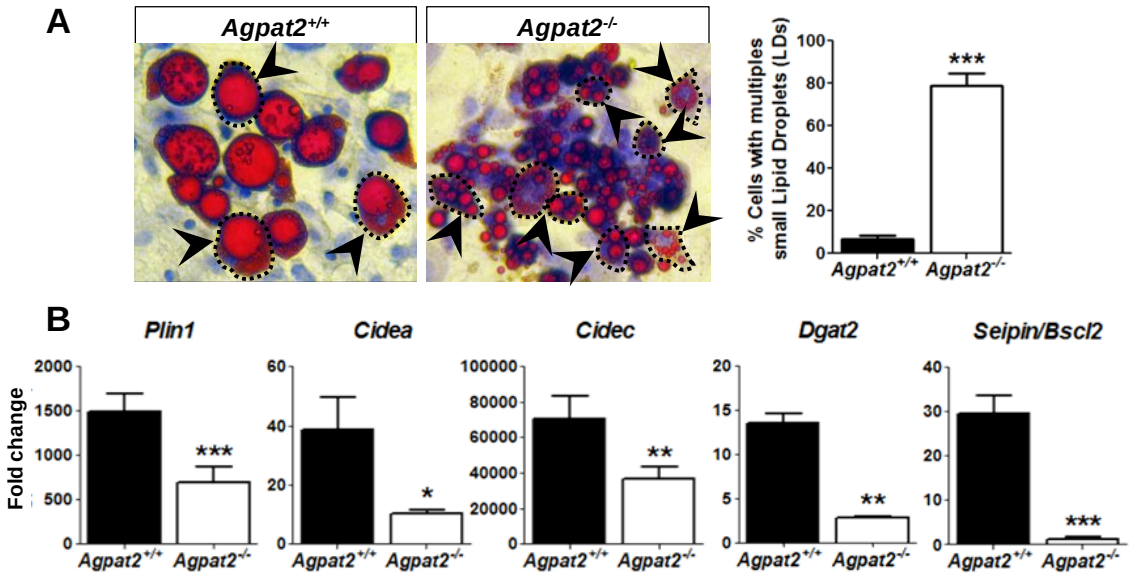

Figure 17: Differentiated *Agpat2*$^{-/-}$ MEFs show abnormalities in the number, size and LD-specific proteins at day 15 of adipocyte differentiation. (A) Representative images (N>6) from 15 days differentiated MEFs stained with Oil-red-O (ORO) and hematoxylin. Black arrowheads and dot lines indicate individual lipid-loaded cells. Graph on the left side represent the percentage of lipid-loaded cells with multiples LDs between 10 – 25 µm of diameter. **(B)** mRNA levels of LDs-specific markers and Seipin were quantified by qPCR. The bars show the means ± standard deviations of three independent experiments (N>6). ***($p<0.001$), **($p<0.01$) and *($p<0.05$) denote significant difference compared to differentiated *Agpat2*$^{+/+}$ MEFs after 15 days of differentiation.

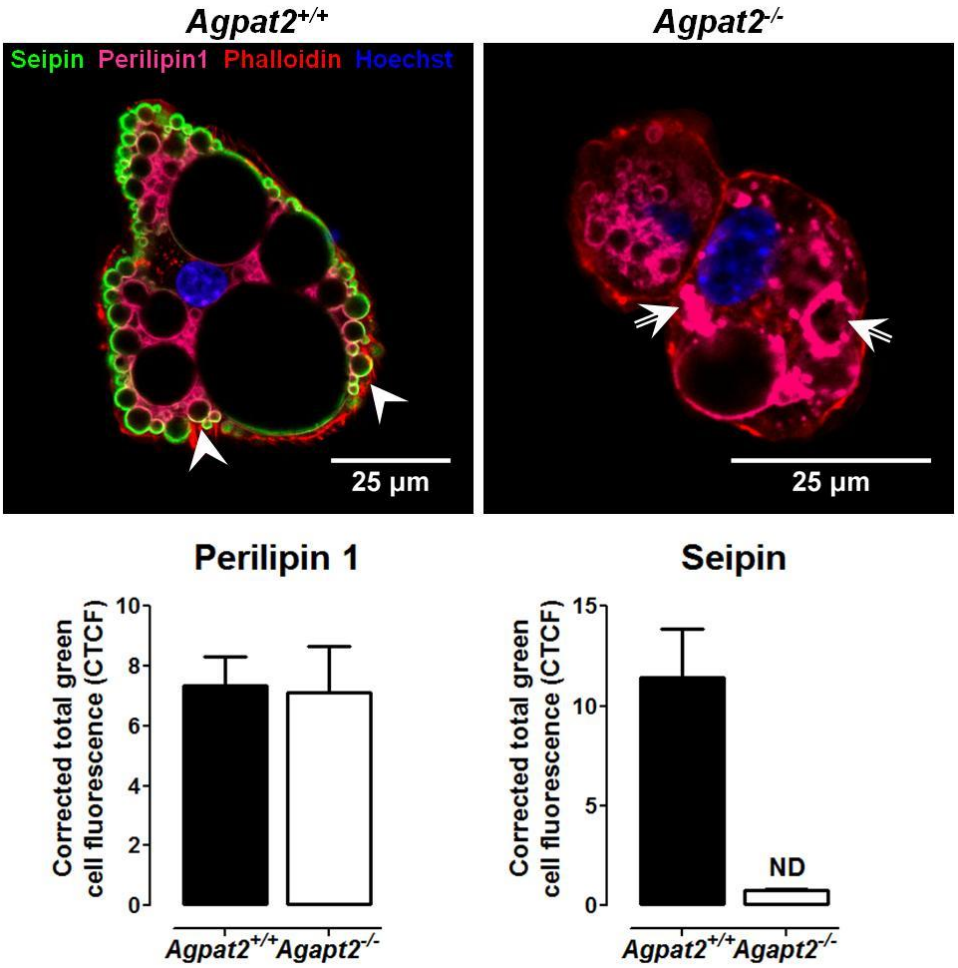

Figure 18: Confocal laser scan microscopy analysis of Perilipin-1 and Seipin co-expression in differentiated cultures of wild-type and *Agpat2*$^{-/-}$ MEFs. Representative images of double Perilipin-1 and Seipin immunostaining show Perilipin-1 (magenta color) localized on LDs and Seipin (green color) mostly distributed at cell's periphery in adipogenically differentiated wild-type MEFs. Colocalization between Seipin and Perilipin-1 was observed at ER-LD junctions in wild-type cells (yellow merge, arrowhead). In contrast, in lipid-loaded *Agpat2*$^{-/-}$ MEFs Perilipin-1 (arrow) has an abnormal distribution and Seipin was completely undetected. Bar graphs represent the corrected total cell fluorescence (CTFC) of Seipin and Perilipin in single differentiated lipid loaded-cells (N>6).

To determine whether LD abnormalities are detectable at early stages of the LD-biogenesis, we monitored LDs' size as well as the mRNA levels of Perilipin-1 and Seipin at different times after adipogenic induction. Light microscopy revealed discernible LDs since day 5 after induction **(Figure 19A)**. At this time point, both *Agpat2*$^{+/+}$ and *Agpat2*$^{-/-}$ MEFs began to acquire spheroid morphology and numerous small LDs with very tight size frequency distribution. Quantitative analysis of the LD diameters showed a distribution from 2 to 10 µm (mode 5 µm), in both genotypes **(Figure 19A, histogram)**, but cellular diameter was remain smaller in *Agpat2*$^{-/-}$ compared with *Agapt2*$^{+/+}$ MEFs, and their LDs appeared qualitatevely less organized. On the following days, LDs in *Agpat2*$^{+/+}$ differentiating MEFs continuously grew in size and were uniformly distributed inside cells. In contrast, LDs in *Agpat2*$^{-/-}$ cells exhibited a wider range of size (2 – 20 µm, mode 10 µm) and had a scattered intracellular distribution **(Figure 19B)**. Finally, at day 15 of differentiation, *Agpat2*$^{+/+}$ lipid-loaded cells had one or two supersized-LD (up to ~ 30 µm in diameter), whereas *Agpat2*$^{-/-}$ cells showed numerous, much smaller and heterogenous LDs, with diameters ranging from 2 to 10 µm (mode 5 µm). In addition to this aberrant LD morphology and distribution, whole cell morphology was abnormal in *Agpat2*$^{-/-}$ differentiating MEFs, suggestive of cellular damage **(Figure 19C).**

Temporal course of Perilipin-1 and Seipin mRNA and protein levels along adipogenic differentiation was also different among MEFs of both genotypes **(Figure 20)**. In *Agpat2*$^{+/+}$ cells, Perilipin-1 and Seipin quickly and robustly increased after the second and third day of induction **(Figure 20A-B)**. In *Agpat2*$^{-/-}$ MEFs, Perilipin-1 mRNA and protein rise was significantly blunted at all time points. In fact, Perilipin-1 mRNA levels were progressively decreased after day 3 whereas Perilipin-1 protein did not increase beyond day 5 in *Agpat2*$^{-/-}$

MEFs. Likewise, Seipin mRNA concentration modestly increased after adipogenic induction in *Agpat2*$^{-/-}$ MEFs. After 3 days of differentation, it was only detectable at basal levels (Ct=27). Seipin protein remained virtually undetectable by western blotting **(Figure 20B)**.

Taken together, these results indicate that the lack of AGPAT2 adversely affects MEFs´s adipogenic differentiation, resulting in a reduced proportion of lipid-loaded cells, lower TGs build up, dysregulated levels of adipocyte-selective genes and proteins as well as abnormal LDs morphology and protein composition.

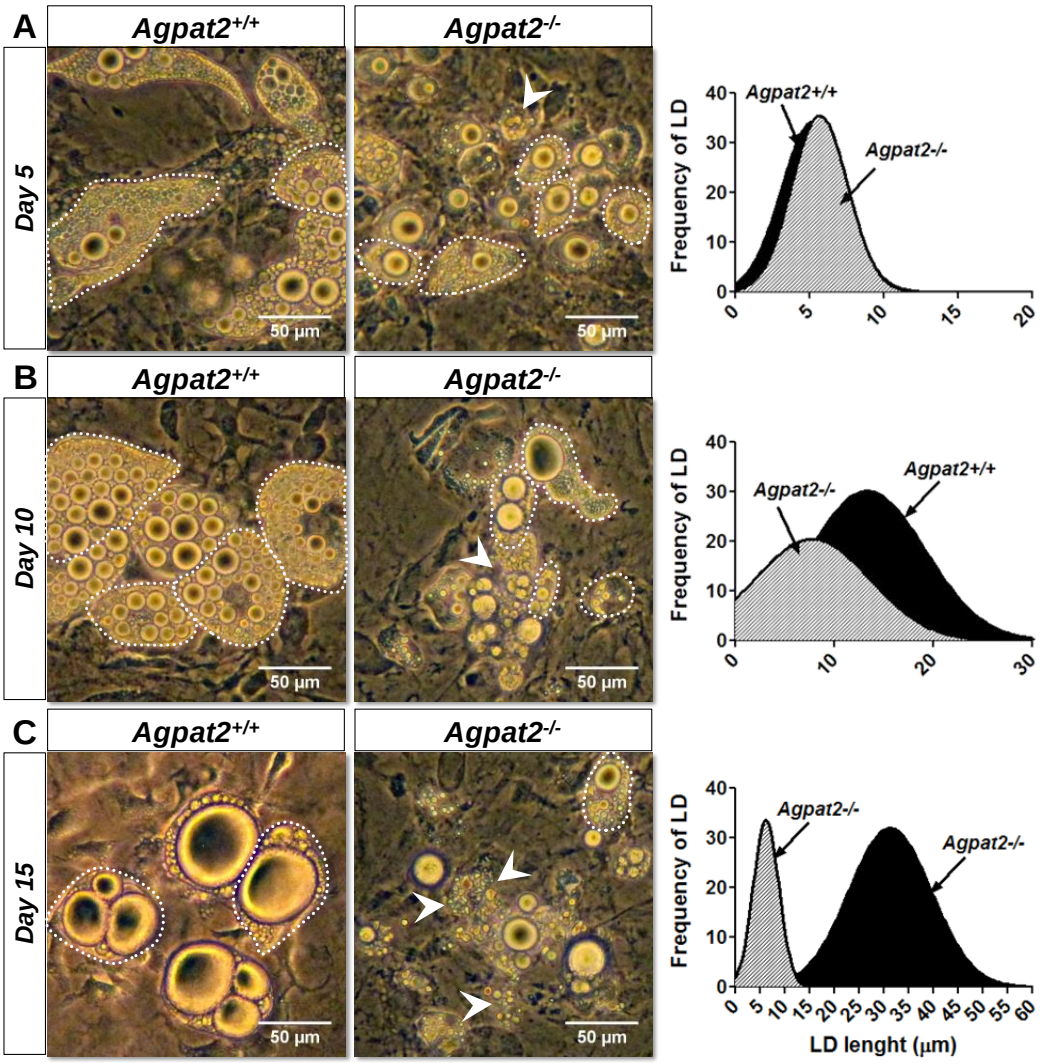

Figure 19: AGPAT2 is essential for normal LD morphology remodeling during adipogenic differentiation in MEFs. Primary *Agpat2*$^{+/+}$ and *Agpat2*$^{-/-}$ MEFs were induced for adipogenesis. At indicated time points (days 5, 10 and 15 post-adipogenic induction) cells were examined under light microscope equipped with relief contrast objectives and photographed to quantify changes in LDs morphology and size. Pictures show representative regions of differentiating cells with clearly visible intracellular LDs. Histograms show a quantitative analysis of LD number and size distribution at early **(A)**, intermediate **(B)** and late differentiation **(C).** A total of 100 cells were analyzed for each quantification.

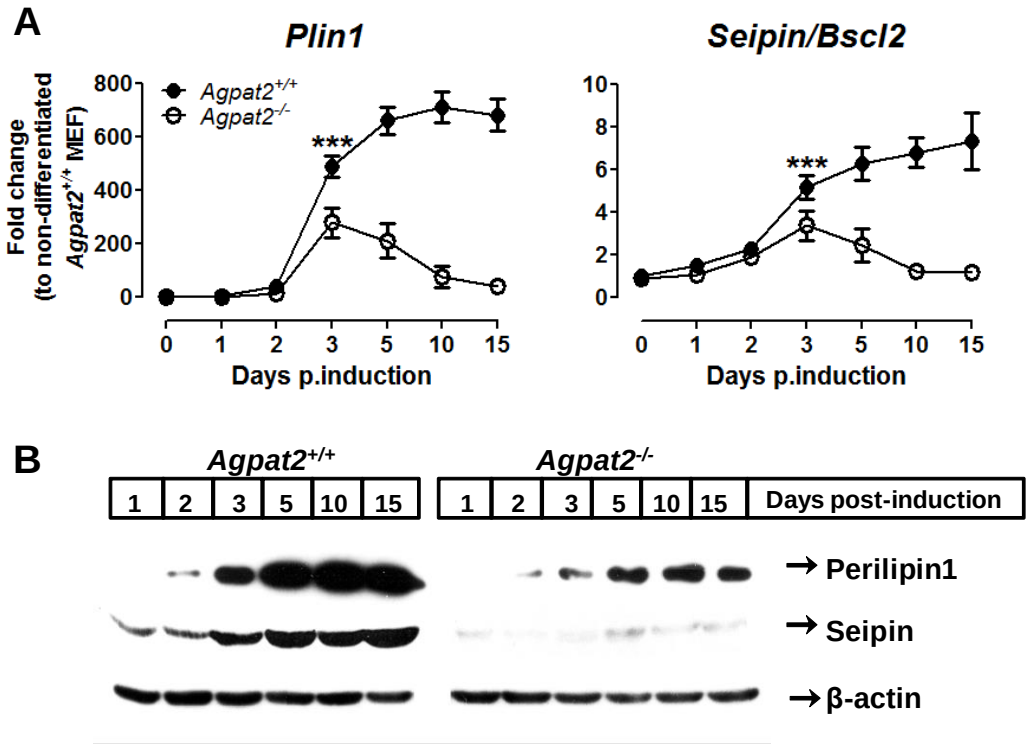

Figure 20: Analysis of Perilipin-1 and Seipin expression during adipocyte differentiation in MEFs. (A) Perilipin-1 (Plin1) and Seipin mRNAs were quantified by qPCR at different days after adipogenic induction. Data were normalized to cyclophilin A and expressed as relative fold changes to non-differentiated *Agpat2*$^{+/+}$ MEFs at day 0. **(B)** Representative western blots of Perilipin-1 and Seipin in *Agpat2*$^{+/+}$ and *Agpat2*$^{-/-}$ MEFs at different days of differentiation (N>3). Whole cell protein lysates (50 µg/well) were separated by SDS-PAGE, electrotransferred onto nitrocellulose membranes, and probed with specific antibodies for Perilipin-1 (~ 62 kDa) and Seipin (~ 45 kDa). β-actin (~45 kDa) was used as loading control. Error bars represent means ± standard deviation of three independent experiments (N > 6). ***($p<0.001$) denote statistically significant difference in comparison with differentiated *Agpat2*$^{+/+}$ MEFs.

4.1.3 Transcriptional regulation of adipogenesis is decreased in *Agpat2*$^{-/-}$MEFs.

To explore the mechanisms by which *Agpat2*$^{-/-}$ MEFs undergo impaired adipogenesis, we evaluated the temporal progression of transcription factors that normally regulate adipogenesis. As expected, adipogenic induction *Agpat2*$^{+/+}$ MEFs resulted in very early induction of C/EBP-β and –δ mRNA and protein levels (24 hours post-induction), followed by upregulation of C/EBPα and PPARγ mRNA and protein after day 2 **(Figure 21A-B)**. Interestingly, similar to observed for Perilipin-1, mRNA levels of adipogenic transcription factors (C/EBPs and PPARγ) were also induced in *Agpat2*$^{-/-}$ MEFs at early days of adipogenic differentiation; however, the extent of this increase was significantly blunted in comparison to *Agpat2*$^{+/+}$ MEFs. Furthermore, the concentration of these transcription factors was progressively and markedly decreased after 3 days of adipogenic differentiation **(Figure 21A)**. Immunoblot analysis showed that C/EBP–β and –δ were increased during the first two days of adipogenic differentiation in *Agpat2*$^{-/-}$ MEFs, but they were almost undetectable 3 days post-induction **(Figure 21B)**. C/EBPα and PPARγ protein levels were significantly reduced in *Agpat2*$^{-/-}$ MEFs.

Single cell confocal immunofluorescence analysis revealed that, in comparison with *Agpat2*$^{+/+}$ MEFs, nuclear PPARγ protein was not reduced in lipid-loaded *Agpat2*$^{-/-}$ cells at early stages of differentiation (day 5) but it was lower at later times (day 10) **(Figure 22B)**. These data indicate that only a low proportion of *Agpat2*$^{-/-}$ MEFs can induce the expression of PPARγ, and although the nuclear content of this transcription factor is normal at early stages, these cells fail to sustain PPARγ levels as adipogenic differentiation progresses. As an alternative posibility, PPARγ expressing *Agpat2*$^{-/-}$ MEFs may be lost (by cell death)

from the differentiating cell culture and, therefore, enrich the cell population with non-adipogenic cells.

To test the hypothesis that PPARγ deficiency underlie the adipogenic failure of *Agpat2*$^{-/-}$ MEFs, we proceeded to force PPARγ expression, by adenoviral-mediated transduction, in these cells.

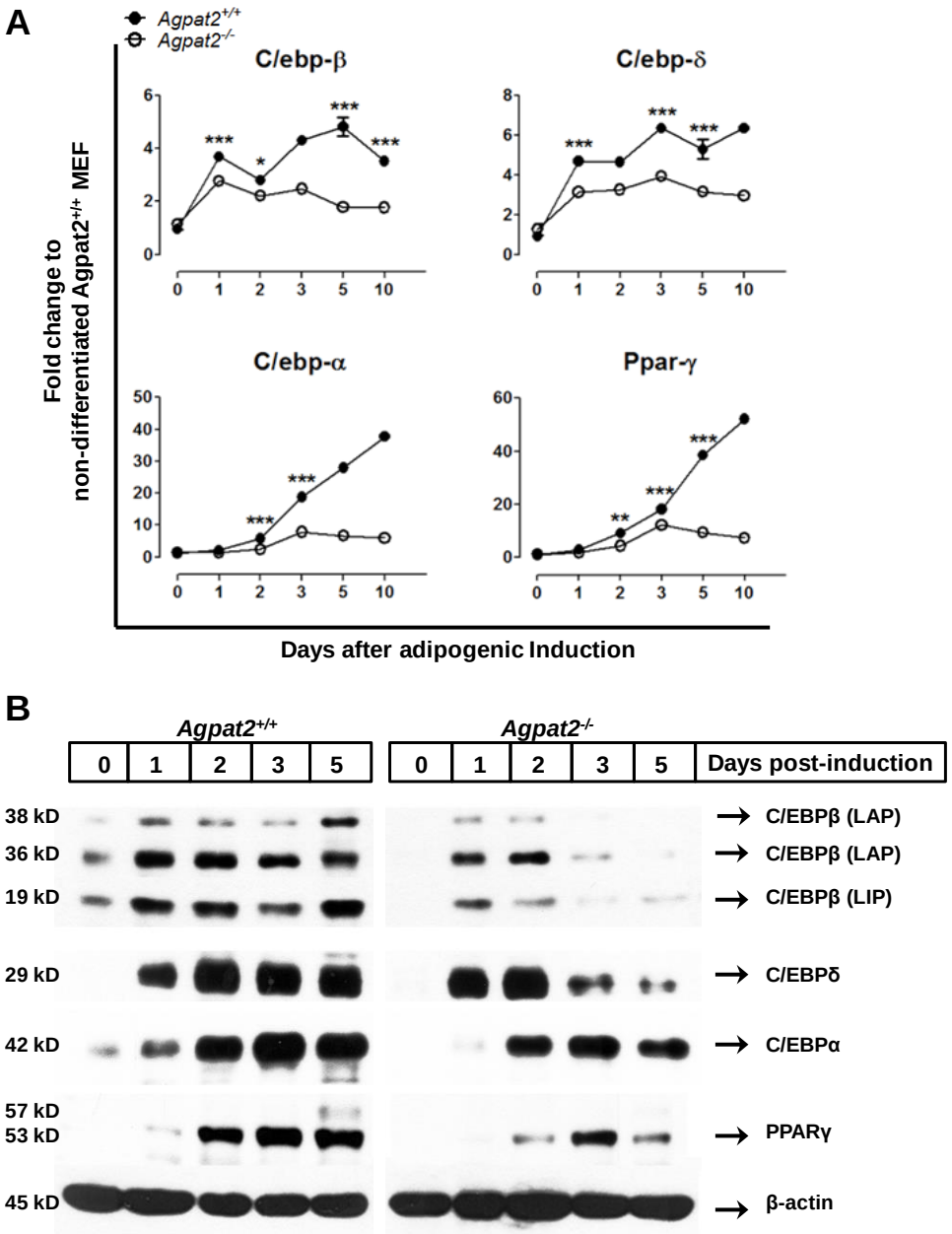

Figure 21. mRNA and protein levels of adipogenic transcriptional regulators are decreased in differentiating *Agpat2*$^{-/-}$ MEFs. (A) qPCR quantification of C/EBPs and PPARγ mRNA levels at early and late stages of adipogenic differentiation. Data were normalized to cyclophilin A and expressed as relative fold changes to non-differentiated *Agpat2*$^{+/+}$ MEFs at day 0. (B) Immunoblot analysis of whole-cell lysates from *Agpat2*$^{-/-}$ and *Agpat2*$^{+/+}$ MEFs at different days of differentiation. 50 µg of proteins were loaded, and β-actin was used as loading control. The data correspond to the mean ± standard deviation of three independent experiments (N>6). ***($p<0.001$), **($p<0.01$) and *($p<0.05$) denote significant difference compared to differentiated *Agpat2*$^{+/+}$ MEFs.

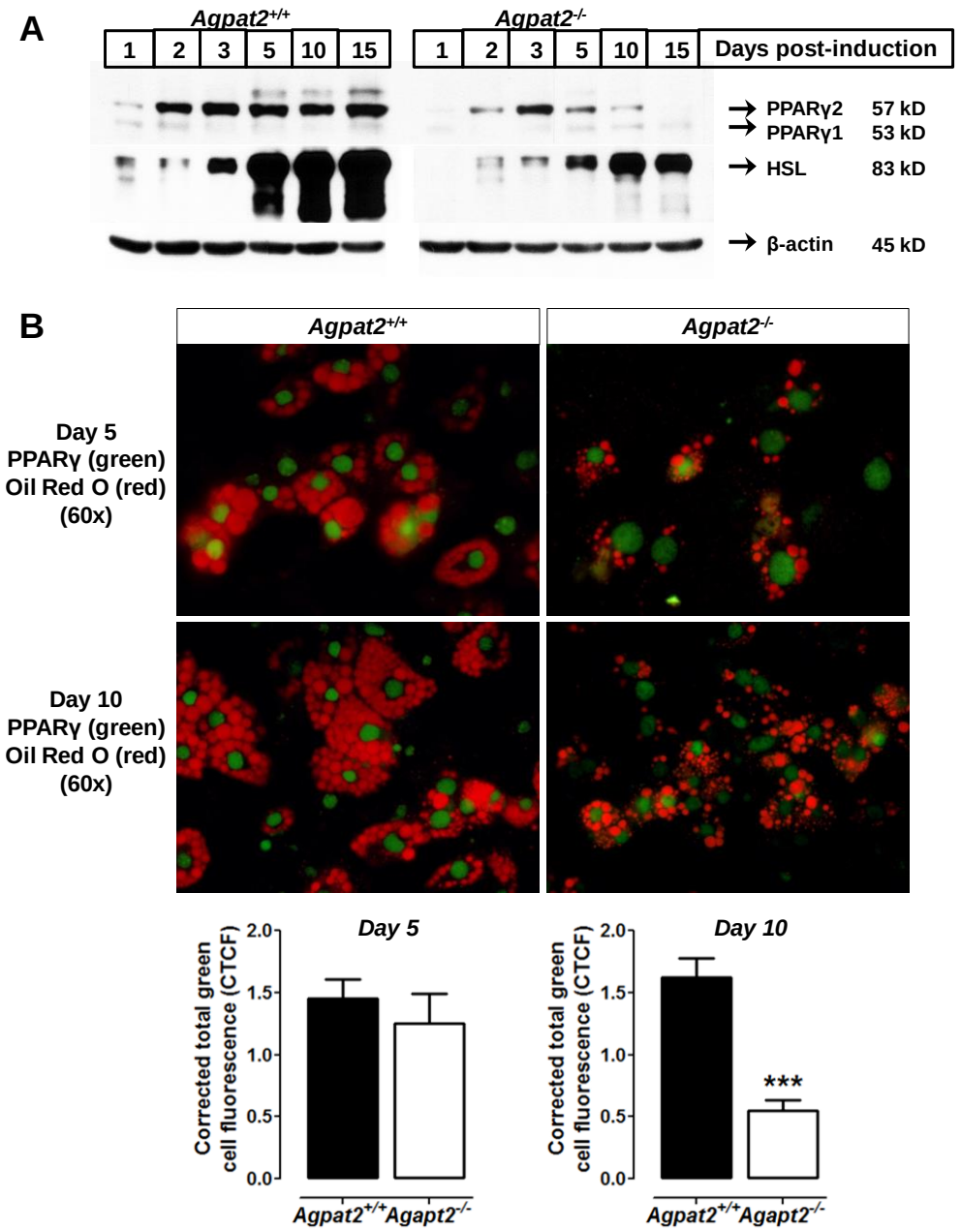

Figure 22: **Nuclear PPARγ is normal at early stages of adipogenic differentiation but is decreased at later times in differentiating *Agpat2*$^{-/-}$ MEFs**. (A) Representative western blot of PPARγ and HSL (hormone sensible lipase), whose gene expression is regulated by PPARγ, in *Agpat2*$^{+/+}$ and *Agpat2*$^{-/-}$ MEFs at different days of differentiation. (B) Confocal immunofluorescence analysis of PPARγ in *Agpat2*$^{+/+}$ and *Agpat2*$^{-/-}$ MEFs at two different stages of adipocyte differentiation. Green fluorescence shows PPARγ nuclear localization in differentiating lipid loaded cells. Lipid droplets were labeled with oil red O (red). Graphs show the corrected total cell fluorescence (CTFC) of PPARγ in each differentiated lipid loaded cell. ***$P < 0.001$. Error bars represent means ± SE, N>6.

4.1.4 Ectopic expression of PPARγ2 enhances adipocyte differentiation but does not amend the LD and cell morphology abnormalities in *Agpat2*$^{-/-}$ MEFs.

To test whether an insufficient mass of nuclear PPARγ underlies the adipogenic failure of *Agapt2*$^{-/-}$ MEFs, we forced the expression of PPARγ2 by adenoviral transduction **(Figure 23A)**. For this, we generated a recombinant adenovirus encoding mouse PPARγ2 under the transcriptional control of CMV promoter. The gene transduction efficiency of our adenoviral vector was tested in undifferentiated MEFs that were infected with growing adenoviral particles concentrations. After a period of 24 hours, the mRNA levels of PPARγ were quantified by qPCR. As shown in **Figure 23B**, adenoviral transduction with MOIs of 10, 25, 50, 100 and 200, proportionally increased PPARγ mRNA concentration in ~2.5, ~50, ~140, ~430 and ~830-fold, respectively. Next, using a MOI of 25, we tested PPARγ protein levels in transduced MEFs for up to 15 days after adenoviral infection. Western blot and inmunofluorescence analyses show that under these experimental conditions, PPARγ protein remained steady during the whole adipogenesis protocol in wild type MEFs **(Figure 23C-D)**.

To test the actions of PPARγ2 forced expression on the adipogenesis of *Agpat2*$^{-/-}$ MEFs, post-confluent *Agpat2*$^{-/-}$ MEFs were infected with PPARγ2 or LacZ encoding adenovirus 1 day before adipogenic induction. 24 hours later, transduced MEFs were induced with the usual adipogenic cocktail (see section of methods). As shown in **Figure 23E**, the over-expression of PPARγ2 in *Agpat2*$^{-/-}$ MEFs resulted in a significantly higher number of lipid loaded cells and an increased level of adipocyte-specific mRNAs at day 15 of differentitation **(Figure 23F, box with vertical lines)**. In contrast, the infection with the

adenovirus encoding LacZ, did not rescue the impaired differentiation induced by AGPAT2 deficiency. Nontheless, in spite of these effects, LDs in the differentiating *Agpat2*$^{-/-}$ MEFs remained smaller in comparison with those in wild type MEFs at day 15 of differentiation **(Figure 23G)**.

These results indicate that PPARγ forced-expression partially reverted adipogenic abnormalities in *Agpat2*$^{-/-}$ MEFs, allowing a larger lipid build up in a significantly higher proportion of cells. However, although many mature adipocyte markers were also relatively increased, full adipogenic differentiation was not reached and, more importantly, LDs remained qualitatively abnormal, with at least one crucial protein, Perilipin-1, remaining physically dissociated from them.

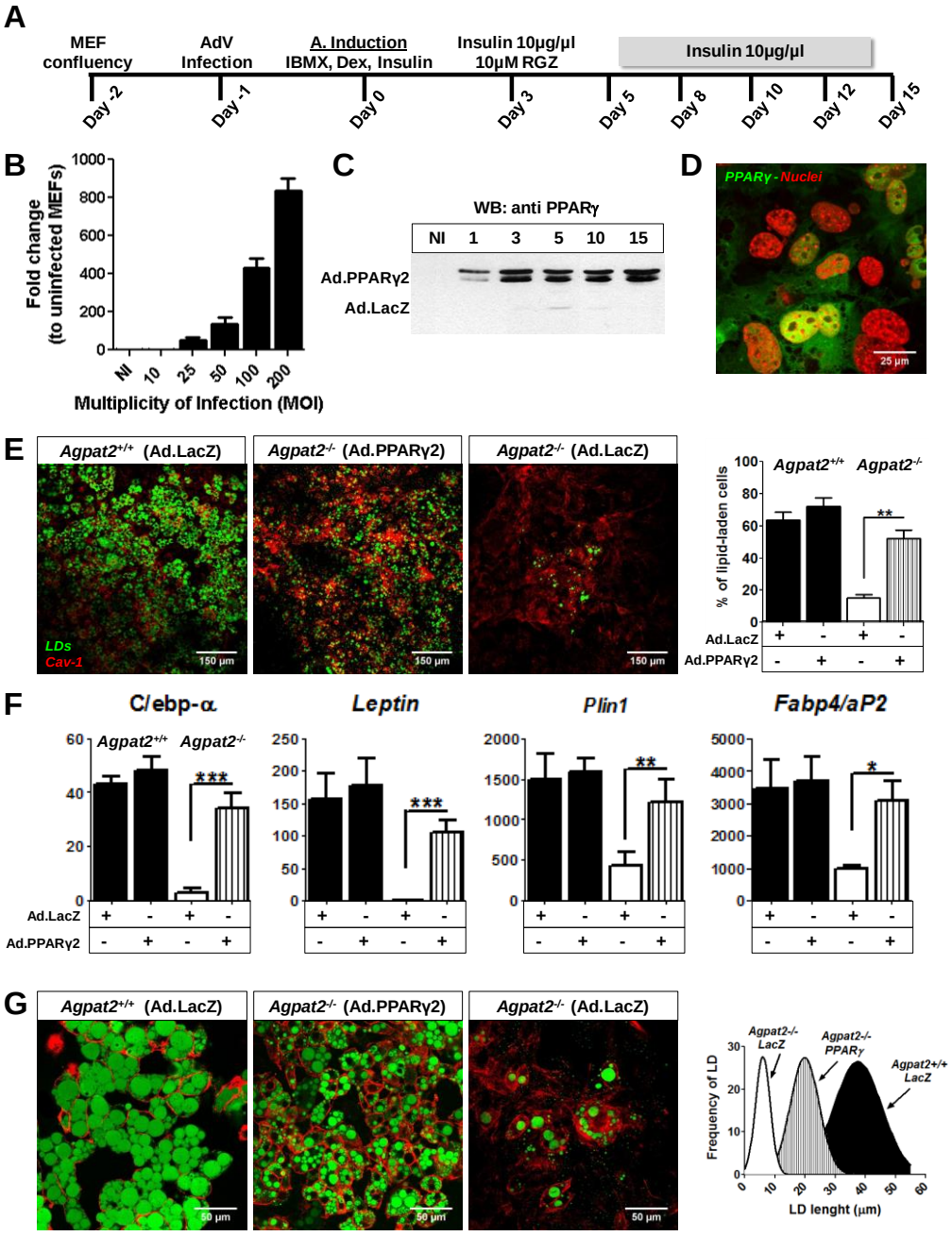
A
MEF confluency
AdV Infection
A. Induction
IBMX, Dex, Insulin
Insulin 10µg/µl
10µM RGZ
Insulin 10µg/µl
Day -2
Day -1
Day 0
Day 3
Day 5
Day 8
Day 10
Day 12
Day 15
B
Fold change (to uninfected MEFs)
Multiplicity of Infection (MOI)
NI
10
25
50
100
200
C
WB: anti PPARγ
NI 1 3 5 10 15
Ad.PPARγ2
Ad.LacZ
D
PPARγ - Nuclei
25 µm
E
Agpat2+/+ (Ad.LacZ)
Agpat2-/- (Ad.PPARγ2)
Agpat2-/- (Ad.LacZ)
LDs
Cav-1
150 µm
% of lipid-laden cells
Agpat2+/+
Agpat2-/-
Ad.LacZ
Ad.PPARγ2
F
C/ebp-α
Leptin
Plin1
Fabp4/aP2
Agpat2+/+
Agpat2-/-
Ad.LacZ
Ad.PPARγ2
G
Agpat2+/+ (Ad.LacZ)
Agpat2-/- (Ad.PPARγ2)
Agpat2-/- (Ad.LacZ)
50 µm
Frequency of LD
LD lenght (µm)
Agpat2-/- LacZ
Agpat2-/- PPARγ
Agpat2+/+ LacZ

Figure 23: Ectopic expression of PPARγ2 partially restores adipocyte differentiation in *Agpat2*$^{-/-}$ MEFs. (A) Schematic time-line shows adipogenic differentiation protocol used on primary cultures of *Agpat2*$^{+/+}$ and *Agpat2*$^{-/-}$ MEFs previously infected with recombinant adenovirus. **(B)** Graph shows infectivity of PPARγ2-AdV using different number of viral particles per cell (MOI=multiplicity of infection). **(C)** Western blot shows the adenoviral-mediated gene expression of PPARγ2 at longer times after infection with a MOI of 25. **(D)** 24h after infection, PPARγ expression was evaluated by immunofluorescence for PPARγ in post-confluent *Agpat2*$^{-/-}$ MEFs infected with PPARγ2-AdV. **(E)** One day before adipogenic induction, confluent MEFs were infected with either control adenovirus expressing LacZ or PPARγ2 and adipogenesis was induced 24 hours later. After 15 days of differentiation, cells were stained with Bodipy 493/503 to analyze the percentage of cells accumulating neutral lipids. Immunofluorescence detection of caveolin-1 was used to identify plasmatic membrane in lipid loaded-cells. Graphs show the percentage of adipogenic differentiation. **(F)** mRNA levels of C/EBPα, Leptin, Plin-1 and Fabp4 were quantified by qPCR. Gene expression was normalized to Cyclophilin and presented as fold-change to non-differentiated *Agpat2*$^{+/+}$ MEFs at day 0. **(G)** Confocal images show the size and morphology of LDs (Bodipy 493/503) on differentiating MEFs. Caveolin-1 is observed in red color. Histogram shows a quantitative analysis of LD number and LD size distribution in differentiated MEFs at day 15. Graphs show the mean ± standard deviations of two independent experiments with N=6. ***($p<0.001$), **($p<0.01$) and *($p<0.05$) denote significant difference compared to differentiated *Agpat2*$^{+/+}$ MEFs.

4.1.5 *Agpat2*$^{-/-}$ MEFs fail to complete the mitotic clonal expansion after adipogenic induction.

As shown in the above sections, impaired adipogenesis in *Agpat2*$^{-/-}$ MEFs is characterized by low abundance of PPARγ expressing cells and lipids-loaded cells. These effects are apparent as early as the second day after adipogenic induction, when MEFs are in a proliferative phase, known as mitotic clonal expansion (MCE) **(Figure 24A)**. Therefore, in order to test whether the low proportion of *Agpat2*$^{-/-}$ MEFs expressing PPARγ is the result of a defective MCE, we quantitatively analyzed the progression of post-confluent growth-arrested *Agpat2*$^{-/-}$ MEFs in the cell cycle after adipogenic induction **(Fig. 24-26)**. As expected, the number of *Agpat2*$^{+/+}$ MEFs significantly increased by ~2-fold within the first 24 hours after adipogenic induction, indicating that MCE starts at very early stages of in *in vitro* MEFs' adipogenesis. By contrast, adipogenic induction resulted in a significantly blunted increase in the cell number of *Agpat2*$^{-/-}$ MEFs 24 hours post-induction, followed by a net decline in the cell population **(Figure 24B)**. Cell-cycle progression markers CDK2, CDK4 and cyclin E1 were increased in both *Agpat2*$^{+/+}$ and *Agpat2*$^{-/-}$ MEFs during first hours of adipogenic induction; however, this elevation was lower in *Agpat2*$^{-/-}$ MEFs beyond 24-48 hrs post-induction. Phosphorylated Rb, which promotes adipose differentiation by controlling G1/S transition and increasing PPARγ levels, reached a maximum 12 hours after induction in *Agpat2*$^{+/+}$ MEFs, remaining at steady levels thereafter. By contrast, in *Agpat2*$^{-/-}$ MEFs phosphorylated Rb was progressively decreased and was undetectable at 24 hours after induction **(Figure 24C)**.

This suggests that *Agpat2*$^{-/-}$ MEFs have the ability to re-enter in the cell cycle after adipogenic induction but that they fail to complete the MCE. To test this latter hypothesis, we analyzed the cell cycle phases and cell proliferation rates by flow cytometry using propidium iodide (PI) and Click-iT EdU/Hoechst 33342 labeling respectively. DNA content analysis showed that equivalent proportion of *Agpat2*$^{+/+}$ and *Agpat2*$^{-/-}$ MEFs in G0/G1 (71 % vs. 72 %) and S (6 % vs. 7 %) phases at the begining of the adipogenic induction (0 hours) **(Figure 25B-C)**. 12 hours later, an equivalent fraction of cells reached the S and G2/M phases in both gentoypes. At the same time point, detection of DNA synthesis by EdU incorporation in proliferating cells showed a ~15% of replicanting cells during the S-phase of the cell cycle of both *Agpat2*$^{+/+}$ and *Agpat2*$^{-/-}$ MEFs, indicating that AGPAT2 deficiency does not block cell proliferation triggered by adipogenic induction **(Figure 26)**. 24 hours after adipogenic induction, we did not observe differences in the proportion of *Agpat2*$^{+/+}$ and *Agpat2*$^{-/-}$ MEFs in S-phase (17 % vs. 18 %) however, the porcentage of *Agpat2*$^{-/-}$ MEFs in G2/M phase was significantly lower (19.2 vs. 12.7 %, $p < 0.05$) and a growing fraction of DNA-synthesizing *Agpat2*$^{-/-}$ MEFs was switched toward a sub-G1 region 24 hours post-adipogenic induction. Notably, this subpopulation increased up to 34 % at 48 hours post-induction **(Figures 25)**.

These results suggest that *Agpat2*$^{-/-}$ MEFs suffer severe anomalies near to or upon completion of MCE, leading a subsequent cell death. Concordantly, western blot analysis of combined adherent and detached MEFs showed activation of caspase 3 in *Agpat2*$^{-/-}$ MEFs upon adipogenic induction **(Figure 27A)**. Furthermore, inmunofluorescence analysis showed abundant cleaved-active caspase-3 exclusively in *Agpat2*$^{-/-}$ MEFs after 24 hours of adipogenic differentiation **(Figure 27B)**. This cleaved caspase-3 was detected in some

EdU-positive *Agpat2*$^{-/-}$ MEFs **(Figure 27C, arrows)** but is was more abundant in non-proliferating cells **(Figure 27C, yellow arrowheads)**. Higher magnification imaging showed that cleaved caspase-3 signal mainly consisted of cytoplasmic bright spots associated with shrunken nuclei and condensed chromatin but also a diffuse signal in the whole cell excluding the nuclear fragments **(Figure 27C, bottom panel)**

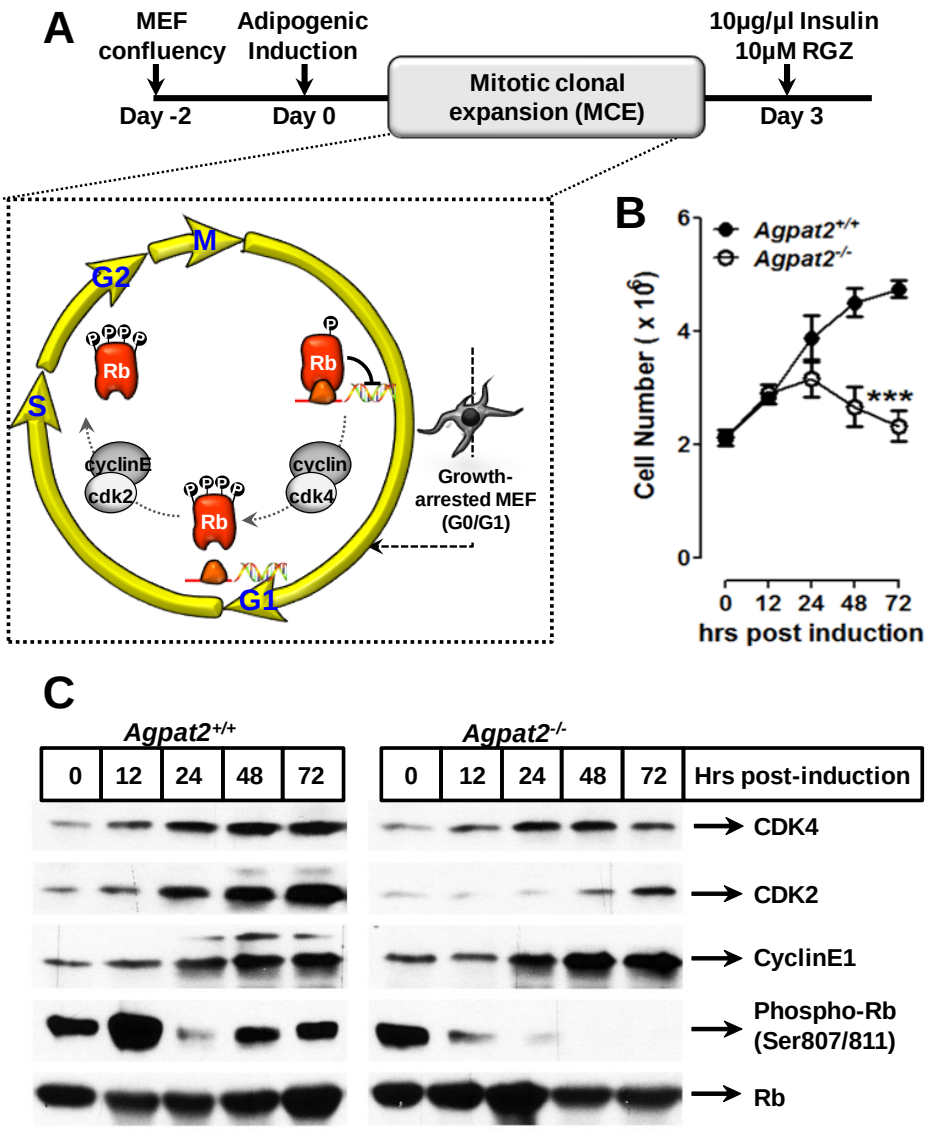

Figure 24. Confluent growth-arrested *Agpat2*$^{-/-}$ MEFs synchronously reenter on the cell cycle but fail to increase their cell number after adipogenic induction. **(A)** At Day 0, postconfluent MEFs were induced to differentiate by using the standard differentiation protocol. **(B)** At the indicated times, cells were harvested and counted in a Neubauer chamber. Graph shows the growth curves until day 3 after induction (72 hours). **(C)** Harvested cells were homogenized and whole-cell protein extracts (50 µg of protein/well) were analyzed by western blotting for CDK4, CDK2, cyclin E and p-Rb cell-cycle regulatory specific proteins.

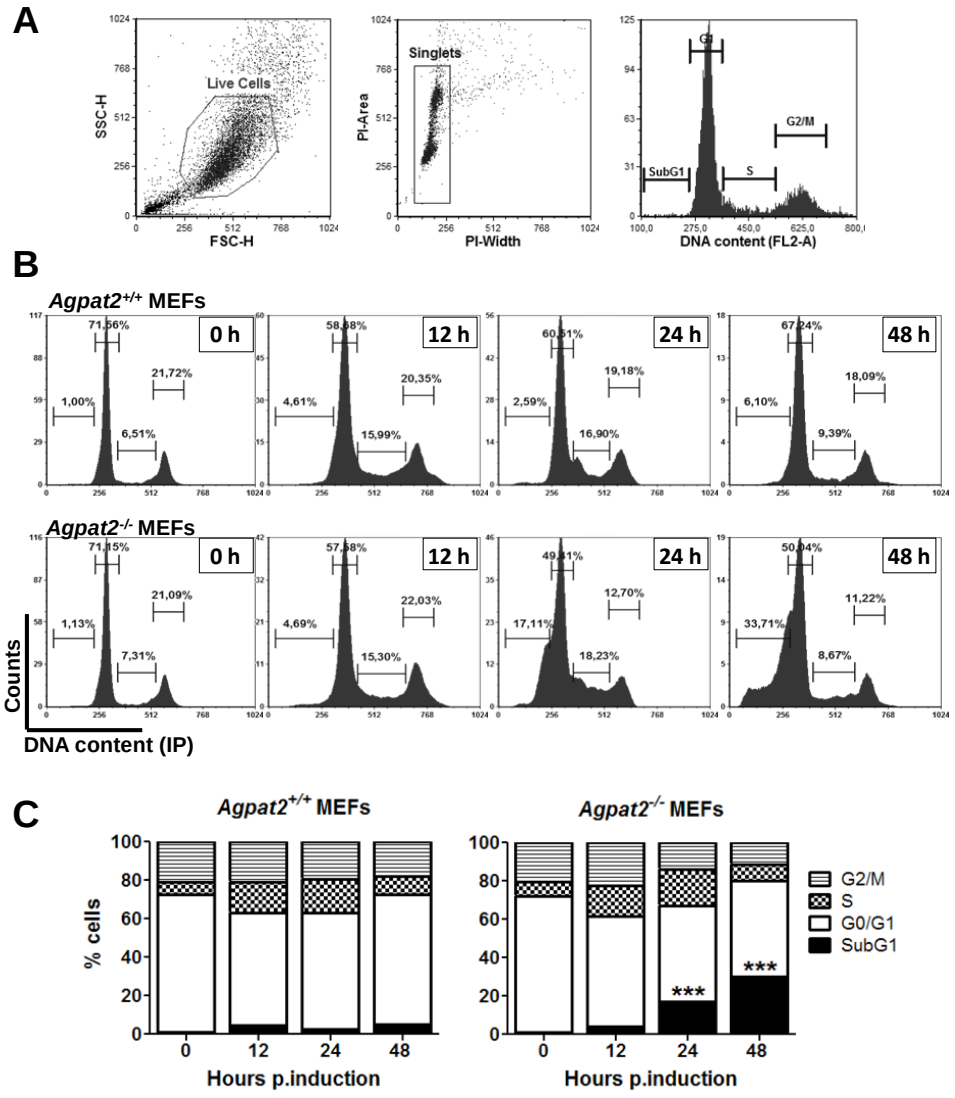

Figure 25. Cell cycle analysis reveals that *Agpat2*$^{-/-}$ MEFs do reenter in the cell cycle after adipogenic induction but undergo loss of the cell viability soon thereafter. At indicated times after adipogenic induction, the distribution of MEFs in the cell cycle (G1 vs. S vs G2/M) was evaluated by propidium iodide staining and fluorescence-activated cell sorter (FACS) analysis. **(B)** DNA content frequency histograms displaying the relative amount of cells in the G1, S and G2/M phase of the cell cycle between 0–48 hours of adipogenic induction. Dead cells are located in the Sub-G1 region. **(C)** Bar histograms show the proportion of cells in the distinct cell cycle phases. Percentages were calculated using FACS Express3 software. Data represent the average of three independent experiments with N=6. ***($p<0.001$) denote significant difference compared with differentiated *Agpat2*$^{+/+}$ MEFs.

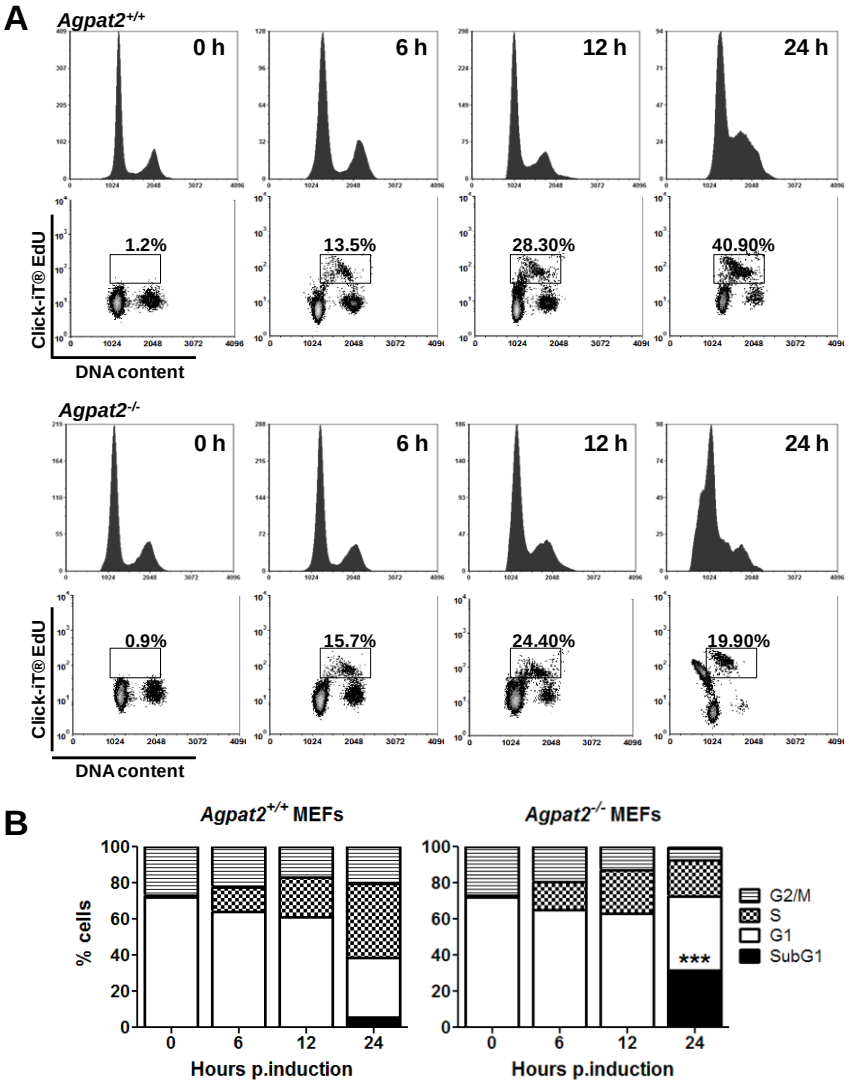

Figure 26: *Agpat2*$^{-/-}$ MEFs undergo early cell death after completion of MCE. At Day 0, postconfluent MEFs were pulsed with 10 µM of EdU and induced to differentiate with the standard protocol. **(A)** Cells were harvested at the indicated times and DNA synthesis during S-phase progression was evaluated by EdU-Click incorporation and analyzed by FACS. **(B)** Bar graphs show the proportion of cells in distinct cell cycle phases. Percentages were calculated using FACS Express3 software. Data represent the average of three independent experiments with N=6. ***($p<0.001$) denote a significant difference compared with differentiated *Agpat2*$^{+/+}$ MEFs.

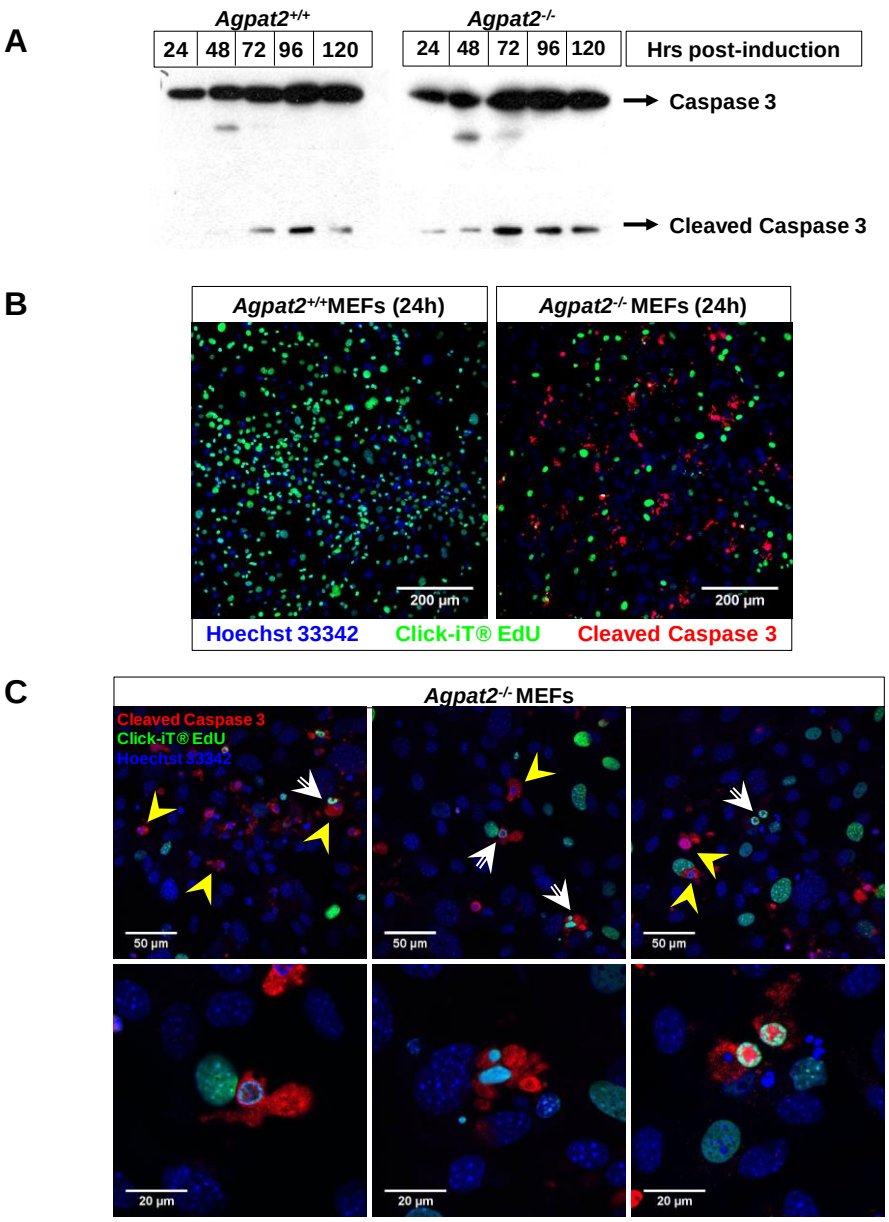

Figure 27: Adipogenic differentiation induces activation of caspase-3 in *Agpat2*$^{-/-}$ MEFs. (A) Western blotting of whole-cell protein extracts combining both detached and adherent cells, show total and cleaved caspase-3 in *Agpat2*$^{+/+}$ and *Agpat2*$^{-/-}$ MEFs upon adipogenic induction **(B)** Confocal immunofluorescence images of *Agpat2*$^{+/+}$ and *Agpat2*$^{-/-}$ MEFs after 24 hours of adipogenic induction. At day 0, MEFs were treated with Edu and adipogenically induced. Immunofluorescence detection of cleaved caspase-3 (red) and proliferating cells (green) was assessed 24h later. **(C)** Images in higher magnification show the distribution of cleaved caspase 3 in *Agpat2*$^{-/-}$ cells.

4.1.6 Akt activation is blunted during the adipogenic differentiation of *Agpat2*$^{-/-}$ MEFs.

Given the significant proportion of *Agpat2*$^{-/-}$ MEFs that undergo cell death after adipogenic induction, we decided to evaluate the activation of key pro-survival signalling pathways that have well recognized roles in adipogenesis. Upon insulin stimulation, activated insulin receptor triggers the recruitment and phosphorylation of a number of adaptor proteins, highlighting the members of insulin receptor substrate family (IRS). These phosphorilated proteins form docking sites for the activation of two main downstream signalling arms: phosphatidylinositol 3-kinase (PI3K)–AKT and the Ras–mitogen-activated protein kinase (MAPK) pathways. Both of these pathways are crucial for adipogenesis since are required for lipogenesis, cell proliferation, growth and survival. Akt may also stimulate PPARγ expression, at least in part, through phosphorylation and inactivation of the transcription factor FoxO1 (117).

To determine whether adipogenic induction activates insulin signalling pathway in *Agpat2*$^{-/-}$ MEFs, we evaluated total levels of insulin receptor (IR) and IRS-1,-2 as well as the phosphorylated and total forms of Akt, Erk and their main downstream target proteins. As shown in **Figure 28**, MEFs of both genotypes exhibited similar levels of total IR, IRS-1, -2, Akt and Erk1/2 (p44/42 MAPK) proteins during adipocyte differentiation. Nevertheless, significant differences in the activation of Akt and Erk were observed between both genotypes. In *Agpat2*$^{+/+}$ MEFs, phosphorylation of Akt at both Ser473 and Thr308 residues was strongly induced, with a maximal activation at day 3 post-adipogenic induction. Concordantly, increased phosphorylation levels of p70S6, which is a target kinase downstream the PI3K/AKT/mTOR pathway, were observed in *Agpat2*$^{+/+}$ MEFs. In

contrast, only low phosphorylation levels of Akt at Thr308 and high levels of PTEN, a negative regulator of PI3K/Akt signaling, were observed in *Agpat2*$^{-/-}$ MEFs.

Agpat2$^{+/+}$ and *Agpat2*$^{-/-}$ MEFs shared similar basal levels of Erk1/2 phosphorylation until day 2 post-adipogenic induction. At day 3 and 5, Erk1/2 was further phosphorylated in *Agpat2*$^{+/+}$ MEFs whereas this increase was rather modest in *Agpat2*$^{-/-}$ MEFs, **(Figure 28B)**.

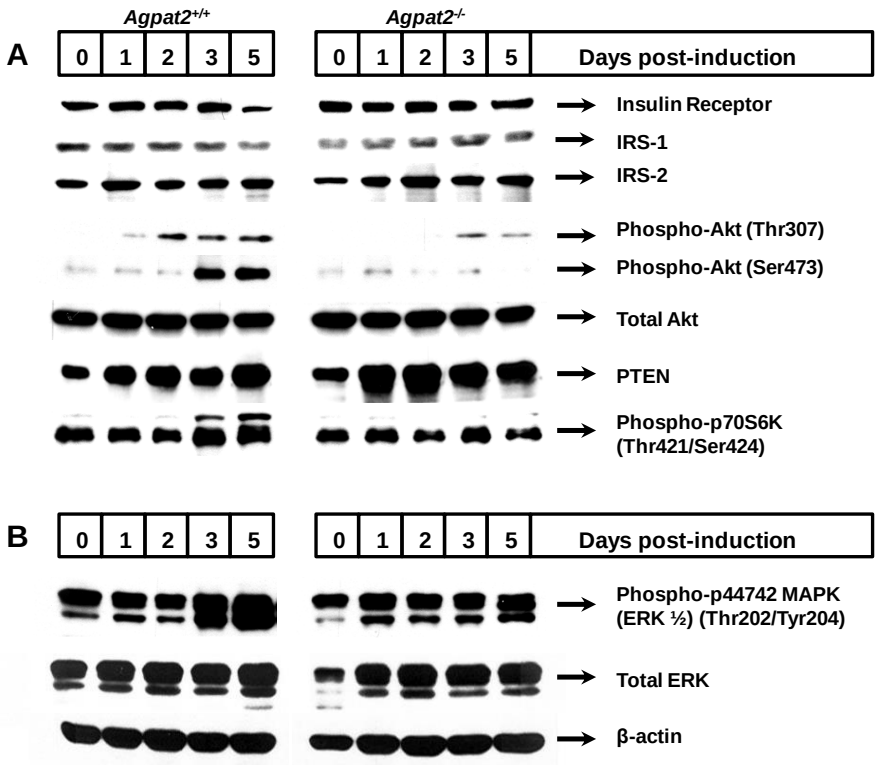

Figure 28: Activation of AKT and ERK signalling pathways is blunted during adipocyte differentiation in *Agpat2*$^{-/-}$ MEFs. Two days post-confluent *Agpat2*$^{+/+}$ and *Agpat2*$^{-/-}$ MEFs were induced to differentiate with the regular hormone cocktail (see Methods section). At the indicated times the cells were harvested and whole protein extracts (50 µg/well) were separated by SDS-PAGE, electrotransferred onto nitrocellulose membranes, and then probed with specific antibodies for the detection of phosphorylated and total proteins.

4.2 *In vivo* studies: WAT and BAT are post-natally lost *Agpat2*$^{-/-}$ mice by massive cell death.

To gain insights on the physiological significance of our *in vitro* findings, we aimed to characterize the development of AT depots in *Agpat2*$^{-/-}$ mice *in vivo*. In murine species WAT development begins late in fetal life and its main expansion takes place postnatally, by both hyperplastic and hypertrophic mechanisms. BAT, in contrast, is fully developed at the time of birth.

As we previously reported, AGPAT2 deficient mice is completely devoid of both WAT and BAT at the time of weaning and this phenotype persists during their whole adult life. Our *in vitro* studies suggest, as a plausible hypothesis, that the lipodystrophic phenotype of *Agpat2*$^{-/-}$ mice can be the result of a failed differentiation of preadipocytes into mature adipocytes. Consequently, although adipose depots are, in fact, absent in the adult *Agpat2*$^{-/-}$ mice, commited preadipocytes could be still present in normal number and anatomic location. Therefore, we aimed to track both, adipose tissue and precursor cells, at different stages of *Agpat2*$^{-/-}$ mice fetal and early postnatal life.

4.2.1 *Agpat2*$^{-/-}$ mice have Pref-1 expressing preadipocytes in anatomical areas where adipose tissue is postnatally developed.

Pref-1 is a bona fide marker of committed adipocyte progenitors suitable for localizing and identifying tissue-resident preadipocytes during early stages of *in vivo* adipogenesis. Adipocyte progenitors have long been thought to reside in or near to the vasculature of adipose tissue. Therefore, to determine whether *Agpat2*$^{-/-}$ mice have preadipocytes, we first performed indirect immunofluorescence on frozen trans-thoracic

slices of whole *Agapt2*$^{+/+}$ and *Agapt2*$^{-/-}$ fetuses and newborn mice. As expected, high expression levels of Pref-1 were found in the anatomical areas where WAT is normally present in the adult animals, such as the subcutaneous connective tissue **(Figure 29A-B, upper panel)**. Indeed, Pref-1 positive cells, with no detectable lipid load, were clearly evident throughout the dermis and hypodermis of *Agpat2*$^{+/+}$ and *Agpat2*$^{-/-}$ mice at embryonic day 18.5 **(Figure 29A,** E18.5**)** and at post-natal day 1.5 **(Figure 29B, P1.5)**. Confocal analysis of BAT depots also showed significant expression of Pref-1 in fetuses (E18.5) and newborn mice (P1.5) from both genotypes. Notably, Pref-1 expressing cells were detected in close proximity to small blood vessels in BAT of both genotypes **(Figure 29, arrowheads)**. Quantification of the relative level of Pref-1 and Zic-1 mRNA showed similar abundance of these preadipocyte markers in BAT from *Agpat2*$^{+/+}$ and *Agpat2*$^{-/-}$ mice at different time-point after birth **(Figure 30).**

These results are compatible with the hypothesis that *Agpat2*$^{-/-}$ mice have a normal population of preadipocytes and that the lipodystrophic phenotype is the consequence of an impaired differentiation of these precursor cells or, alterantively, and increased adipocyte cell death.

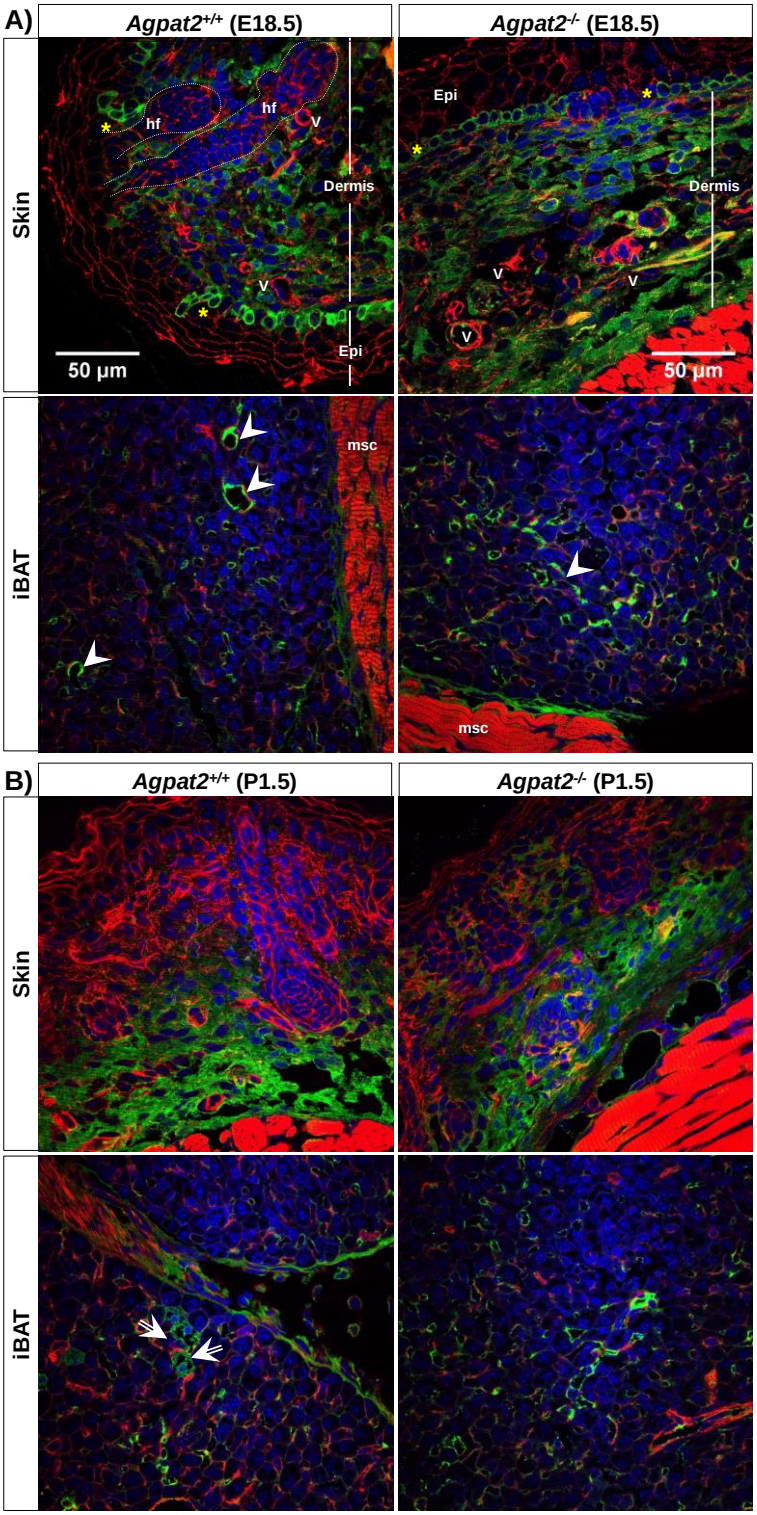
A)
Agpat2+/+ (E18.5)
Agpat2-/- (E18.5)
Skin
iBAT
hf
hf
V
Dermis
V
Epi
50 µm
Epi
Dermis
V
V
V
50 µm
msc
msc
B)
Agpat2+/+ (P1.5)
Agpat2-/- (P1.5)
Skin
iBAT

Figure 29: *Agpat2*$^{-/-}$ mice have Pref-1 expressing cells in the anatomical areas where adipose tissue is postnatally developed. Immunofluorescence staining of Pref-1 (green) in transversal sections through the scapular region of **(A)** E18.5 fetuses and **(B)** P1.5 newborn mice. β-actin expression is shown in red and nuclei were counterstained with DAPI (blue). Epi=Epidermis, hf=hair follicle, V=Vessel, msc=muscle.

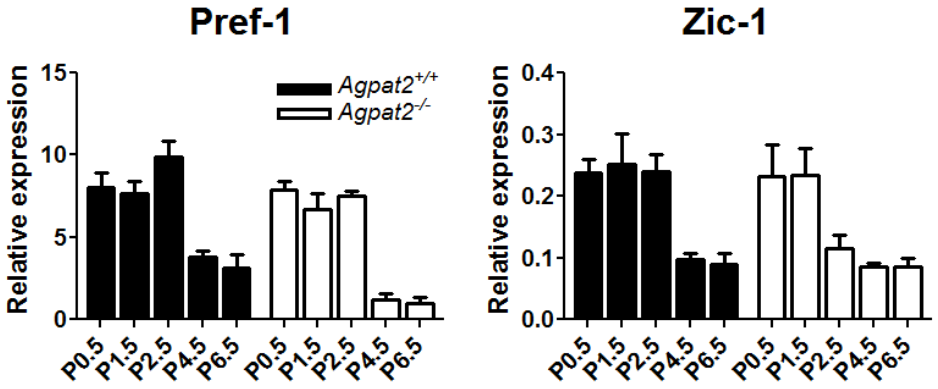

Figure 30: Relative mRNA expression of preadipocyte markers is normal *Agapt2*$^{-/-}$ mice. Expression of Pref-1 and Zic-1 mRNAs was assessed by qPCR in interscapular BAT depots at different post-natal time points (from birth (P0.5) to 6 days-old mice (P6.5)). Graphs show the relative abundance of each transcript normalized to cyclophilin (Ct =20). The bars show the means ± standard deviations of N=8. No statistical differences were observed between both genotypes.

4.2.2 Postnatal adipose tissue growth and survival are impaired in *Agapt2*$^{-/-}$ mice.

Oil Red-O staining of thoracic region transverse sections of E18.5 and P1.5 mice showed well-defined BAT and WAT depots in all the wild type and *Agpat2*$^{-/-}$ mice examined **(Figure 31A-32A)**. Indeed, substantial BAT at interscapular, thoracic, dorsal cephalic and cervical regions was observed in both genotypes **(Figure 31-32A, see Figure S6 for detailed anatomy description)**. Furthermore, upon higher magnification at the dorsal area, a well-defined layer of subcutaneous Oil-red O stained, Perilipin-1 expressing adipocytes was evident in animals of both genotypes **(Figures 31A-B, 32B)**.

In contrast, in all P4.5 *Agpat2*$^{-/-}$ mice examined, BAT and WAT depots were much smaller than in their wild type littermates, and showed remarkable morphological abnormalities at the macroscopic level **(Figure 33)**. In fact, at this time point of post-natal age, wild type iBAT was a well-defined biolobular soft organ with a brownish color and surrounded by large amounts of WAT. In contrast, iBAT in *Agpat2*$^{-/-}$ P4.5 pups was markedly smaller, with a very stiff texture and a much yellowish color **(Figure 33A)**. Oil Red-O staining of transverse sections of P4.5 *Agpat2*$^{-/-}$ mice revealed a severe decrease in the total number of adipocytes at subcutaneous **(Figure 33B, arrowhead)** and iBAT regions **(Figure 33B, arrow)**. In addition, large foci of infiltrating cells were spread throughout the BAT lobules of *Agpat2*$^{-/-}$ mice (**Figure 33B, yellow asterisks**). WAT of P4.5 *Agpat2*$^{+/+}$ mice was continuously expanding, basically at expenses of individual adipocyte growth **(Figure 33B, left panel, arrowhead)**. Consistently with Oil Red-O staining, biochemical quantification of tissue TGs showed significantly lower levels of total TGs in subcutaneous and iBAT depots of P4.5 *Agpat2*$^{-/-}$ mice **(Figure 33C).**

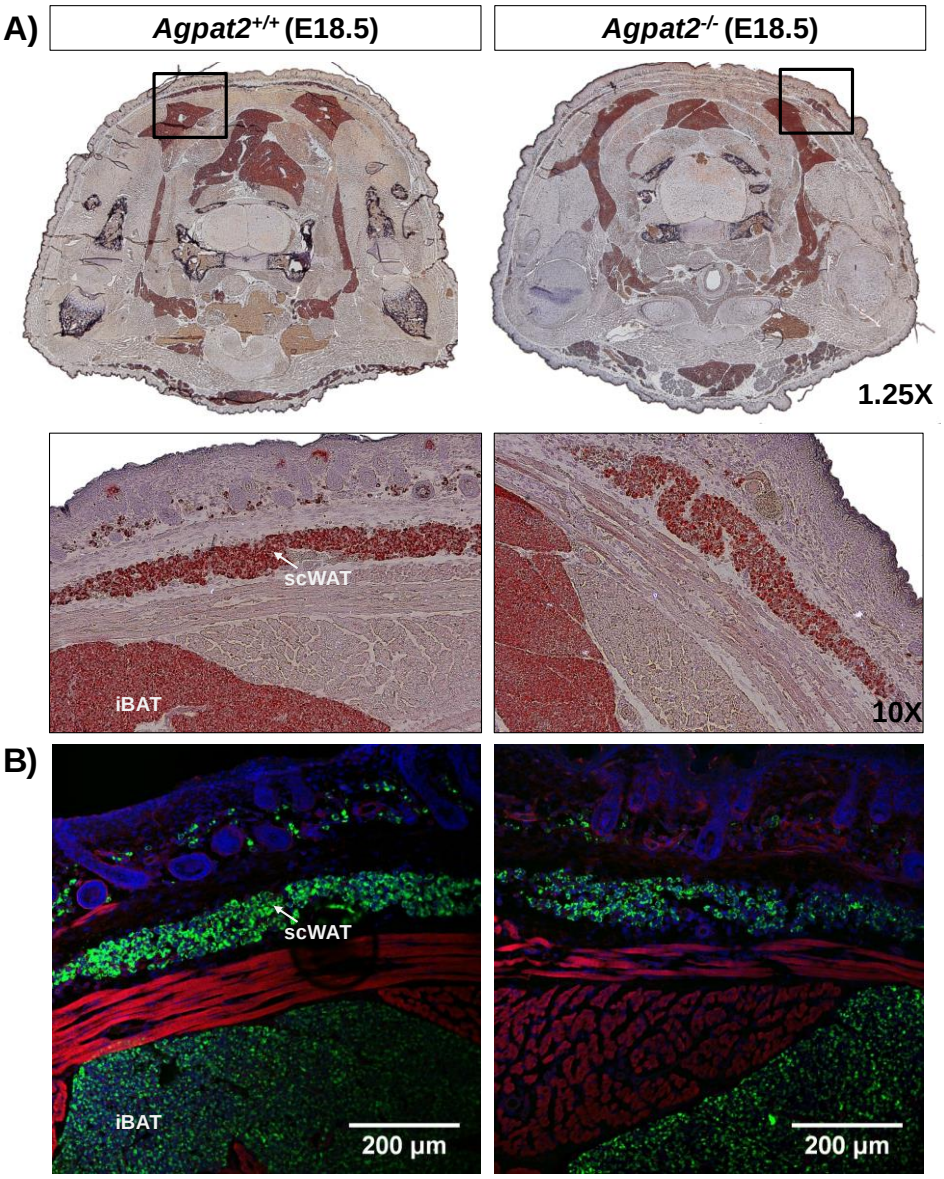

Figure 31: Fetal development of adipose tissue is normal in *Agpat2*$^{-/-}$ mice. **(A, top panel)** Oil Red-O and Hematoxylin staining of transversal thoracic sections from E18.5 embryos. **(A, bottom panel)** Higher magnification of the area depicted in squares shows a well-defined tissue containing numerous lipid-loaded cells, which are strongly stained with Oil Red O. (scWAT: subcutaneous white adipose tissue, iBAT: interscapular brown adipose tissue). **(B)** Immunofluorescence staining of Perilipin-1 (green) of the same sections shown above, demonstrates than ORO-positive depots (scWAT and BAT) are indeed adipocytes. β-actin positive cells are observed in red color and nuclei are stained with DAPI (blue).

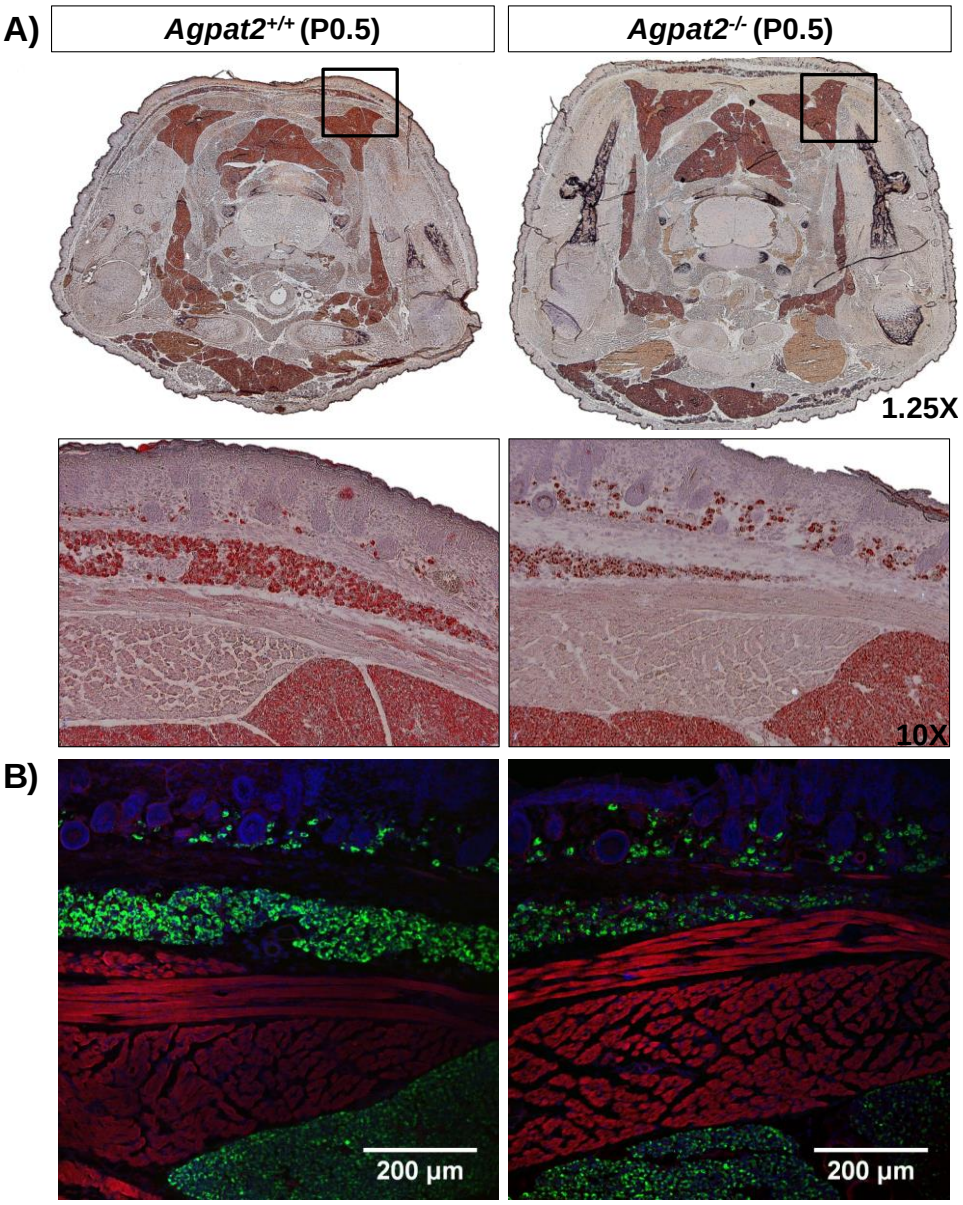

Figure 32: Adipose tissue depots are presents with normal distribution in *Agpat2*$^{-/-}$ newborn mice. **(A, top panel)** Oil Red-O and Hematoxylin staining of transversal thoracic sections from E18.5 embryos. **(A, bottom panel)** Higher magnification of the area depicted in squares clearly shows well-defined tissues containing numerous lipid-loaded cells, which are strongly stained with Oil Red O. **(B)** Immunofluorescence staining of Perilipin-1 (green) of the same sections shown above, demonstrates than ORO-positive depots (scWAT and BAT) are indeed adipocytes. β-actin positive cells are observed in red color and nuclei are stained with DAPI (blue).

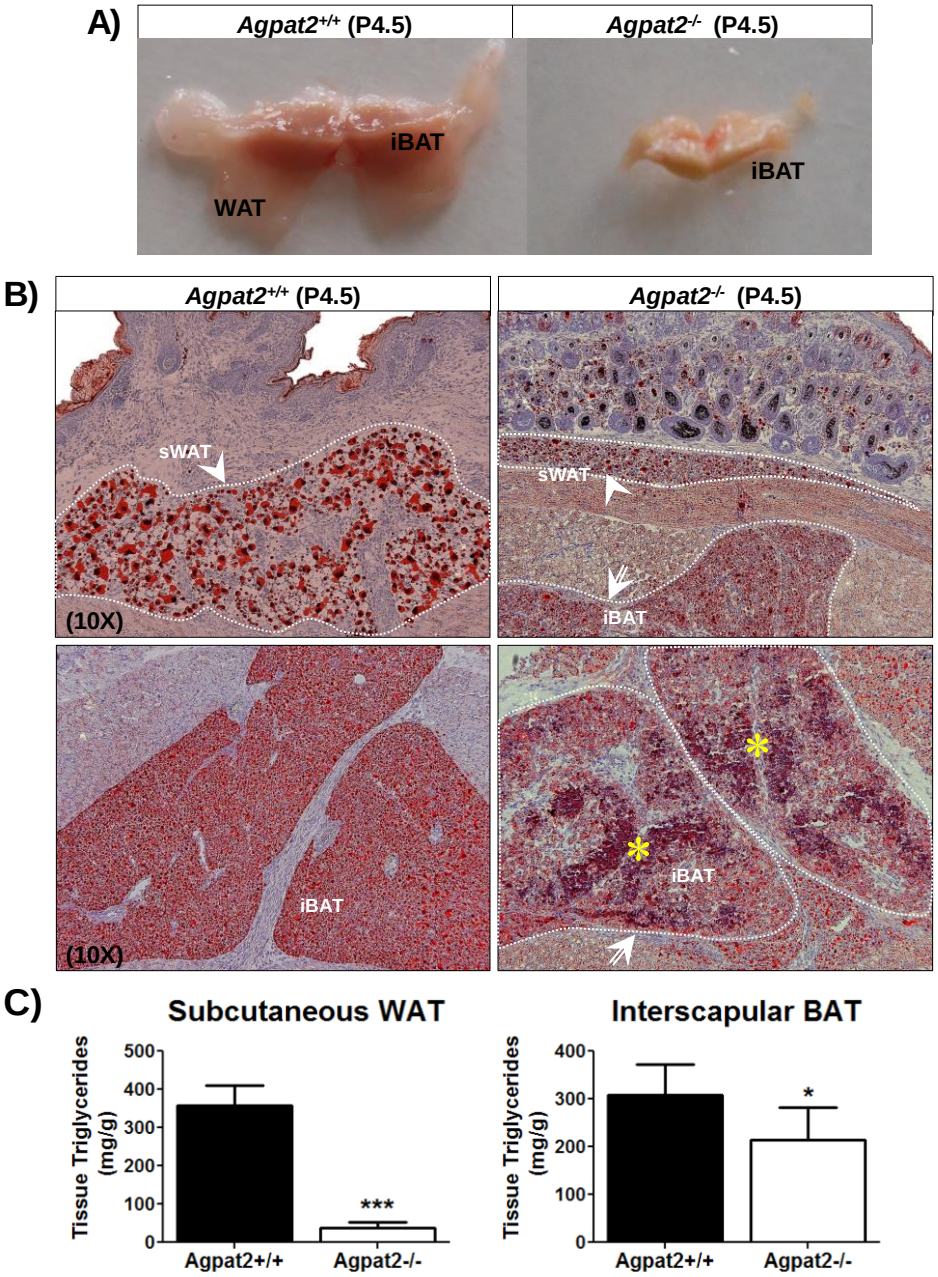

Figure 33: Abnormal morphology of BAT and WAT in 4.5 days-old *Agpat2*$^{-/-}$ mice. (A) Gross anatomy of whole interscapular brown adipose tissue (iBAT) depot surrounded by white adipose tissue (WAT) from a 4.5 days-old *Agpat2*$^{+/+}$ male mouse (left) and a *Agpat2*$^{-/-}$ male sibling (right). **(B)** Representative images (N=6) of subcutaneous (upper panel) and interscapular area (lower panel) of whole body transverse cryosections stained with ORO and Hematoxylin. **(C)** Skin (containing scWAT) and iBAT triglyceride content from 4.5 days-old pups. ***($p<0.001$) and *($p<0.05$) denote significant difference compared to *Agpat2*$^{+/+}$

Three-dimensional surface reconstructions of WAT and BAT sections stained with Perilipin-1 revealed a number of notorious differences at the cellular level among genotypes **(Figure 34)**. WAT of *Agpat2*$^{+/+}$ mice has large white adipocytes with a single "supersized" LD homogenously surrounded by Perilipin-1 **(Figure 34A)**. BAT of *Agpat2*$^{+/+}$ was composed by smaller adipocytes with multiple Perilipin-1 coated LDs **(Figure 34B)**. In contrast, WAT and BAT of *Agpat2*$^{-/-}$ mice have a disorganized architecture with heterogenous distribution of Perilipin-1, that was coating small LDs but also was found in lipid-free aggregates, similar to what we observed in adipogenically induced *Agpat2*$^{-/-}$ MEFs. **(Figure 14B)**. Further, multiple cellular nucleus likely corresponding to non-adipocyte cells were abundant both in WAT and BAT from P4.5 *Agpat2*$^{-/-}$ mice.

The serial analysis of the AT development from postnatal day 1 (P0.5) to postnatal day 6 (P6.5), revealed that at P0.5, WAT of both genotypes was composed by small adipocytes and fibroblastic-like cells **(Figure 35, upper panel)**. At P2.5 WAT in wild type mice, consisted of a homogeneous population of unilocular adipocytes containing a single lipid droplet **(Figure 35, second line, left panel)**. In contrast, WAT in P2.5 *Agpat2*$^{-/-}$ mice showed an abnormal morphology characterized by fewer and smaller adipocytes with brightly eosinophilic cytoplasm and several irregular LDs **(Figure 35, second line, right panel)**. Moreover, a significant amount of non-adipocytic cells infiltrated the tissue. All these anomalies were increasing with the following post-natal days **(Figure 35, pictures of P4.5 and P6.5 days-old tissues)** and were also observed in subcutaneous WAT **(Figure 36)**. Here, dermal and hypodermal *Agpat2*$^{+/+}$ adipocytes were widely distributed between hair follicles and also under the panniculus carnosus muscle. In contrast, in the *Agpat2*$^{-/-}$

mice, the subcutaneous adipocytes were almost completely absent. In fact, higher magnification of the hypodermal area revealed a significant infiltration of foam cells **(Figure 36, black arrows)** and small lipid-loaded cells, possibly corresponding to dying adipocytes **(Figure 36, yellow arrows).**

Histological evaluation of postnatal BAT showed similar findings. At P0.5, iBAT of *Agpat2*$^{-/-}$ mice seemed well-organized with clearly demarcated and richly vascularized lobules containing great number of adipocytes with eosinophilic multiloculated cytoplasm, suggesting that brown adipocyte adipogenesis normally occurs in AGPAT2 deficient mice **(Figure 37, upper panel)**. At P2.5, iBAT of *Agpat2*$^{-/-}$ mice displayed pathological changes in its cellular composition **(Figure 37, second line)**, mostly consisting of numerous unilocular cells resembling small white adipocytes. Lately, massive brown adipocyte death and mononuclear infiltration were the hallmark features of the remmant BAT, whose parenchyme was largely replaced by amorphous bashophilic material, cytoplasmic debris, scattered mononuclear cells and giant histiocytes surrounding large lipid vacuoles likely formed by the fusion of broken adipocytes **(Figure 37, pictures of P4.5 and P6.5 days-old tissues)**.

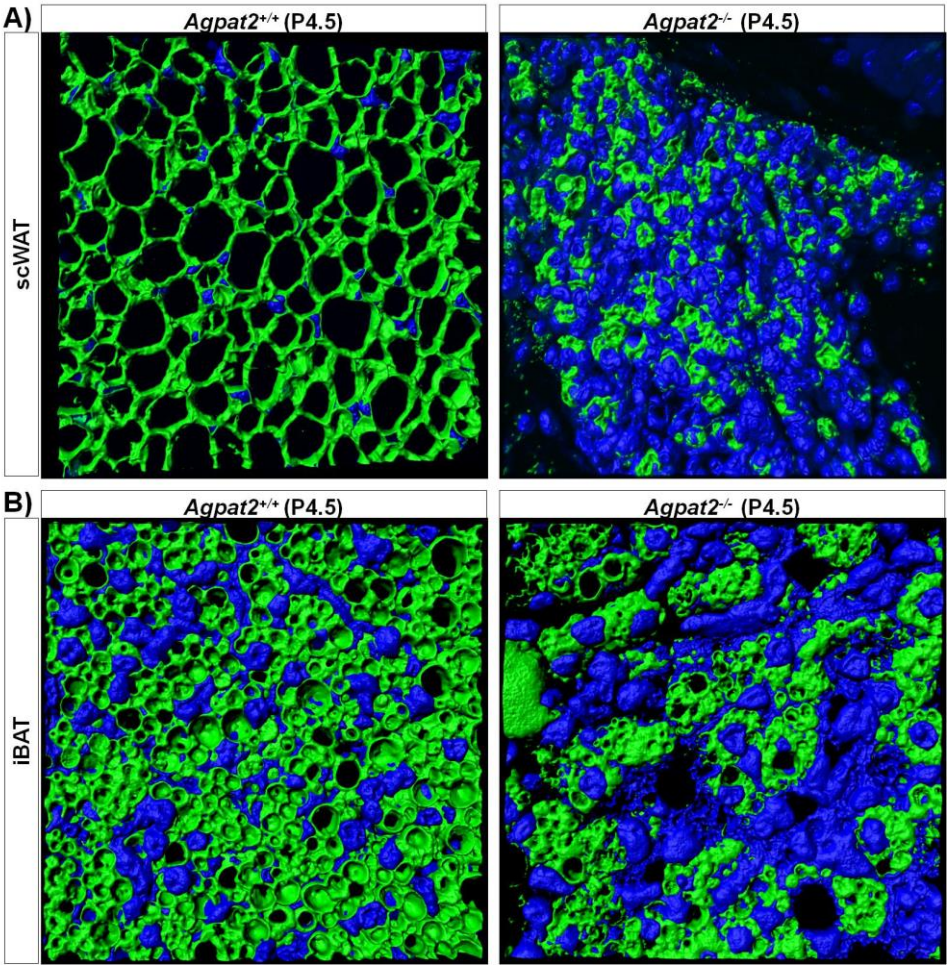

Figure 34: Three-dimensional (3D) digital reconstruction of Perilipin-1 stained adipose tissue depots from *Agpat2*$^{+/+}$ and *Agpat2*$^{-/-}$ mice at P4.5. (A) subcutaneous WAT and interscapular BAT **(B)** were stained with Perilipin-1 (green) and DAPI. Right images show adipose tissue from *Agpat2*$^{+/+}$ mice and left images show adipose tissue from *Agpat2*$^{-/-}$ mice.

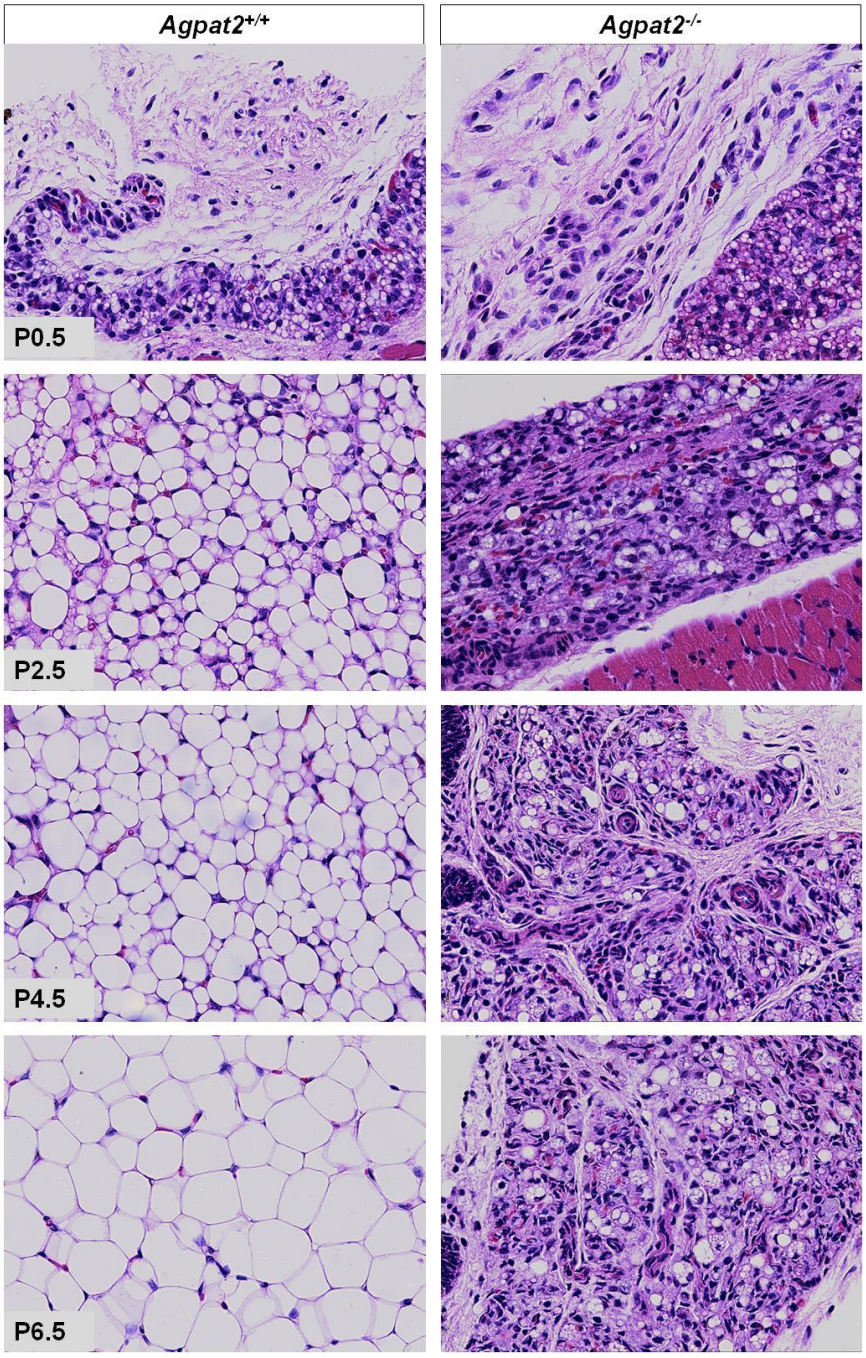

Figure 35. White adipose tissue development and expansion are early impaired after birth in *Agapt2*$^{-/-}$ mice. Paraffin-embedded sections of white adipose tissue from *Agpat2*$^{+/+}$ (left panels) and *Agpat2*$^{-/-}$ mice (right panels) were obtained at different days of post-natal life and stained with Hematoxylin and Eosin. Slides were photographed at 40x of magnification.

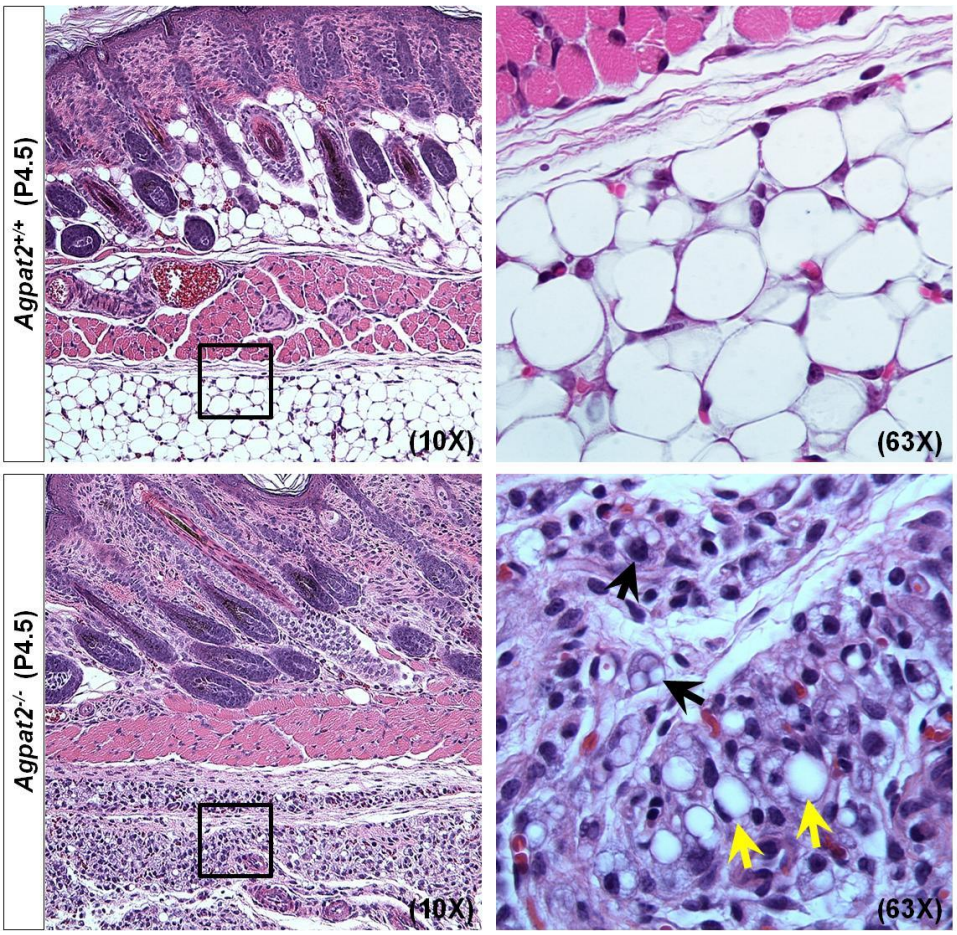

Figure 36. Atrophic adipocytes are present in the subcutaneous region of *Agapt2*$^{-/-}$ mice. Representative images (N=6) of Hematoxylin and Eosin stained cross sections of paraffin-embedded skin specimens from *Agpat2*$^{+/+}$ (upper panels) and *Agpat2*$^{-/-}$ littermates (lower panels) at P4.5 show complete absence of subcutaneous adipose tissue both in the dermis and the subcutaneous layer under the striated muscle (*panniculus carnosus*) in Agpat2$^{-/-}$ mice. Higher magnifications (63X) of the indicated areas (squares) are shown in the right panels. Black arrows indicate the presence of foam cells. Yellow arrows indicate abnormal adipocyte like-cells in subcutaneous region of *Agpat2*$^{-/-}$ mice but not in *Agpat2*$^{+/+}$ mice.

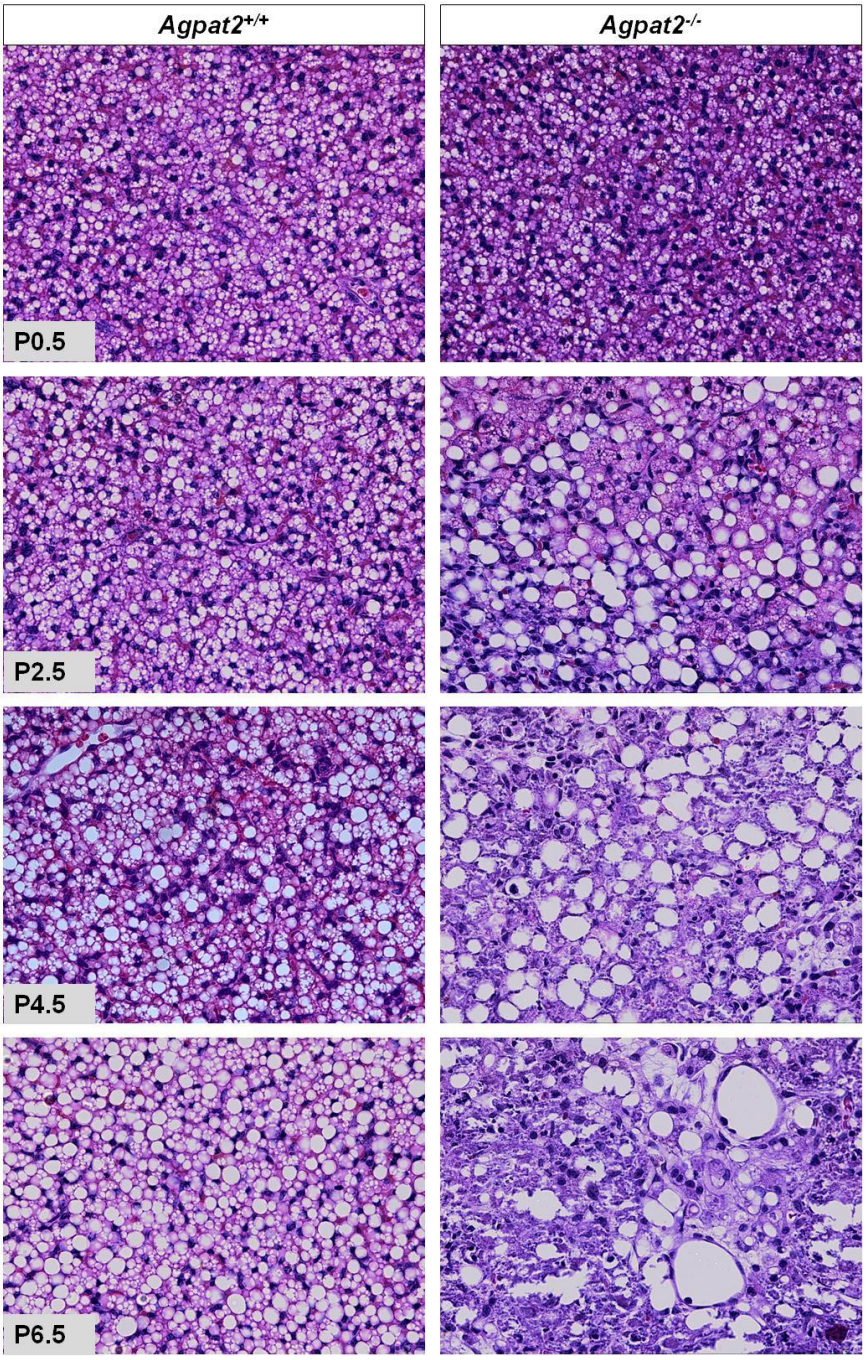

Figure 37. Postnatal brown adipose tissue development and expansion are impaired in *Agapt2*$^{-/-}$ mice. Paraffin-embedded sections of iBAT from *Agpat2*$^{+/+}$ (left panels) and *Agpat2*$^{-/-}$ mice (right panels) were obtained at different days of post-natal life and stained with Hematoxylin and Eosin. Slides were photographed at 40x of magnification.

4.2.3 mRNA levels of key adipocyte markers is normal in newborn *Agapt2*$^{-/-}$ mice but it is decreased concomitantly with the pathological changes observed in the adipose tissue.

The mRNA concentration of common adipocyte as well as BAT markers was quantified in the iBAT of *Agpat2*$^{-/-}$ mice at different postnatal times. As shown in **Figure 38**, the relative expression of these markers was equivalent between newoborn (P0.5), *Agpat2*$^{+/+}$ and *Agpat2*$^{-/-}$ mice. This pattern notably changed as soon as the second day after birth, when the relative expression of PPARγ, adiponectin, CIDEA and seipin (BSCL2) was significantly decreased in the *Agpat2*$^{-/-}$ pups. After 4.5 days, the mRNA levels of all the markers was severely reduced in *Agpat2*$^{-/-}$ mice, indicating a very substantial loss of adipose tissue.

These *in vivo* results are reminiscent of our findings in cultured *Agpat2*$^{-/-}$ MEFs, that die soon after the adipogenic program is started with a hormone cocktail (see section of results, figures 25-27).

Considered together, our data suggest the *Agapt2*$^{-/-}$ mice have preadipocytes in normal number and location but that, soon after adipogenic program starts, differentiating adipocytes suffer cell that result in lack of any mature adipose depot.

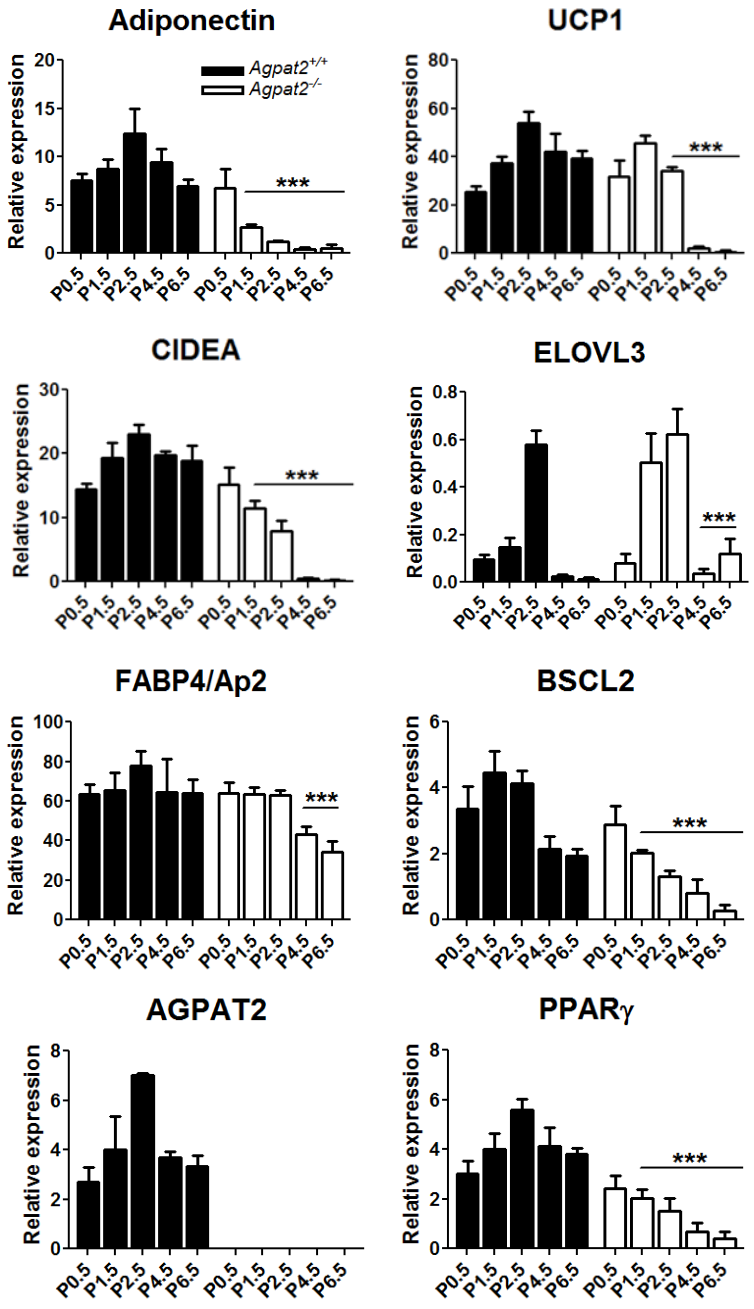

Figure 38. Gene expression of common adipocyte and BAT specific markers is normal in newborn *Agapt2*$^{-/-}$ mice but it is decreased soon after birth. Adipose tissue mRNA markers were assessed by qPCR in iBAT depots at different post-natal time points (from birth (P0.5) to 6 days-old mice (P6.5)). Graphs represent the relative abundance of each transcript normalized to cyclophilin (Ct =20). The bars show the means ± standard deviations of N=6. ***($p<0.001$) denote significant difference compared to differentiated *Agpat2*$^{+/+}$ mice.

4.2.4 mRNA levels of AGPAT family members is not changed in the adipose tissue of *Agpat2*$^{-/-}$ mice.

Because AGPAT enzymes are involved in neutral lipid synthesis, we asked how the other isoforms of the AGPAT family are regulated in WAT and BAT depots of *Agpat2*$^{-/-}$ mice. For this, we evaluated the mRNA levels of all 11 known AGPAT isoforms in the iBAT of newborn *Agpat2*$^{-/-}$ mice. As shown in **Figure 39**, no differences were detected in the mRNA levels of all these genes between animals of both genotypes. Interestingly, AGPAT2, AGPAT3 and AGPAT6 were main isoforms expressed in iBAT at this time point (**Figure 38**). These results suggest that the absence of AGPAT2 does not elicit any compensatory response in the gene transcription of other adipose AGPATs in mice.

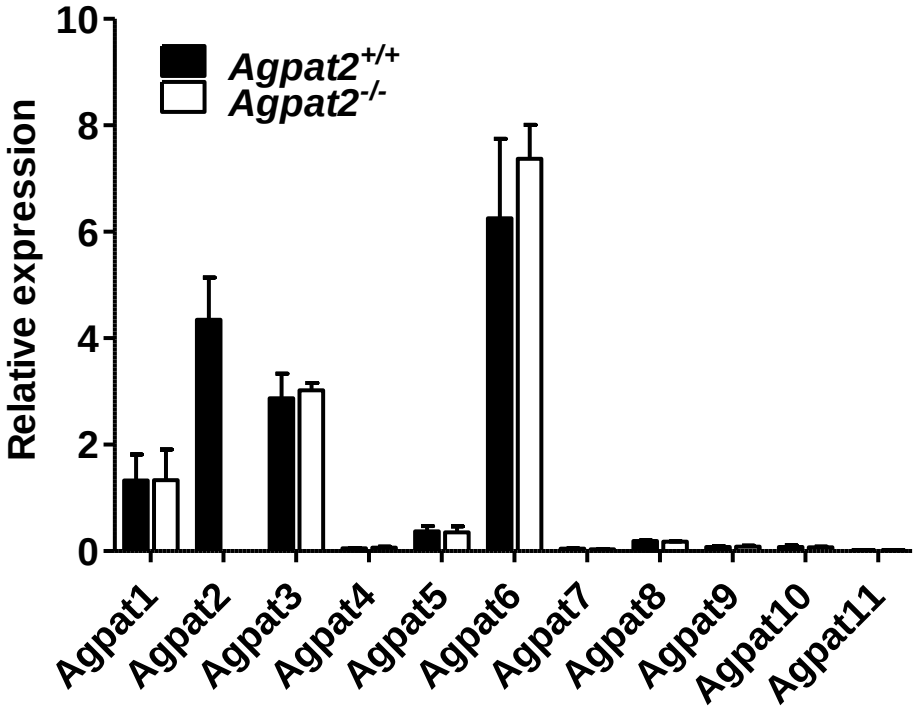

Figure 39: mRNA levels of 1-acylglycerol-3-phsophate O-acyltransferase (AGPAT) isoforms in iBAT of *Agpat2*$^{+/+}$ and *Agapt2*$^{-/-}$ newborn mice. Data were obtained by qPCR from a pool of three individual mice in two independent experiments. The relative abundance of each transcript was normalized to cyclophilin (Ct =20). Values shown represent means ±SD in arbitrary units.

4.2.5 Adipose tissue involution during early post-natal life of AGPAT2 deficient mice is associated with massive macrophage infiltration and adipocyte cell death.

As mentioned in section 4.2.2, disappearing adipocytes in adipose tissue from P4.5 *Agpat2*$^{-/-}$ mice is quickly replaced by infiltrating cells. To determine the lineage of these cells, macrophagic cell-surface marker Mac-2 was evaluated by immunoflourescence in adipose tissue sections of *Agpat2*$^{-/-}$ and *Agpat2*$^{+/+}$ mice from P0.5 to P4.5

Mac2-stained macrophages were undetectable in adipose depots of both genotypes at P0.5 **(Figure 40, left panel)**. In contrast, these cells were highly abundant in subcutaneous WAT **(Figure 40A)** and iBAT **(Figure 40B)** *Agpat2*$^{-/-}$ mice at P4.5 whereas were totally absent in their *Agpat2*$^{+/+}$ littermates (data not shown), suggesting that macrophages rapidly infiltrate *Agpat2*$^{-/-}$ adipose depots as adipocytes dissapear from these tissues.

iBAT gene expression analysis showed that the mRNA levels of inflammation regulatory genes NFκB, Caspase-1, IL-6 and TNFα directly correlated with the abundance of Mac-2 expressing cells in *Agpat2*$^{-/-}$ mice at all developmental stages and that those inversely correlated with the mass of neutral lipid loaded cells **(Figure 41)**. Importantly, all of these transcripts remained unchanged in liver, skeletal muscle and spleen of *Agpat2*$^{-/-}$ mice and their levels were equivalent to the ones detected in *Agpat2*$^{+/+}$ mice **(**data not shown) suggesting that macrophages exclusively infiltrate the involuting adipose tissue of *Agpat2*$^{-/-}$ mice.

To determine the mechanisms of AT cell death in *Agpat2*$^{-/-}$ mice, the presence of chromatin fragmentation was assessed by terminal deoxynucleotidyl transferase dUTP nick end

labeling (TUNEL). WAT and iBAT was completely devoid of TUNEL-positive cells in the *Agpat2*$^{+/+}$ mice **(Figure 42**). In sharp contrast, countless TUNEL-positive cells were evident in both WAT and BAT of P4.5 *Agpat2*$^{-/-}$ mice, indicating that these adipose tissues have already suffered massive cell death, possibly by apoptosis, at that time point **(Figure 42)**.

Considering all the *in vivo* data presented in the above sections, it is apparent that AGPAT2, although dispensable for preadipocytes determination, it is absolutely required for the full expansion of the adipose tissue after birth, possibly at the level of the lipid droplet formation.

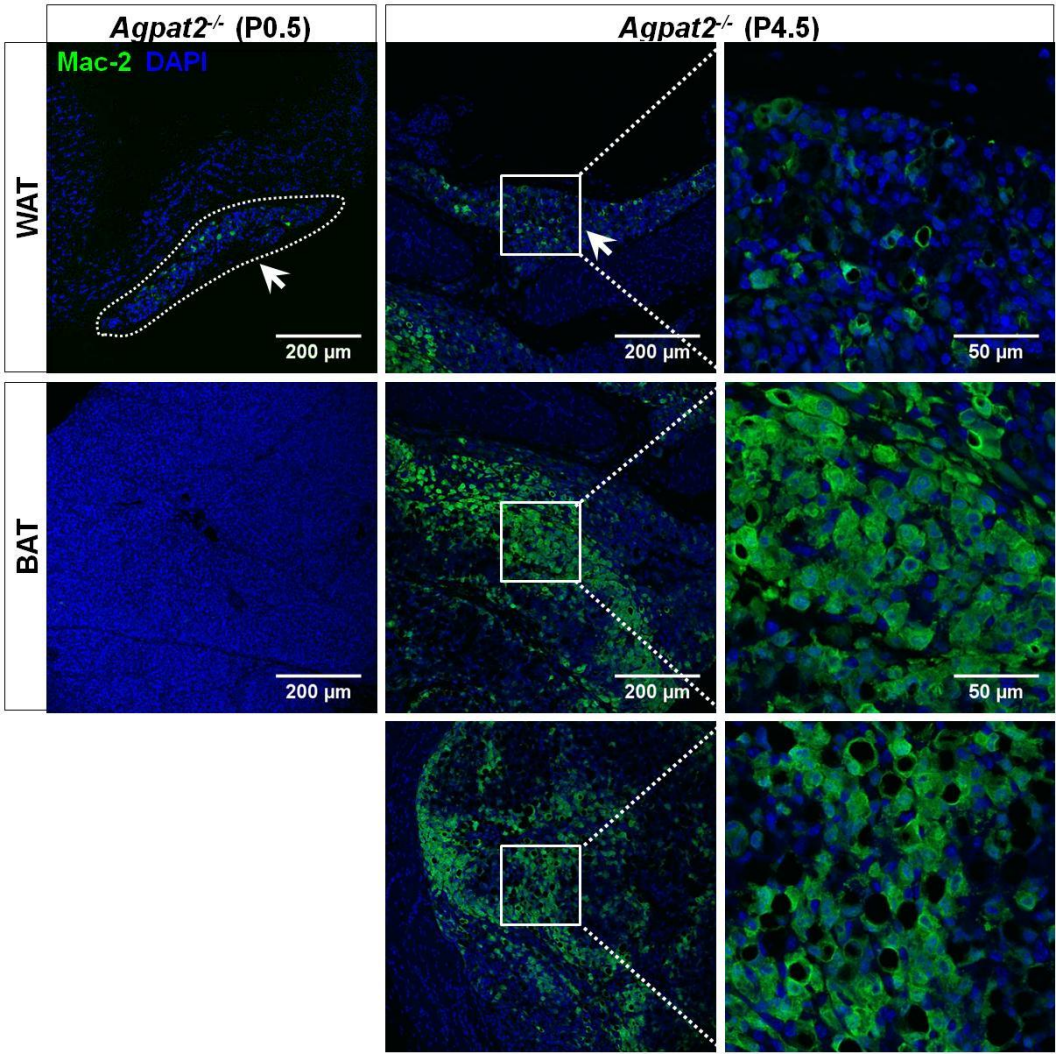

Figure 40: Macrophages infiltrate the involuting adipose tissue of *Agpat2*$^{-/-}$ mice. Paraffin-embedded sections of developing subcutaneous WAT and interscapular BAT from *Agpat2*$^{+/+}$ and *Agpat2*$^{-/-}$ littermates were stained with anti-Mac-2 (macrophage specific marker) and detected by immunofluorescence. Mac-2 positive macrophages are shown in green color and nuclei in blue (DAPI).

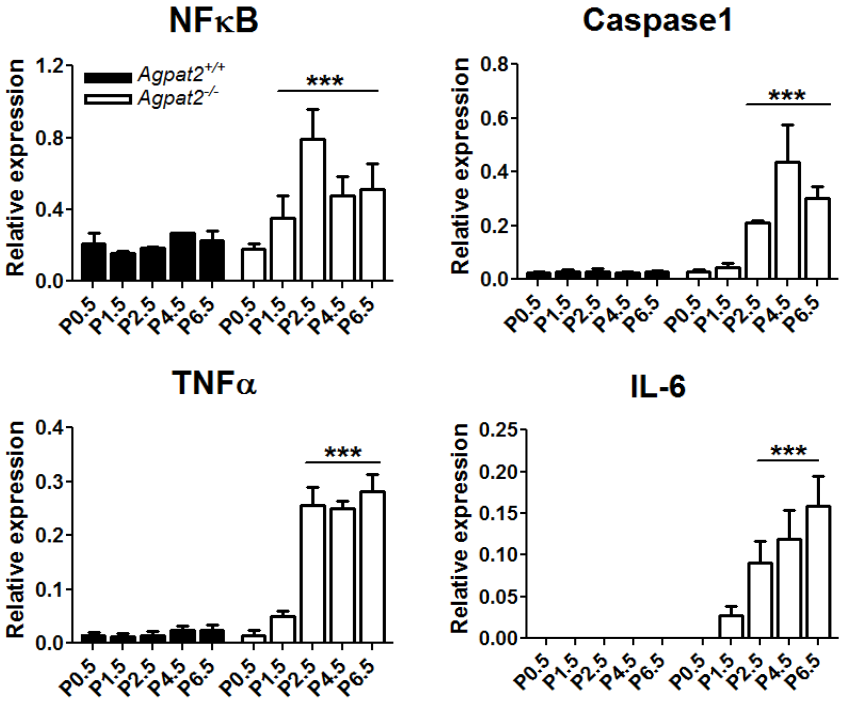

Figure 41. The mRNA level of genes involved in inflammatory response are increased in the adipose tissue of *Agapt2*$^{-/-}$ mice. Interscapular BAT gene expression was assessed by qPCR at different post-natal time points (from birth (P0.5) to 6.5 days-old mice (P6.5)). Graphs show the relative abundance of each transcript normalized to cyclophilin (Ct =20). Undetermined or higher Ct values (Ct>38) were detected for all transcripts evaluated in *Agpat2*$^{+/+}$ mice. The bars show the means ± standard deviations of N=8. ***($p<0.001$) denote significant difference compared to *Agpat2*$^{+/+}$ mice at day P0.5.

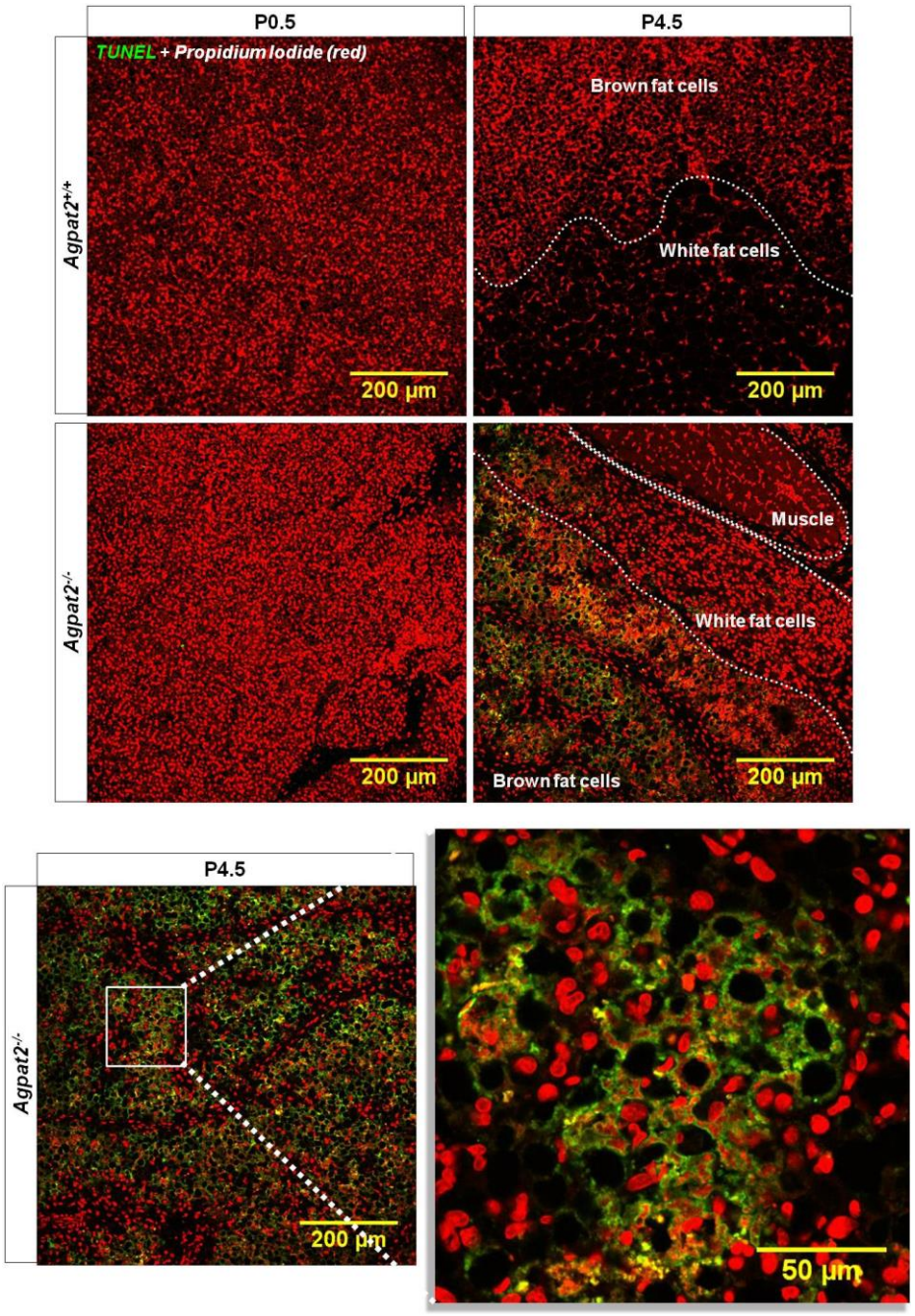

Figure 42: The loss of adipose tissue in *Agapt2*$^{-/-}$ mice is associated with massive accumulation of TUNEL labeled cells. Paraffin-embedded sections of developing adipose tissue from *Agpat2*$^{+/+}$ and *Agpat2*$^{-/-}$ littermates were assessed by TUNEL staining to detect apoptotic cells. Green fluorescence is indicative of TUNEL-positive nuclei while red fluorescence (propidium iodide staining) is indicative of TUNEL-non reactive nuclei. P0 and P4.5 denoted tissues isolated from newborn and 4.5 days-old mice, respectively.

5. DISCUSSION

5.1 General considerations

The aim of this thesis was to characterize the molecular, cellular and *in vivo* mechanisms of adipose tissue deficiency in *Agpat2*$^{-/-}$ mice, with the hope of shedding light on the basic processes that command normal adipose tissue differentiation, growing and remodeling.

Loss of AGPAT2 function result in complete absence of adipose tissue, i.e. lipodystrophy, in humans and mice, but the precise mechanisms responsible for this severe phenotype have not been determined yet. AGPAT2 catalyzes the conversion of LPA to PA, a critical intermediate step in the glycerophospholipid biosynthesis pathway **(Figure 11)**. The simplest and most direct hypothesis for adipose deficiency in *Agpat2*$^{-/-}$ mice is the lack of AGPAT2 precludes TGs synthesis, and thus, leads to "TG-depleted adipocytes". However, gene deletion of upstream or downstream enzymes in the glycerolipid synthesis pathway, such as GPATs and DGATs, although severely decreasing TGs synthesis rate, do not cause lipodystrophy, suggesting that AGPAT2 activity has additional regulatory roles besides the sole TGs biosynthesis. Furthermore, hepatic *de novo* lipogenesis is strongly increased in *Agpat2*$^{-/-}$ mice (2), indicating that other AGPAT isoforms may compensate the AGPAT2 deficiency in terms of TGs generation, at least in hepatocytes.

Thus, our main working hypothesis was that lipodystrophy in *Agpat2*$^{-/-}$ mice most likely results from abnormalities in the differentiation process of adipocyte precursor cells. Previous investigations by others support this notion. Gale et al, reported that siRNA-

induced knockdown of AGPAT2 expression in OP9 cells signficantly delays C/EBPβ gene expression and reduces the mRNA levels of several C/EBPs, PPARγ as well as other adipocyte markers, thus preventing adipogenic differentiation *in vitro* (115). A pathological analysis of 10-day-old AGPAT2 knockout mice found small adipocyte-like cells made by Vogel et al., led these authors to conclude that AGPAT2 might not be required for early adipocytes differentiation (118).

To gain insights on the pathophysiology of AGPAT2-dependent lipodystrophy, I characterized the effects of AGPAT2 deficiency during adipogenic differentiation of primary MEFs cultures. The MEFs experimental system has extensively been used for adipogenesis studies *in vitro* (25). In particular, this model is useful for examining the role of AGPAT2, in which early postnatal lethality together with the complete absence of adipose tissue in adult mice made studies of *in vivo* adipogenesis studies in adult *Agpat2*$^{-/-}$ mice completely impractical. Since MEFs are essentially heterogeneous mixture of primary cells, I first aimed to determine if *Agpat2*$^{-/-}$ and *Agpat2*$^{+/+}$ cultured MEFs had equivalent content of mesenchymal precursors. Importantly, I found that our experimental procedures resulted in MEFs with equal proportion of Sca1+, CD29+, CD44+, CD45- and CD11b- mesenchimal markers in both genotypes **(Figure 13)**. This control was crucial because all the phenotypic differences in terms of adipogenic response could have merely be the result of different proportion of adipogenically competent cells between genotypes. Consequently, after demonstrating that *Agpat2*$^{-/-}$ MEFs have normal mesenchimal components, I used this system to study the impact of AGPAT2 deficiency on adipogenic differentiation program.

In addition, as a second complementary approach to demonstrate my hypothesis I also studied the existence of preadipocytes and adipose tissue in neonatal *Agpat2*$^{-/-}$ mice.

In the next sub-sections I discuss the main results of this work and their implications on the adipose tissue development.

5.2 Adipogenic differentiation of MEFs shows that AGPAT2 is required for normal adipogenesis because it is required for preadipocyte/adipocytes survival

The *in vitro* adipogenesis studies revealed that *Agpat2*$^{-/-}$ MEFs do fail to undergo significant adipocyte differentiation, as indicated by 1) the presence of fewer lipid accumulating cells, with abnormal LDs, 2) lower expression of mature adipocyte-selective markers and TGs content and 3) higher levels of total LPA + PA species.

The blunted expression of C/EBPβ, PPARγ and multiple adipocyte-related proteins as well as the reduced TGs acumulated are consistent with the data previously published by Gale et al. (115). In this thesis, we demonstrate that this aberrant process is owed to premature cell death during MCE, instead of inappropriate induction of key adipogenic transcriptional regulators. In fact, soon after the adipogenic program is hormonally induced, *Agpat2*$^{+/+}$ MEFs actively proliferate for the next 48 hours, resulting is a 3-fold increase in their cell number **(Figure 24A)**. *Agpat2*$^{-/-}$ MEFs also reenter the cell cycle and actively proliferate, however, a significant proportion of them die just few hours after the induction, resulting in null changes in the cell number. Of note, *Agpat2*$^{-/-}$ MEFs cell death only happens if they are adipogenically induced and possibly accounts for the low proportion of PPARγ expressing and lipid-accumulating cells at the end of the differentiation **(Figure 14C)**. In agreement with our results, other investigators have recently reported that the

adipogenic differentiation of cultured muscle-derived multipotent cells (MDMC) isolated from CGL-1 patients, results in significant cell death rate (~18.3% compared with ~10% in control MDMC) after 3 days of adipogenic induction (116).

Therefore, our findings indicate that AGAPT2 is required for differentiating MEFs well before intracellular lipid accumulation becomes apparent. But then another fundamental question automatically arises: *what mechanisms does AGPAT2 play a crucial role in the preadipocyte/adipocyte survival?* To address this question it might be necessary to characterize the full complement of glycerophospholipid species at very early times of adipogenic differentiation in *Agpat2*$^{-/-}$ MEFs. It is likely that dysregulated levels of specific LPA and PA species triggered by AGPAT2 deficiency induce either lack of pro-adipogenic lipid species or accumulation of lipotoxic compounds that determine reduced adipocyte survival and/or growth.

Supporting this idea, it has been shown that the pharmacological inhibition of AGPAT2 significantly decreases the cell proliferation and survival rate of malignant cells in culture, possibly as a result in imbalanced glycerophospholipid cellular content. In fact, AGPAT2 is highly expressed in a wide variety of neoplastic and tumor stroma cells while it is negligible in normal tissue cells and its inhibition results in attenuation of both Ras/Raf/Erk and PI3K/Akt signalling pathways (119-121).

Noteworthly, both ERK and PI3K/Akt signalling pathways are required for normal adipogenesis. I found that Akt and ERK pathways have a very blunted activation during the adipogenic differentiation of *Agpat2*$^{-/-}$ MEFs. Similarly, a reduced Akt phosphorylation was reported in human MDMC of CGL-1 patients after insulin stimulation (116). Frther studies

will be necessary to address the exact mechanisms by which AGPAT2 deficiency determines impaired activation of Akt in adipogenically-induced MEFs.

5.3 Abnormalities in the LD biogenesis and morphology in differentiated *Agpat2*$^{-/-}$ MEFs

Surprisingly and in contradiction with several published studies performed in adipogenic cell lines and human primary MDMCs (116), here I show that an appreciable proportion of *Agpat2*$^{-/-}$ MEFs (~20-30%) do accumulate inrtacelullar neutral lipids and do express all the examined LD-related proteins. Interestingly, these lipid-loaded *Agpat2*$^{-/-}$ cells are much smaller than their wild type controls, in spite of that they express normal levels of PPARγ at the single cell level. At the 10th day of differentiation, however, we noted a reduction in the nuclear abundance of PPARγ in the lipid-loaded *Agpat2*$^{-/-}$ cells and a lower proportion of lipid-loaded cells in comparison with the previous days, suggesting that cell death could be still happening in differentiating cultures of *Agpat2*$^{-/-}$ MEFs.

In the *Agpat2*$^{-/-}$ lipid-loaded cells, Perilipin-1 has an scattered pattern of expression, either in association with LDs or as lipid-free cytoplasmic agreggates. FABP4 and ATGL proteins also have an abnormal intracellular distribution in *Agpat2*$^{-/-}$ differentiating MEFs. The transcriptional expression of all these proteins is regulated by PPARγ and funtionally, they are required for appropriate adipocyte maturation. Perilipin-1 promotes unilocular lipid droplet formation, FABP4 binds intracellular fatty acids and ATGL hydrolyzes TGs stored in the LDs.. Currently, this adipocyte phenotype has never been reported before and leads us to speculate that these "lipodistrophic adipocytes" are nonfunctional because they

undergo an abnormal growth, develop abnormal intracellular distribution of LD-associated proteins and have smaller LD.

Accordingly to the literature, mature adipose LDs arise by two mechanisms: by the fusion or coalescence of small LDs and/or by growth or expansion of smaller-immature LDs. Coalescence is an active process whereby a transient pore is formed beetween two LDs or LD-ER. This mechanism is regulated by the LD monolayer curvature that results from its specific phospholipid composition. If the curvature is positive (as determined by the predominant abundance of positively curved lipids such as LPC, LPA, LPE and others) this results in a frustrated coalescence and the pore is closed. By contrast, if the curvature of the monolayer is negative (as determined by the predominant abundance of negatively curved lipids such as PA, DAG, cholesterol, fatty acids) the fusion between two LDs is favoured (122). Accordingly with this model, a dysregulation in the glycerophospholipid content in *Agpat2*$^{-/-}$ differentiating MEFs could directly affect the formation, growth and stability of the LDs during the adipogenesis and result in the multiple and small LDs observed in these cells in this thesis **(Figure 14b, 19).**

Other recently proposed mechanism by which LDs can growth requires the relocalization of TG-synthesizing enzymes from the ER to LDs (83). Accordingly, there are two subpopulations of LDs: the small ones that appear static and the large ones that grow in size after fatty acid loading. Large LDs grow by addition of TG, synthesized locally by moving de novo TG synthesis enzymes along membrane bridges to the LD surface. In contrast, the LDs that do not acquire these TG enzymes remain small after their initial formation. This recent publication show that depletion of the LD-localized TG synthesis enzymes GPAT4, AGPAT3, and DGAT2 resulted in a reduction of the large LD population

in Drosophila S2 cells treated with oleate. Conversely, depletion of TG-synthesis enzymes that remain localized within the ER during LD formation (e.g., AGPAT1, AGPAT2, AGPAT4, and DGAT1) had not effect on the number of large LDs.

5.4 Defective adipogenesis of *Agpat2*$^{-/-}$ MEFs is partially reversed by PPARγ2 over-expression.

Here we showed that over-expression of PPARγ2 in *Agpat2*$^{-/-}$ MEFs promotes adipocyte phenotype after adipogenic induction, resulting in elevated percentage of lipid-loaded cells with high expression of adipocyte-specific markers. Integrating these observations with the fact that a low porportion of *Agpat2*$^{-/-}$ MEFs can actually form LDs, because early cell death, it is suggested that early events trigger the cell death before that PPARγ can be expressed. Likely, these events depend on the metabolic status of the cells since PPARγ-dependent adipogenesis ocurrs upon completion of MCE in cultured MEFs.

Even though adipocyte phenotype can be partially rescued by PPARγ2 overexpression, differentiating *Agpat2*$^{-/-}$ MEFs cell-size and LDs volumen remained smaller in comparison with their wild type controls, indicating that morphological defects owing to AGPAT2 deficiency are not directly related with PPARγ transcriptional regulation. In fact, dysregulation of intracellular lipid species seems to play a central rol in the cellular remodelling along the adipogenic differentiation. As we have mentioned before (see section 1.4), major glycerophospholipids are derived from PA, which is also an important constituent of cell membranes and, together with LPA, act as potent signaling molecules. Notably, adipogenic induction in 3T3-L1 cells that have suffer *Agpat2* knockdown, results in abnormal levels of all major phospholipids (PC, PE, PI, PS and PA). Therefore, even

thought we have not determined what lipid species directly contribute to the premature cell death in adipogenically induced *Agpat2*$^{-/-}$ MEFs yet, the elevated levels of total PA species (LPA+PA) reflect alterations in the cellular lipid homeostasis, that can induce different forms of cellular stress and abonormal normal cell growth and differentiation.

5.5 *BSCL2* gene expression, the gene mutated in the most severe forms of human CGL and encoding the protein Seipin, is suppressed in differentiating *Agpat2*$^{-/-}$ MEFs.

The complete lack of seipin in adipogenically induced *Agpat2*$^{-/-}$ MEFs was an unexpected finding of this thesis **(Figures 17-18 and 20)**. Seipin is a 462 aminoacids long ER protein (123) with two putative transmembrane domains (124). Mutations in *BSCL2*, the Seipin encoding gene, cause congenital generalized lipodystrophy type 2, the most severe form of lipodystrophy in humans (125). Seipin is widely expressed across tissues, it is abundantly present in adipocytes and its levels are highly regulated during adipogenic differentitation of 3T3L1 cells (126). Indeed, although Seipin functions still remain unknown, its shRNA mediated knock down prevents adipogenic differentiation of cultured preadipocyte cell lines (126). In yeasts, Seipin is localized in the juncture of ER and LDs, and its gene deletion results in irregular lipid droplets often clustered alongside the ER (123). Seipin inactivation in Drosophila and yeasts results in accumulation of PA, whereas its deletion in human lymphoblastoid cell-lines alters the fatty acid composition by decreasing fatty acids desaturation activity (127).

In my thesis studies, I made two novel findings relative to the role of Seipin in the adipogenic differentiation of MEFs. First, I show that Seipin induction during normal adipogenesis absolutely requires functional AGPAT2. As I showed, after 48 hours post-

induction Seipin is highly upregulated at both mRNA and protein levels in *Agpat2*$^{+/+}$ MEFs **(Figure 20).** By contrast, although Seipin mRNA levels remain similar between *Agpat2*$^{-/-}$ and *Agpat2*$^{+/+}$ MEFs during the first 3 days after adipogenic induction, its subsequent induction is completely abrogated in *Agpat2*$^{-/-}$ MEFs. Considering that AGPAT2 deficiency in differentiating MEFs results in abnormal LDs morphology **(Figure 14B, Figure 19)** which is similar to what is observed in FLD1/seipin mutant yeast, we can speculate that the failure of *Agpat2*$^{-/-}$ MEFs to induce Seipin expression during their adipogenic transformation could play a role in the inability of these cells to acquire a mature LD phenotype.

The second relevant observation relative to Seipin biology in this thesis was the extensive co-localization of this protein with Perilipin-1 on LDs surface **(Figure 18)**. Digital reconstruction of confocal imaging of differentiating *Agpat2*$^{+/+}$ MEFs revealed that this potential interaction happens on both small and large LDs **(Figure S2)**. Because the very close physical proximity between LDs and the ER, it will be necessary to use high-resolution microscopy to further characterize the topological properties of this protein-protein interactions. Nonetheless, the lack of Seipin induction can also explain why lipid-loaded cells from differentiating *Agpat2*$^{-/-}$ MEFs have significant clustering of Perilipin-1, even forming LD-free clumps.

It is well known that Perilipin-1, an adipocyte-specific LD-associated protein, is essential for promoting unilocular lipid droplet growth; however, the molecular mechanisms underlying Perilipin-1 actions remain poorly understood. To date, most of the studies regard Perilipin-1 as an exclusively LDs coating protein. However, it has recently been shown that Perilipin-1 also localizes in the ER and the cytosol, from where it is

recruited onto growing LDs (128). Interestingly, in our studies we also observed Perilipin-1 in sub-cellular regions of wild type MEFs away from LDs at early stages of *in vitro* adipogenic differentiation. In fact, when these wild type cells have reached full adipogenic differentiation, Perilipin-1 is only apparent in association with LDs. Considering these finding is noteworthy that Perilipin-1 moves between ER-LDs. Seipin-deficient yeasts inefficiently locate Tgl3p (a TGs lipase) on the surface of LD, supporting the idea that Seipin may control the loading of lipids and possibly proteins into droplets (94). It is unclear, however, whether this defect is secondary to the development of ER-stress associated with Seipin deficiency.

Currently, we are working on the mechanisms linking AGPAT2 with BSCL2 gene expression during adipogenesis and on the pathways that connect the functions of these two lipodystrophy-associated proteins.

5.6 Adipose depots in *Agpat2*$^{-/-}$ mice are lost soon after birth as a result of accelerated cell death and acute adipose inflammation.

We consider that there is a remarkable consistency between our *in vitro* and *in vivo* findings. As we have discussed above, *Agpat2*$^{-/-}$ MEFs seem capable to start the adipogenic differentiation with normal initial changes in the cell-cycle regulation. However, this is soon followed by cell death and abnormal adipogenic differentiation at the gene expression and cellular remodelling level. *In vivo*, we found BAT and WAT depots in embryos and newborn *Agpat2*$^{-/-}$ mice that were morphologically equivalent with the ones in wild type littermates **(Figure 31-32).** However, the existing adipocytes in *Agpat2*$^{-/-}$ mice start to die as soon as the second day after birth, suggesting that signals coming from the maternal milk

or derived from the feeding behavior (nutritional, metabolic, hormonal or neural) somehow results in adipocytes cell death in coincidence with the activation of the postnatal adipogenic program in mice. In fact, multilocular brown adipocytes from *Agpat2*$^{-/-}$ lactating pups (>P1.5) were first turned in hypertrophic unilocular cells and then lately die. Similarly, immature white adipocytes were quickly lost without signs of further maturation

Thus, massive cell death and inflammation of all adipose depots is responsible for the ablation of this tissue in the *Agpat2*$^{-/-}$ mice. Although we did not determine the molecular mechanisms responsible for this acute adipose death in *Agpat2*$^{-/-}$ mice, it is clear that the absence of this enzyme leads a rapid postpartum destruction of adipocytes regardless of different origins and metabolic functions between BAT and WAT.

These findings demonstrated that AGPAT2 has a role on the survival of adipocytes even before lipids accumulate intracellularly. We speculate that adipocytes death might be due to cytotoxic lipid species accumulation not safely stored in LDs or by an imbalanced composition of critical glycerophospholipids.

It is widely accepted that some fatty acids are toxic for adipocytes and that diets supplemented with certain conjugated linoleic acid result in frank lipoatrophy in mice (129). If LDs are unable to expand, it is possible that toxic lipids are accumulated into adipocytes allowing their death. On the other hand, phospholipids are important components of biological membranes and precursors of numerous signaling molecules and also they provide platforms for the vesicle trafficking, signal transduction and biosynthesis. Here, we found that total cellular PA content, including its lyso-precursors, was elevated in adipogenically differentiating *Agpat2*$^{-/-}$ MEFs, suggesting that in presence of AGPAT2,

MEFs rapidly use these species to produce large amounts of glycerolipids required to achieve appropriate adipogenic differentiation.

Therefore, to gain more insight into the physiological role of phospholipids in the regulation of adipogenesis, we performed mass spectrometry and electron microscopy analysis in adipose tissue samples from newborn *Agpat*$^{+/+}$ and *Agpat2*$^{-/-}$ mice. Mass spectrometry analysis revealed elevated levels of Lyso-PC and significant reduction of PI, PG and PA species in BAT from *Agpat2*$^{-/-}$ mice **(Figure S3)**. Furthermore, electron microscopy of white adipocytes showed numerous abnormalities in *Agpat2*$^{-/-}$ mice, such as lack of caveolae, strongly electron-dense granules, dilated organelles, membrane aggregation, cytosolic vacuolation and small LDs **(Figure S4)**, whereas that brown adipocytes from *Agpat2*$^{-/-}$ were also characterized by a reduced proportion of mitochondrias **(Figure S5).** All these abnormal traits observed in the adipose tissue of *Agpat2*$^{-/-}$ mice are consistent with the alterated phospholipid composition and allowing us to postulate a possible mechanism by which the deficiency of AGPAT2 impairs the adipocyte differentiation and survival **(Figure 43-44).**

Finally, adipose tissue inflammation in neonatal *Agpat2*$^{-/-}$ mice could be a physiological mechanism required for clearing the extracellular space of adipocytes debris. In obese mice and humans, white adipose tissue inflammation results when adipose tissue enlargement is not longer capable of buffering the excess nutrient leading a excessive production of free radicals and “ER stress” followed by a vast infiltration of macrophages at sites where adipocytes undergo necrotic-like death (130). Severe inflammation and dramatic macrophage infiltration in white and brown adipose tissue has also recently been also reported in aP2-nSREBP-1c transgenic (Tg) mice which is an established model of

lipodystrophy (131). These mice have elevated levels of proinflamatory cytokines and macrophage infiltration into all adipose tissue depots, suggesting that, the severe adipose tissue inflammation in aP2-nSREBP-1c Tg mice seems to be involved more with a patological adipose tissue remodeling than impaired adipogenesis. Likewise, I showed here that adipogenesis was completely normal in adipogenically induced primary cultures of aP2-nSREBP-1c MEFs **(Figure 14F)**.

In conclusion, in this thesis we demonstrate that early cell death is the primary event responsible for the loss of adipose tissue in the AGPAT2 deficient mice. Our findings suggest that AGPAT2 regulates adipocyte early survival upon adipogenic differentiation and is required for normal LDs biogenesis by allowing the normal gene expression and subcellular distribution of LD associated proteins (**Figures 43**).

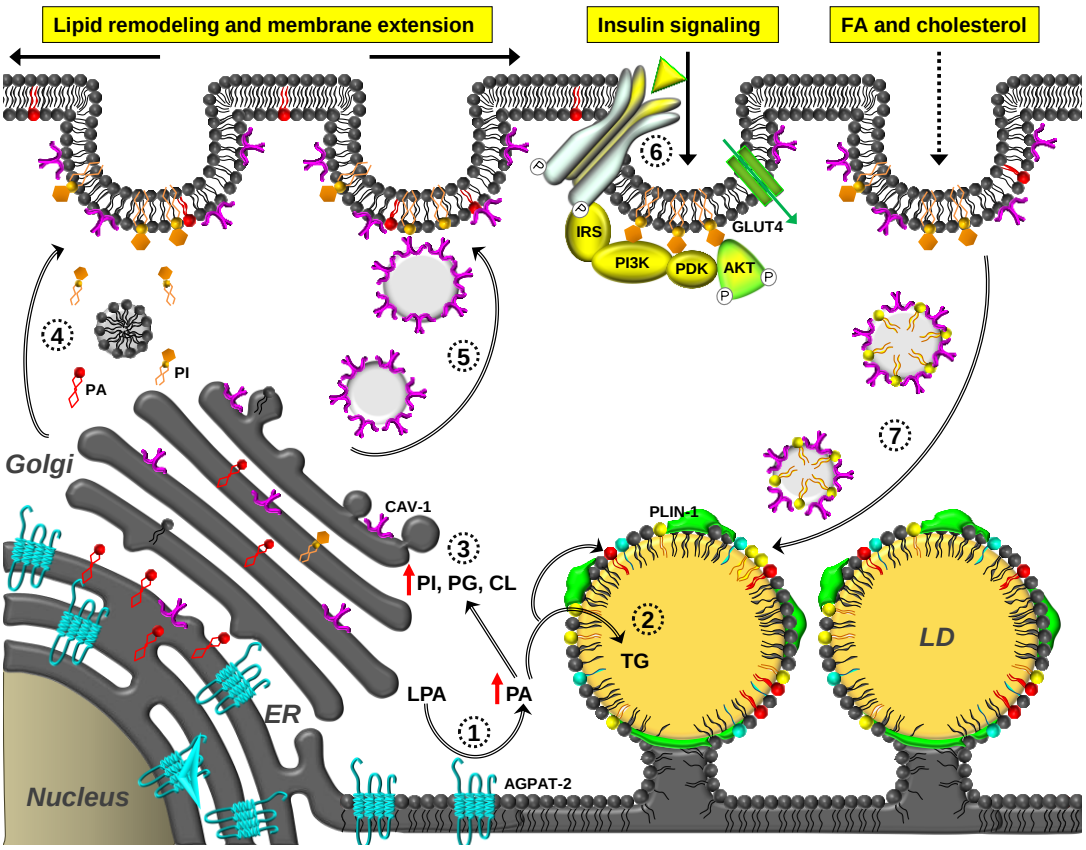

Figure 43. Model for the regulatory role of AGPAT2 on adipocyte differentiation. Consistent with a role in adipogenesis, enzymatic activity of AGPAT2 might promote adipocyte maturation by generating PA substrate for other glycerophospholipid biosynthesis, membrane remodeling and lipid signaling (Step 1). At early adipogenic stages, the enzymes implicated in the *de novo* glycerolipid synthesis pathway, including AGPAT2, produce TGs. These neutral lipids are rapidly stored in nascent lipid droplets (LD) (Step 2). As differentiation progresses, the elevated expression of AGPAT2 induces a massive conversion of LPA to PA for TG and also glycerophospholipid synthesis, mainly phosphatidylinositol (PI) and phosphatidylglycerol (PG), in the endoplasmic reticulum (ER, Step 3). PIs are transported to the plasma membrane where they are used as precursor for phosphoinositides and other signalling lipids, which would facilitate vesicle budding towards the cytosol and mediate the recruitment of vesicle coating proteins that will additionally affect plasma membrane curvature, such as caveolin-1 (CAV-1) and others (Step 4). This lipid and protein plasma membrane remodeling determines the formation of caveolae that appear to be critical for insulin signaling (Step 5). Upon nutritional and hormone signalling, insulin receptors, IRS substrates and downstream kinases are located in caveolae microdomains of plasma membrane, allowing its enhanced tyrosine phosphorylation and enhancement of IR signal transduction (Step 6). In the present model, conical-shaped lipids such PA, unsaturated fatty acids and cholesterol are also incorporated in the LD monolayer favoring a negative spontaneous monolayer curvature which results in coalescence (or fusion), generating large LDs (Step 7).

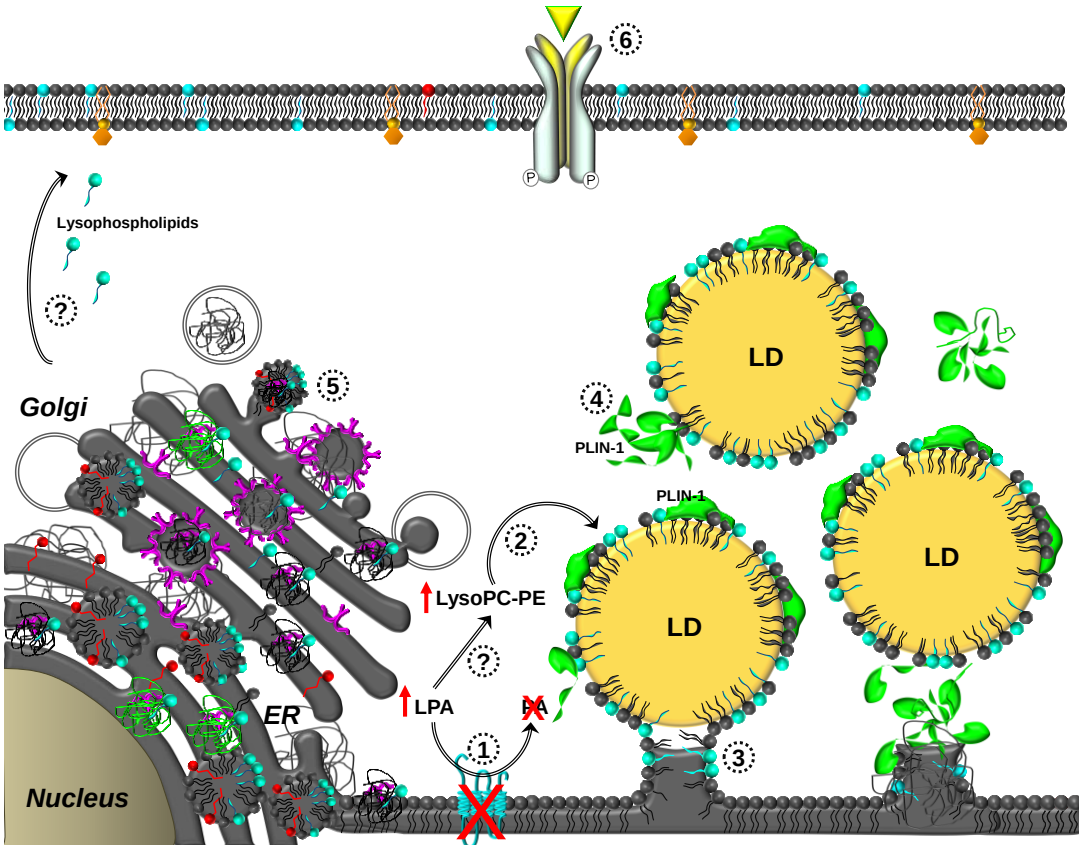

Figure 44: Lack of AGPAT2 impairs the adipocyte development resulting in small lipid-loaded-cells which undergo an early cell death. During fetal life, developing AGPAT2-deficient adipocytes store TGs in small lipid droplets, likely owing to the activity of other AGPATs. After birth, the production of PA decreases markedly and lyso-phospholipids species are accumulated (Step 1). Lysophosphatidylcholine (LysoPC), which could be produced from LPA, is an inverted conical-shaped lipid that favors the formation of positive monolayer curvatures. Therefore, if LysoPC is accumulated in the ER or LD membranes, the pore or bridge between LD-ER or LD-LD is unstable, which induces the early budding and pinching-off of LDs (Step2-3). The resulting LDs have a loose packing of lipids which could restrict the protein targeting to LD monolayer, inducing clustering of LD membrane proteins in the cytosol and ER (Step 4). Accumulation of lipids and proteins in the ER results in an impaired ER transport and function (Step 5). Furthermore, impaired vesicular trafficking and/or inadequate lipid remodeling of the plasma membrane could disrupt caveolae formation thereby permitting a delayed and less efficient IR signal transduction (Step 6).

6. CONCLUDING REMARKS

In this work I have studied the molecular mechanisms underlying the lack of adipose tissue in the AGPAT2 deficient mouse.

As shown here, AGPAT2 deficiency in MEFs, results in an impaired adipogenesis characterized by a reduced proportion of MEFs undergoing neutral lipid accumulation at the end of adipocyte differentiation. These abnormally differentiated *Agpat2*$^{-/-}$ MEFs have smaller size in comparison to wild type control and have scattered and multiple smaller lipid droplets (LDs) with anomalous intracellular distribution of proteins associated with LDs biogenesis and lipid metabolism. Furthermore, the expression of key adipogenic transcription factors (c/EBPs, PPARγ) and mature adipocytes markers is significantly lower in *Agpat2*$^{-/-}$ MEFs at all the time points evaluated. However, single cell confocal analysis showed that nuclear content of PPARγ, the master regulator of adipogenesis, is normal in LDs-containing *Agpat2*$^{-/-}$ MEFs, but is present in a significantly lower proportion of these cells. Moreover, the over-expression of PPARγ2 at the beginning of the differentiation enhances the proportion of *Agpat2*$^{-/-}$ MEFs that are differentiated to adipocyte-like cells but do not amend neither the smaller cell size nor abnormal LDs morphology in *Agpat2*$^{-/-}$ MEFs.

Additionally, we demonstrated by gene expression and confocal analysis that expression of Seipin protein, also associated with human congenital generalized lipodystrophy, is highly induced upon adipogenic differentiation in wild type MEFs and that it colocalizes with Perilipin-1 on the surface of LDs in lipid loaded cells. However, the gene expression of Seipin is severely impaired in differentiated *Agpat2*$^{-/-}$ MEFs, possibly

implicating Seipin deficiency in the pathogenesis of the lipodystrophy dependent on AGPAT2 mutations.

We also identified that the reduced differentiation to adipocyte-like cells in *Agpat2*$^{-/-}$ MEFs is owed to a massive cell death of these cells undergoing after activation of mitotic clonal expansion, upon adipogenic induction and to a reduced activation of Akt pathway, which strongly suggests that impaired adipogenesis in AGPAT2 deficient adipocyte precursors can be resulting from impaired lipid signaling.

Complementing these *in vitro* studies, we analyzed adipose tissue development in *Agpat2*$^{-/-}$ mice. Contradicting our working hypothesis that AGPAT2 deficient mice never develop adipose tissue, detailed histological and gene expression analyses in *Agpat2*$^{-/-}$ embryos and newborn mice showed that both developing subcutaneous WAT and BAT are normal in these mice until the second day after birth. After this period, adipose depots undergo a rapid involution along with a massive adipocytes cell death and macrophage infiltration, which results in complete adipose destruction by the 6th day after birth. These findings indicate that AGPAT2 is absolutely required for the full development, growth and maintenance of adipose tissue during early post natal life in mice and that its deficiency is detrimental for adipocyte survival.

Notably, both our *in vitro* adipogenesis studies in MEFs and our morphological/molecular characterization of adipose tissue in mice, consistently show that AGPAT2 is required for cell survival only after adipogenic induction. It is possible that AGPAT2 plays a critical role in the balance of key glycerolipid metabolite(s) during adipogenic differentiation that is essential for the normal balance between pro-survival/growth and death signals. Additionally, the inability to build normal LDs in

differentiating preadipocytes, should determine cellular stress triggered cell death, possibly through ER stress or lipotoxic pathways.

Future studies will be essential to unveil the exact molecular mechanisms and mediators by which AGPAT2 deficiency results in cell death after adipogenic induction. For this, it will be required to know the full lipidomic composition of differentiating preadipocytes by unbiased lipidomic approaches. The identification of the lipid metabolites that coordinate the transcriptional and cell remodeling events underlying normal and pathologic adipogenic differentiation will open new possibilities for therapeutic manipulation of adipose tissue disorders, including lipodistrophy, common obesity and various other LDs-related diseases, such as fatty liver disease, muscle dystrophy and pancreatic beta-cell dysunction.

7. APPENDIX

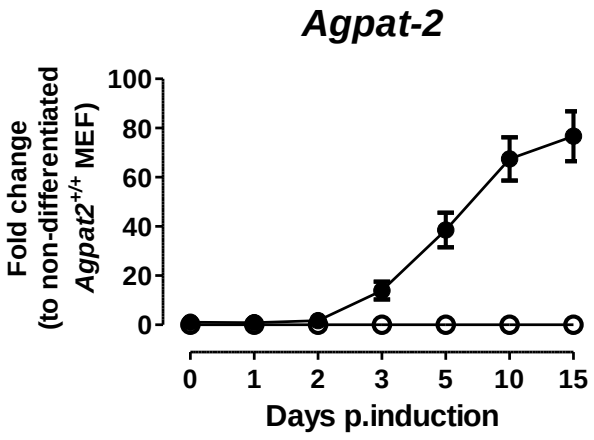

Figure Supplementary 1: Analysis AGPAT2 expression during adipocyte differentiation in wild-type MEFs. (A) qPCR analyze of Seipin mRNA at different days after adipogenic induction. Data were normalized to cyclophilinA and are expressed as relative fold changes compared to non-differentiated *Agpat2*$^{+/+}$ MEFs at day 0.

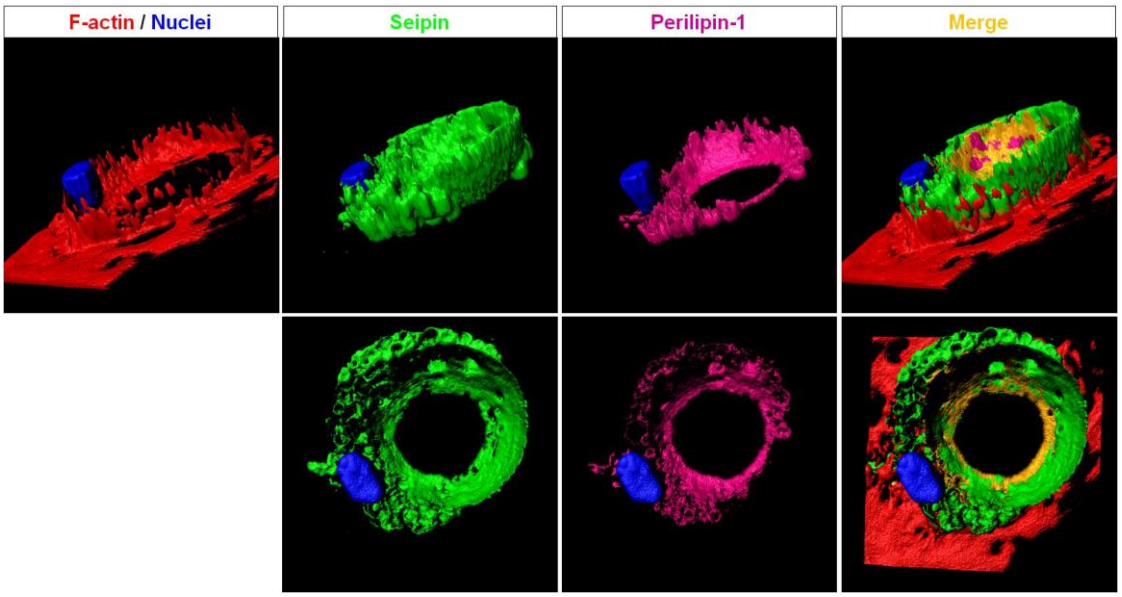

Figure Supplementary 2: Seipin and Perilipin interaction during adipocyte differentiation. Three dimentrional (3D)-views of a wild-type mouse embryonic fibroblast differentiated to adipocyte-like cell shows that ER-localized Seipin (green), an unknown function protein, interacts with Perilipin-1 (yellow merge) at the lipid droplet boundary. Nucleus stained with Hoechst (blue) and F-Actin filamentous with phalloidin (red).

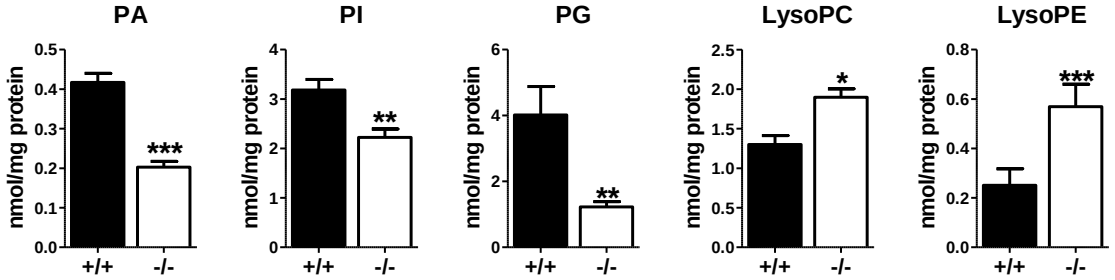

Figure Supplementary 3: Glycerophospholipid analysis in BAT from newborn mice. Total phospholipids were quantified in lipid extracts made from *Agpat2*$^{+/+}$ and *Agpat2*$^{-/-}$ iBAT depots by ESI-MS and normalized to total protein content. PA: phosphatidic acid, PI: phosphatidylinositol, PG: phosphatidylglycerol, LysoPC: lysophosphatidylcholine, LysoPE: lysophosphatidylethanolamine. The bars show the means ± standard deviations of N>5 ***($p<0.001$), **($p<0.01$) and *($p<0.05$) denote significant difference compared to *Agpat2*$^{+/+}$ data.

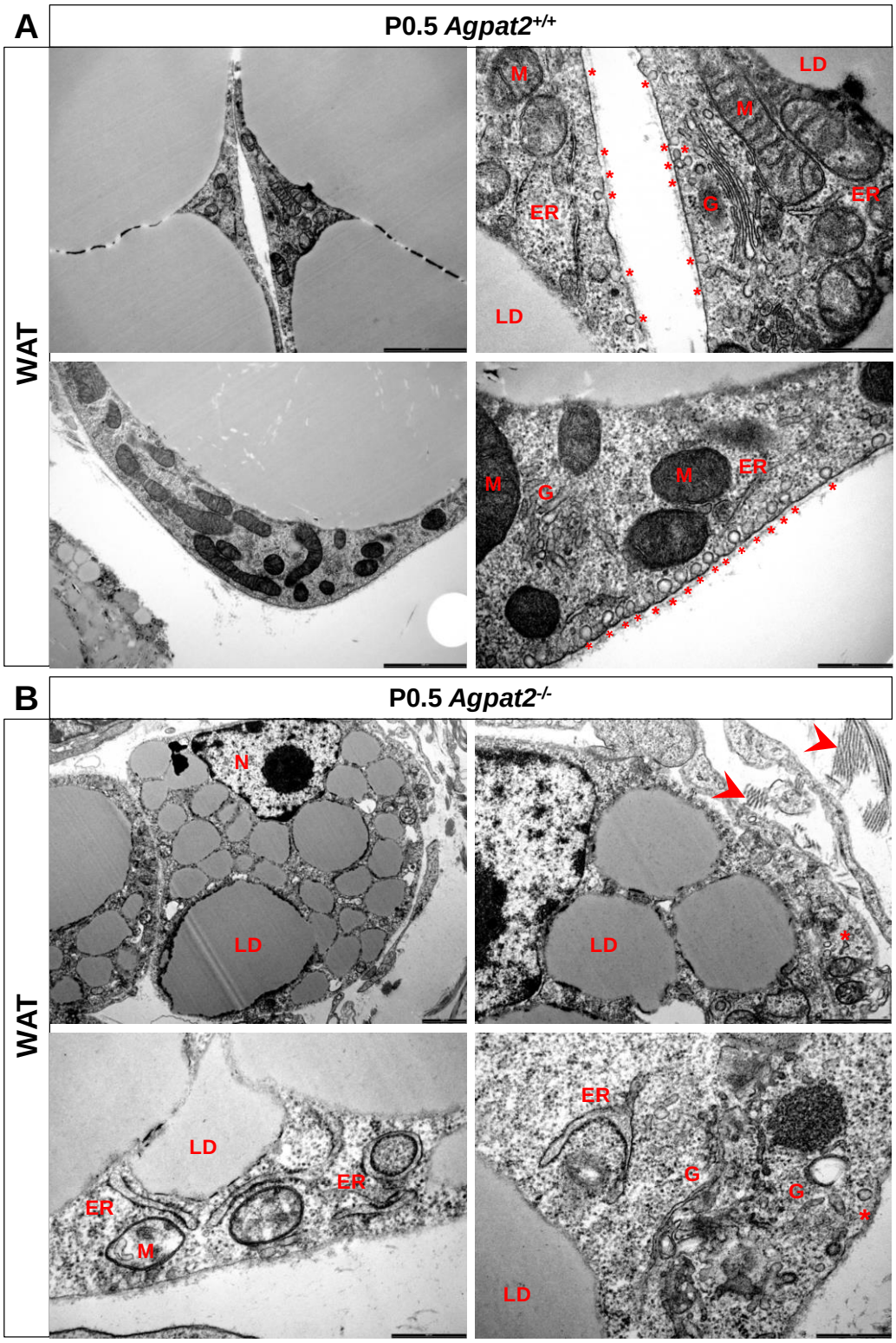
A
P0.5 Agpat2+/+
WAT
M
LD
M
ER
G
ER
LD
M
G
M
ER
B
P0.5 Agpat2-/-
WAT
N
LD
LD
LD
ER
ER
M
ER
G
G
LD

Figure Supplementary 4: Electron microscopy of adipocytes in white adipose tissue from P0.5 mice. (A) Pictures of white adipocytes from subcutaneous WAT of *Agpat2*$^{+/+}$ mice showing large LDs and organelles such as mitochondria (M), ER and Golgi (G) with a well-defined morphology and distribution. High abundance of caveolae are showed as discrete flask-shaped pits (red asterisks). **(B)** White adipocytes from subcutaneous skin of *Agpat2*$^{-/-}$ mice show numerous abnormalities such as cell and LD size, dilated organelles, vacuoles and absolute absence of caveolae at the plasma membrane.

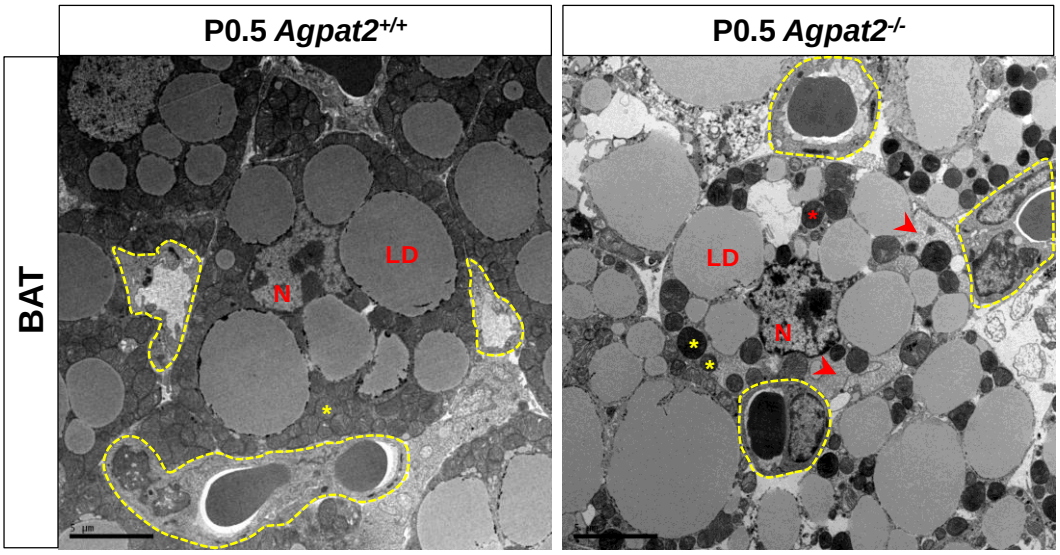

Figure Supplementary 5: Electron microscopy of multilocular adipocytes in brown adipose tissue from P0.5 mice. Pictures show adipocytes of brown adipose tissue and their characteristic mitochondria (yellow asterisks), lipid droplets (LD) and nucleus (N). Capillaries (dotted area) are in close contact with adipocytes. *Agpat2*$^{-/-}$ brown adipocytes have numerous abnormalities such as electron dense mitochondria, dilated ER (red arrowheads) and vacuoles.

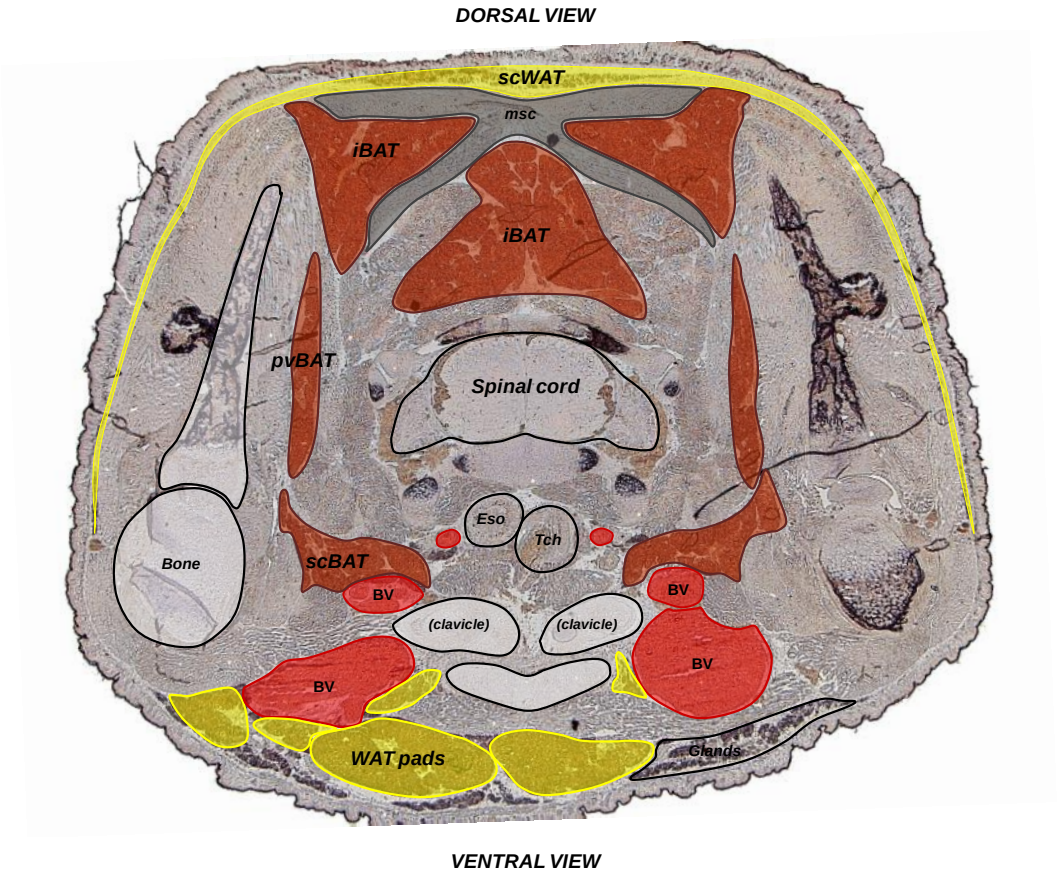

Figure Supplementary 6: Anatomical details of an Oil Red-O and Haematoxylin stained transversal section at the scapular region of P1.5 newborn mice. Yellow and brown color represent white and brown adipose tissue depots, respectively. Red color indicates blood vessels. Bone, muscle and glands also are indicated. scWAT: subcutaneous white adipose tissue, iBAT: interscapular brown adipose tissue, pvBAT: paravertebral BAT, scBAT: supraclavicular BAT. Eso: Esophagus, Tch: Trachea, BV: Blood vessel, Msc: Muscle.

8. REFERENCES

1. Agarwal, A. K., and A. Garg. 2006. Genetic basis of lipodystrophies and management of metabolic complications. *Annu Rev Med* 57:297-311.
2. Cortes, V. A., D. E. Curtis, S. Sukumaran, X. Shao, V. Parameswara, S. Rashid, A. R. Smith, J. Ren, V. Esser, R. E. Hammer, A. K. Agarwal, J. D. Horton, and A. Garg. 2009. Molecular mechanisms of hepatic steatosis and insulin resistance in the AGPAT2-deficient mouse model of congenital generalized lipodystrophy. *Cell Metab* 9:165-176.
3. Gesta, S., Y. H. Tseng, and C. R. Kahn. 2007. Developmental origin of fat: tracking obesity to its source. *Cell* 131:242-256.
4. Cristancho, A. G., and M. A. Lazar. Forming functional fat: a growing understanding of adipocyte differentiation. *Nat Rev Mol Cell Biol* 12:722-734.
5. Cinti, S. 2005. The adipose organ. *Prostaglandins Leukot Essent Fatty Acids* 73:9-15.
6. Hassan, M., N. Latif, and M. Yacoub. Adipose tissue: friend or foe? *Nat Rev Cardiol* 9:689-702.
7. Lee, M. J., Y. Wu, and S. K. Fried. Adipose tissue remodeling in pathophysiology of obesity. *Curr Opin Clin Nutr Metab Care* 13:371-376.
8. Gil, A., J. Olza, M. Gil-Campos, C. Gomez-Llorente, and C. M. Aguilera. Is adipose tissue metabolically different at different sites? *Int J Pediatr Obes* 6 Suppl 1:13-20.
9. Baglioni, S., G. Cantini, G. Poli, M. Francalanci, R. Squecco, A. Di Franco, E. Borgogni, S. Frontera, G. Nesi, F. Liotta, M. Lucchese, G. Perigli, F. Francini, G. Forti, M. Serio, and M. Luconi. Functional differences in visceral and subcutaneous fat pads originate from differences in the adipose stem cell. *PLoS One* 7:e36569.
10. Grundy, S. M., H. B. Brewer, Jr., J. I. Cleeman, S. C. Smith, Jr., and C. Lenfant. 2004. Definition of metabolic syndrome: Report of the National Heart, Lung, and Blood Institute/American Heart Association conference on scientific issues related to definition. *Circulation* 109:433-438.
11. Cinti, S. 2012. The adipose organ at a glance. *Disease models & mechanisms* 5:588-594.
12. Garg, A. 2006. Adipose tissue dysfunction in obesity and lipodystrophy. *Clinical cornerstone* 8 Suppl 4:S7-S13.
13. Norgan, N. G. 1997. The beneficial effects of body fat and adipose tissue in humans. *International journal of obesity and related metabolic disorders : journal of the International Association for the Study of Obesity* 21:738-746.
14. Wells, J. C. 2006. The evolution of human fatness and susceptibility to obesity: an ethological approach. *Biological reviews of the Cambridge Philosophical Society* 81:183-205.
15. Trujillo, M. E., and P. E. Scherer. 2006. Adipose Tissue-Derived Factors: Impact on Health and Disease. *Endocr Rev*:er.2006-0033.
16. Maury, E., and S. M. Brichard. 2010. Adipokine dysregulation, adipose tissue inflammation and metabolic syndrome. *Molecular and cellular endocrinology* 314:1-16.
17. Lidell, M. E., M. J. Betz, O. Dahlqvist Leinhard, M. Heglind, L. Elander, M. Slawik, T. Mussack, D. Nilsson, T. Romu, P. Nuutila, K. A. Virtanen, F. Beuschlein, A. Persson, M. Borga, and S. Enerback. Evidence for two types of brown adipose tissue in humans. *Nat Med* 19:631-634.

18. Virtanen, K. A., M. E. Lidell, J. Orava, M. Heglind, R. Westergren, T. Niemi, M. Taittonen, J. Laine, N. J. Savisto, S. Enerback, and P. Nuutila. 2009. Functional brown adipose tissue in healthy adults. *The New England journal of medicine* 360:1518-1525.
19. Cypess, A. M., S. Lehman, G. Williams, I. Tal, D. Rodman, A. B. Goldfine, F. C. Kuo, E. L. Palmer, Y. H. Tseng, A. Doria, G. M. Kolodny, and C. R. Kahn. 2009. Identification and importance of brown adipose tissue in adult humans. *N Engl J Med* 360:1509-1517.
20. van der Lans, A. A., J. Hoeks, B. Brans, G. H. Vijgen, M. G. Visser, M. J. Vosselman, J. Hansen, J. A. Jorgensen, J. Wu, F. M. Mottaghy, P. Schrauwen, and W. D. van Marken Lichtenbelt. 2013. Cold acclimation recruits human brown fat and increases nonshivering thermogenesis. *J Clin Invest* 123:3395-3403.
21. Yoneshiro, T., S. Aita, M. Matsushita, T. Kayahara, T. Kameya, Y. Kawai, T. Iwanaga, and M. Saito. 2013. Recruited brown adipose tissue as an antiobesity agent in humans. *J Clin Invest* 123:3404-3408.
22. Stanford, K. I., R. J. Middelbeek, K. L. Townsend, D. An, E. B. Nygaard, K. M. Hitchcox, K. R. Markan, K. Nakano, M. F. Hirshman, Y. H. Tseng, and L. J. Goodyear. 2013. Brown adipose tissue regulates glucose homeostasis and insulin sensitivity. *J Clin Invest* 123:215-223.
23. Tam, C. S., V. Lecoultre, and E. Ravussin. 2012. Brown adipose tissue: mechanisms and potential therapeutic targets. *Circulation* 125:2782-2791.
24. Cannon, B., and J. Nedergaard. 2004. Brown adipose tissue: function and physiological significance. *Physiological reviews* 84:277-359.
25. Rosen, E. D., and O. A. MacDougald. 2006. Adipocyte differentiation from the inside out. *Nat Rev Mol Cell Biol* 7:885-896.
26. Lowe, C. E., S. O'Rahilly, and J. J. Rochford. Adipogenesis at a glance. *J Cell Sci* 124:2681-2686.
27. Tang, Q. Q., and M. D. Lane. Adipogenesis: from stem cell to adipocyte. *Annu Rev Biochem* 81:715-736.
28. Rosen, E. D., and O. A. MacDougald. 2006. Adipocyte differentiation from the inside out. *Nat Rev Mol Cell Biol* 7:885-896.
29. Lefterova, M. I., and M. A. Lazar. 2009. New developments in adipogenesis. *Trends in Endocrinology & Metabolism* 20:107-114.
30. Spalding, K. L., E. Arner, P. O. Westermark, S. Bernard, B. A. Buchholz, O. Bergmann, L. Blomqvist, J. Hoffstedt, E. Naslund, T. Britton, H. Concha, M. Hassan, M. Ryden, J. Frisen, and P. Arner. 2008. Dynamics of fat cell turnover in humans. *Nature* 453:783-787.
31. Cawthorn, W. P., E. L. Scheller, and O. A. MacDougald. 2012. Adipose tissue stem cells meet preadipocyte commitment: going back to the future. *Journal of lipid research* 53:227-246.
32. Christodoulides, C., C. Lagathu, J. K. Sethi, and A. Vidal-Puig. 2009. Adipogenesis and WNT signalling. *Trends Endocrinol Metab* 20:16-24.
33. Wang, Y., and H. S. Sul. 2009. Pref-1 regulates mesenchymal cell commitment and differentiation through Sox9. *Cell metabolism* 9:287-302.
34. Sul, H. S. 2009. Minireview: Pref-1: role in adipogenesis and mesenchymal cell fate. *Mol Endocrinol* 23:1717-1725.
35. Rodeheffer, M. S., K. Birsoy, and J. M. Friedman. 2008. Identification of white adipocyte progenitor cells in vivo. *Cell* 135:240-249.

36. Tang, W., D. Zeve, J. M. Suh, D. Bosnakovski, M. Kyba, R. E. Hammer, M. D. Tallquist, and J. M. Graff. 2008. White fat progenitor cells reside in the adipose vasculature. *Science* 322:583-586.
37. Gupta, R. K., Z. Arany, P. Seale, R. J. Mepani, L. Ye, H. M. Conroe, Y. A. Roby, H. Kulaga, R. R. Reed, and B. M. Spiegelman. Transcriptional control of preadipocyte determination by Zfp423. *Nature* 464:619-623.
38. Farmer, S. R. 2006. Transcriptional control of adipocyte formation. *Cell metabolism* 4:263-273.
39. Tang, Q. Q., T. C. Otto, and M. D. Lane. 2003. Mitotic clonal expansion: a synchronous process required for adipogenesis. *Proc Natl Acad Sci U S A* 100:44-49.
40. Tang, Q. Q., and M. D. Lane. 1999. Activation and centromeric localization of CCAAT/enhancer-binding proteins during the mitotic clonal expansion of adipocyte differentiation. *Genes Dev* 13:2231-2241.
41. Tang, Q. Q., T. C. Otto, and M. D. Lane. 2003. CCAAT/enhancer-binding protein beta is required for mitotic clonal expansion during adipogenesis. *Proc Natl Acad Sci U S A* 100:850-855.
42. Morrison, R. F., and S. R. Farmer. 1999. Role of PPARgamma in regulating a cascade expression of cyclin-dependent kinase inhibitors, p18(INK4c) and p21(Waf1/Cip1), during adipogenesis. *J Biol Chem* 274:17088-17097.
43. Patel, Y. M., and M. D. Lane. 2000. Mitotic clonal expansion during preadipocyte differentiation: calpain-mediated turnover of p27. *J Biol Chem* 275:17653-17660.
44. Fajas, L., R. L. Landsberg, Y. Huss-Garcia, C. Sardet, J. A. Lees, and J. Auwerx. 2002. E2Fs regulate adipocyte differentiation. *Dev Cell* 3:39-49.
45. Rosen, E. D., C. H. Hsu, X. Wang, S. Sakai, M. W. Freeman, F. J. Gonzalez, and B. M. Spiegelman. 2002. C/EBPalpha induces adipogenesis through PPARgamma: a unified pathway. *Genes Dev* 16:22-26.
46. Lefterova, M. I., Y. Zhang, D. J. Steger, M. Schupp, J. Schug, A. Cristancho, D. Feng, D. Zhuo, C. J. Stoeckert, Jr., X. S. Liu, and M. A. Lazar. 2008. PPARgamma and C/EBP factors orchestrate adipocyte biology via adjacent binding on a genome-wide scale. *Genes Dev* 22:2941-2952.
47. Wu, Z., E. D. Rosen, R. Brun, S. Hauser, G. Adelmant, A. E. Troy, C. McKeon, G. J. Darlington, and B. M. Spiegelman. 1999. Cross-regulation of C/EBP alpha and PPAR gamma controls the transcriptional pathway of adipogenesis and insulin sensitivity. *Mol Cell* 3:151-158.
48. Tontonoz, P., E. Hu, and B. M. Spiegelman. 1994. Stimulation of adipogenesis in fibroblasts by PPAR gamma 2, a lipid-activated transcription factor. *Cell* 79:1147-1156.
49. Lefterova, M. I., and M. A. Lazar. 2009. New developments in adipogenesis. *Trends in endocrinology and metabolism: TEM* 20:107-114.
50. McIntyre, T. M., A. V. Pontsler, A. R. Silva, A. St Hilaire, Y. Xu, J. C. Hinshaw, G. A. Zimmerman, K. Hama, J. Aoki, H. Arai, and G. D. Prestwich. 2003. Identification of an intracellular receptor for lysophosphatidic acid (LPA): LPA is a transcellular PPARgamma agonist. *Proc Natl Acad Sci U S A* 100:131-136.
51. Zhu, Y., C. Qi, J. R. Korenberg, X. N. Chen, D. Noya, M. S. Rao, and J. K. Reddy. 1995. Structural organization of mouse peroxisome proliferator-activated receptor gamma (mPPAR gamma) gene: alternative promoter use and different splicing yield two mPPAR gamma isoforms. *Proc Natl Acad Sci U S A* 92:7921-7925.

52. Vidal-Puig, A., M. Jimenez-Linan, B. B. Lowell, A. Hamann, E. Hu, B. Spiegelman, J. S. Flier, and D. E. Moller. 1996. Regulation of PPAR gamma gene expression by nutrition and obesity in rodents. *J Clin Invest* 97:2553-2561.
53. Vidal-Puig, A. J., R. V. Considine, M. Jimenez-Linan, A. Werman, W. J. Pories, J. F. Caro, and J. S. Flier. 1997. Peroxisome proliferator-activated receptor gene expression in human tissues. Effects of obesity, weight loss, and regulation by insulin and glucocorticoids. *J Clin Invest* 99:2416-2422.
54. Stapleton, C. M., D. G. Mashek, S. Wang, C. A. Nagle, G. W. Cline, P. Thuillier, L. M. Leesnitzer, L. O. Li, J. B. Stimmel, G. I. Shulman, and R. A. Coleman. Lysophosphatidic acid activates peroxisome proliferator activated receptor-gamma in CHO cells that over-express glycerol 3-phosphate acyltransferase-1. *PLoS One* 6:e18932.
55. Itoh, T., L. Fairall, K. Amin, Y. Inaba, A. Szanto, B. L. Balint, L. Nagy, K. Yamamoto, and J. W. Schwabe. 2008. Structural basis for the activation of PPARgamma by oxidized fatty acids. *Nat Struct Mol Biol* 15:924-931.
56. Waku, T., T. Shiraki, T. Oyama, Y. Fujimoto, K. Maebara, N. Kamiya, H. Jingami, and K. Morikawa. 2009. Structural insight into PPARgamma activation through covalent modification with endogenous fatty acids. *J Mol Biol* 385:188-199.
57. Altmann, R., M. Hausmann, T. Spottl, M. Gruber, A. W. Bull, K. Menzel, D. Vogl, H. Herfarth, J. Scholmerich, W. Falk, and G. Rogler. 2007. 13-Oxo-ODE is an endogenous ligand for PPARgamma in human colonic epithelial cells. *Biochem Pharmacol* 74:612-622.
58. Fernández-Real, J. M. M.-N. a. J. M. 2012. Adipocyte Differentiation. In *Adipose Tissue Biology*. M. E. Symonds, ed.
59. Tontonoz, P., and B. M. Spiegelman. 2008. Fat and beyond: the diverse biology of PPARgamma. *Annu Rev Biochem* 77:289-312.
60. Barak, Y., M. C. Nelson, E. S. Ong, Y. Z. Jones, P. Ruiz-Lozano, K. R. Chien, A. Koder, and R. M. Evans. 1999. PPAR gamma is required for placental, cardiac, and adipose tissue development. *Mol Cell* 4:585-595.
61. He, W., Y. Barak, A. Hevener, P. Olson, D. Liao, J. Le, M. Nelson, E. Ong, J. M. Olefsky, and R. M. Evans. 2003. Adipose-specific peroxisome proliferator-activated receptor gamma knockout causes insulin resistance in fat and liver but not in muscle. *Proc Natl Acad Sci U S A* 100:15712-15717.
62. Jones, J. R., C. Barrick, K. A. Kim, J. Lindner, B. Blondeau, Y. Fujimoto, M. Shiota, R. A. Kesterson, B. B. Kahn, and M. A. Magnuson. 2005. Deletion of PPARgamma in adipose tissues of mice protects against high fat diet-induced obesity and insulin resistance. *Proc Natl Acad Sci U S A* 102:6207-6212.
63. Koutnikova, H., T. A. Cock, M. Watanabe, S. M. Houten, M. F. Champy, A. Dierich, and J. Auwerx. 2003. Compensation by the muscle limits the metabolic consequences of lipodystrophy in PPAR gamma hypomorphic mice. *Proc Natl Acad Sci U S A* 100:14457-14462.
64. Zhang, J., M. Fu, T. Cui, C. Xiong, K. Xu, W. Zhong, Y. Xiao, D. Floyd, J. Liang, E. Li, Q. Song, and Y. E. Chen. 2004. Selective disruption of PPARgamma 2 impairs the development of adipose tissue and insulin sensitivity. *Proc Natl Acad Sci U S A* 101:10703-10708.
65. Agarwal, A. K., and A. Garg. 2002. A novel heterozygous mutation in peroxisome proliferator-activated receptor-gamma gene in a patient with familial partial lipodystrophy. *The Journal of clinical endocrinology and metabolism* 87:408-411.

66. Hegele, R. A., H. Cao, C. Frankowski, S. T. Mathews, and T. Leff. 2002. PPARG F388L, a transactivation-deficient mutant, in familial partial lipodystrophy. *Diabetes* 51:3586-3590.
67. Jeninga, E. H., O. van Beekum, A. D. van Dijk, N. Hamers, B. I. Hendriks-Stegeman, A. M. Bonvin, R. Berger, and E. Kalkhoven. 2007. Impaired peroxisome proliferator-activated receptor gamma function through mutation of a conserved salt bridge (R425C) in familial partial lipodystrophy. *Mol Endocrinol* 21:1049-1065.
68. Ludtke, A., J. Buettner, H. H. Schmidt, and H. J. Worman. 2007. New PPARG mutation leads to lipodystrophy and loss of protein function that is partially restored by a synthetic ligand. *J Med Genet* 44:e88.
69. Jeninga, E. H., M. Gurnell, and E. Kalkhoven. 2009. Functional implications of genetic variation in human PPARgamma. *Trends Endocrinol Metab* 20:380-387.
70. Deeb, S. S., L. Fajas, M. Nemoto, J. Pihlajamaki, L. Mykkanen, J. Kuusisto, M. Laakso, W. Fujimoto, and J. Auwerx. 1998. A Pro12Ala substitution in PPARgamma2 associated with decreased receptor activity, lower body mass index and improved insulin sensitivity. *Nat Genet* 20:284-287.
71. Tsai, Y. S., H. J. Kim, N. Takahashi, H. S. Kim, J. R. Hagaman, J. K. Kim, and N. Maeda. 2004. Hypertension and abnormal fat distribution but not insulin resistance in mice with P465L PPARgamma. *J Clin Invest* 114:240-249.
72. Walther, T. C., and R. V. Farese, Jr. 2012. Lipid droplets and cellular lipid metabolism. *Annual review of biochemistry* 81:687-714.
73. Murphy, D. J. 2001. The biogenesis and functions of lipid bodies in animals, plants and microorganisms. *Prog Lipid Res* 40:325-438.
74. Reue, K. A thematic review series: lipid droplet storage and metabolism: from yeast to man. *Journal of lipid research* 52:1865-1868.
75. Farese, R. V., Jr., and T. C. Walther. 2009. Lipid droplets finally get a little R-E-S-P-E-C-T. *Cell* 139:855-860.
76. Ohsaki, Y., J. Cheng, M. Suzuki, Y. Shinohara, A. Fujita, and T. Fujimoto. 2009. Biogenesis of cytoplasmic lipid droplets: from the lipid ester globule in the membrane to the visible structure. *Biochim Biophys Acta* 1791:399-407.
77. Bickel, P. E., J. T. Tansey, and M. A. Welte. 2009. PAT proteins, an ancient family of lipid droplet proteins that regulate cellular lipid stores. *Biochim Biophys Acta* 1791:419-440.
78. Ducharme, N. A., and P. E. Bickel. 2008. Lipid droplets in lipogenesis and lipolysis. *Endocrinology* 149:942-949.
79. Walther, T. C., and R. V. Farese, Jr. Lipid droplets and cellular lipid metabolism. *Annu Rev Biochem* 81:687-714.
80. Yang, L., Y. Ding, Y. Chen, S. Zhang, C. Huo, Y. Wang, J. Yu, P. Zhang, H. Na, H. Zhang, Y. Ma, and P. Liu. The proteomics of lipid droplets: structure, dynamics, and functions of the organelle conserved from bacteria to humans. *Journal of lipid research* 53:1245-1253.
81. Brasaemle, D. L., G. Dolios, L. Shapiro, and R. Wang. 2004. Proteomic analysis of proteins associated with lipid droplets of basal and lipolytically stimulated 3T3-L1 adipocytes. *J Biol Chem* 279:46835-46842.
82. Stone, S. J., M. C. Levin, P. Zhou, J. Han, T. C. Walther, and R. V. Farese, Jr. 2009. The endoplasmic reticulum enzyme DGAT2 is found in mitochondria-associated membranes and has a mitochondrial targeting signal that promotes its association with mitochondria. *The Journal of biological chemistry* 284:5352-5361.

83. Wilfling, F., H. Wang, J. T. Haas, N. Krahmer, T. J. Gould, A. Uchida, J. X. Cheng, M. Graham, R. Christiano, F. Frohlich, X. Liu, K. K. Buhman, R. A. Coleman, J. Bewersdorf, R. V. Farese, Jr., and T. C. Walther. Triacylglycerol synthesis enzymes mediate lipid droplet growth by relocalizing from the ER to lipid droplets. *Dev Cell* 24:384-399.
84. Agarwal, A. K., and A. Garg. 2003. Congenital generalized lipodystrophy: significance of triglyceride biosynthetic pathways. *Trends in endocrinology and metabolism: TEM* 14:214-221.
85. Ahmadian, M., R. E. Duncan, K. Jaworski, E. Sarkadi-Nagy, and H. S. Sul. 2007. Triacylglycerol metabolism in adipose tissue. *Future Lipidol* 2:229-237.
86. Tauchi-Sato, K., S. Ozeki, T. Houjou, R. Taguchi, and T. Fujimoto. 2002. The surface of lipid droplets is a phospholipid monolayer with a unique Fatty Acid composition. *J Biol Chem* 277:44507-44512.
87. Kuerschner, L., C. Moessinger, and C. Thiele. 2008. Imaging of lipid biosynthesis: how a neutral lipid enters lipid droplets. *Traffic* 9:338-352.
88. Harris, C. A., J. T. Haas, R. S. Streeper, S. J. Stone, M. Kumari, K. Yang, X. Han, N. Brownell, R. W. Gross, R. Zechner, and R. V. Farese, Jr. DGAT enzymes are required for triacylglycerol synthesis and lipid droplets in adipocytes. *Journal of lipid research* 52:657-667.
89. Gonzalez-Baro, M. R., T. M. Lewin, and R. A. Coleman. 2007. Regulation of Triglyceride Metabolism. II. Function of mitochondrial GPAT1 in the regulation of triacylglycerol biosynthesis and insulin action. *Am J Physiol Gastrointest Liver Physiol* 292:G1195-1199.
90. Vergnes, L., A. P. Beigneux, R. Davis, S. M. Watkins, S. G. Young, and K. Reue. 2006. Agpat6 deficiency causes subdermal lipodystrophy and resistance to obesity. *Journal of lipid research* 47:745-754.
91. Agarwal, A. K. Lysophospholipid acyltransferases: 1-acylglycerol-3-phosphate O-acyltransferases. From discovery to disease. *Curr Opin Lipidol* 23:290-302.
92. Peterfy, M., J. Phan, P. Xu, and K. Reue. 2001. Lipodystrophy in the fld mouse results from mutation of a new gene encoding a nuclear protein, lipin. *Nat Genet* 27:121-124.
93. Harris, C. A., J. T. Haas, R. S. Streeper, S. J. Stone, M. Kumari, K. Yang, X. Han, N. Brownell, R. W. Gross, R. Zechner, and R. V. Farese. 2011. DGAT enzymes are required for triacylglycerol synthesis and lipid droplets in adipocytes. *J Lipid Res* 52:657-667.
94. Cartwright, B. R., and J. M. Goodman. 2012. Seipin: from human disease to molecular mechanism. *Journal of lipid research* 53:1042-1055.
95. Smith, S. J., S. Cases, D. R. Jensen, H. C. Chen, E. Sande, B. Tow, D. A. Sanan, J. Raber, R. H. Eckel, and R. V. Farese, Jr. 2000. Obesity resistance and multiple mechanisms of triglyceride synthesis in mice lacking Dgat. *Nature genetics* 25:87-90.
96. Garg, A. 2011. Lipodystrophies: Genetic and Acquired Body Fat Disorders. *J Clin Endocr Metab* 96:3313-3325.
97. Garg, A. Clinical review#: Lipodystrophies: genetic and acquired body fat disorders. *J Clin Endocrinol Metab* 96:3313-3325.
98. Rother, K. I., and R. J. Brown. Novel Forms of Lipodystrophy: Why should we care? *Diabetes Care* 36:2142-2145.
99. Domingo, P., V. Estrada, J. Lopez-Aldeguer, F. Villaroya, and E. Martinez. Fat redistribution syndromes associated with HIV-1 infection and combination antiretroviral therapy. *AIDS Rev* 14:112-123.
100. Agarwal, A. K., V. Simha, E. A. Oral, S. A. Moran, P. Gorden, S. O'Rahilly, Z. Zaidi, F. Gurakan, S. A. Arslanian, A. Klar, A. Ricker, N. H. White, L. Bindl, K. Herbst, K. Kennel, S. B.

Patel, L. Al-Gazali, and A. Garg. 2003. Phenotypic and genetic heterogeneity in congenital generalized lipodystrophy. *The Journal of clinical endocrinology and metabolism* 88:4840-4847.

101. Agarwal, A. K., R. I. Barnes, and A. Garg. 2004. Genetic basis of congenital generalized lipodystrophy. *International journal of obesity and related metabolic disorders : journal of the International Association for the Study of Obesity* 28:336-339.
102. Van Maldergem, L., J. Magre, T. E. Khallouf, T. Gedde-Dahl, Jr., M. Delepine, O. Trygstad, E. Seemanova, T. Stephenson, C. S. Albott, F. Bonnici, V. R. Panz, J. L. Medina, P. Bogalho, F. Huet, S. Savasta, A. Verloes, J. J. Robert, H. Loret, M. De Kerdanet, N. Tubiana-Rufi, A. Megarbane, J. Maassen, M. Polak, D. Lacombe, C. R. Kahn, E. L. Silveira, F. H. D'Abronzo, F. Grigorescu, M. Lathrop, J. Capeau, and S. O'Rahilly. 2002. Genotype-phenotype relationships in Berardinelli-Seip congenital lipodystrophy. *J Med Genet* 39:722-733.
103. Ostermeyer, A. G., J. M. Paci, Y. Zeng, D. M. Lublin, S. Munro, and D. A. Brown. 2001. Accumulation of caveolin in the endoplasmic reticulum redirects the protein to lipid storage droplets. *J Cell Biol* 152:1071-1078.
104. Razani, B., and M. P. Lisanti. 2001. Caveolin-deficient mice: insights into caveolar function human disease. *J Clin Invest* 108:1553-1561.
105. Razani, B., T. P. Combs, X. B. Wang, P. G. Frank, D. S. Park, R. G. Russell, M. Li, B. Tang, L. A. Jelicks, P. E. Scherer, and M. P. Lisanti. 2002. Caveolin-1-deficient mice are lean, resistant to diet-induced obesity, and show hypertriglyceridemia with adipocyte abnormalities. *J Biol Chem* 277:8635-8647.
106. Hill, M. M., M. Bastiani, R. Luetterforst, M. Kirkham, A. Kirkham, S. J. Nixon, P. Walser, D. Abankwa, V. M. Oorschot, S. Martin, J. F. Hancock, and R. G. Parton. 2008. PTRF-Cavin, a conserved cytoplasmic protein required for caveola formation and function. *Cell* 132:113-124.
107. Liu, L., and P. F. Pilch. 2008. A critical role of cavin (polymerase I and transcript release factor) in caveolae formation and organization. *J Biol Chem* 283:4314-4322.
108. Liu, L., D. Brown, M. McKee, N. K. Lebrasseur, D. Yang, K. H. Albrecht, K. Ravid, and P. F. Pilch. 2008. Deletion of Cavin/PTRF causes global loss of caveolae, dyslipidemia, and glucose intolerance. *Cell metabolism* 8:310-317.
109. Agarwal, A. K., S. Sukumaran, V. A. Cortes, K. Tunison, D. Mizrachi, S. Sankella, R. D. Gerard, J. D. Horton, and A. Garg. 2011. Human 1-acylglycerol-3-phosphate O-acyltransferase isoforms 1 and 2: biochemical characterization and inability to rescue hepatic steatosis in Agpat2(-/-) gene lipodystrophic mice. *The Journal of biological chemistry* 286:37676-37691.
110. Agarwal, A. K. 2012. Lysophospholipid acyltransferases: 1-acylglycerol-3-phosphate O-acyltransferases. From discovery to disease. *Current opinion in lipidology* 23:290-302.
111. Takeuchi, K., and K. Reue. 2009. Biochemistry, physiology, and genetics of GPAT, AGPAT, and lipin enzymes in triglyceride synthesis. *Am J Physiol Endocrinol Metab* 296:E1195-1209.
112. Simon, M. F., D. Daviaud, J. P. Pradere, S. Gres, C. Guigne, M. Wabitsch, J. Chun, P. Valet, and J. S. Saulnier-Blache. 2005. Lysophosphatidic acid inhibits adipocyte differentiation via lysophosphatidic acid 1 receptor-dependent down-regulation of peroxisome proliferator-activated receptor gamma2. *J Biol Chem* 280:14656-14662.

113. Zhang, P., K. Takeuchi, L. S. Csaki, and K. Reue. Lipin-1 phosphatidic phosphatase activity modulates phosphatidate levels to promote peroxisome proliferator-activated receptor gamma (PPARgamma) gene expression during adipogenesis. *J Biol Chem* 287:3485-3494.
114. Tsukahara, T., S. Hanazawa, T. Kobayashi, Y. Iwamoto, and K. Murakami-Murofushi. Cyclic phosphatidic acid decreases proliferation and survival of colon cancer cells by inhibiting peroxisome proliferator-activated receptor gamma. *Prostaglandins Other Lipid Mediat* 93:126-133.
115. Gale, S. E., A. Frolov, X. Han, P. E. Bickel, L. Cao, A. Bowcock, J. E. Schaffer, and D. S. Ory. 2006. A regulatory role for 1-acylglycerol-3-phosphate-O-acyltransferase 2 in adipocyte differentiation. *The Journal of biological chemistry* 281:11082-11089.
116. Subauste, A. R., A. K. Das, X. Li, B. G. Elliott, C. Evans, M. El Azzouny, M. Treutelaar, E. Oral, T. Leff, and C. F. Burant. Alterations in lipid signaling underlie lipodystrophy secondary to AGPAT2 mutations. *Diabetes* 61:2922-2931.
117. Laplante, M., S. Horvat, W. T. Festuccia, K. Birsoy, Z. Prevorsek, A. Efeyan, and D. M. Sabatini. 2012. DEPTOR cell-autonomously promotes adipogenesis, and its expression is associated with obesity. *Cell metabolism* 16:202-212.
118. Vogel, P., R. Read, G. Hansen, J. Wingert, C. M. Dacosta, L. M. Buhring, and M. Shadoan. Pathology of congenital generalized lipodystrophy in Agpat2-/- mice. *Vet Pathol* 48:642-654.
119. Coon, M., A. Ball, J. Pound, S. Ap, D. Hollenback, T. White, J. Tulinsky, L. Bonham, D. K. Morrison, R. Finney, and J. W. Singer. 2003. Inhibition of lysophosphatidic acid acyltransferase beta disrupts proliferative and survival signals in normal cells and induces apoptosis of tumor cells. *Mol Cancer Ther* 2:1067-1078.
120. La Rosee, P., T. Jia, S. Demehri, N. Hartel, P. de Vries, L. Bonham, D. Hollenback, J. W. Singer, J. V. Melo, B. J. Druker, and M. W. Deininger. 2006. Antileukemic activity of lysophosphatidic acid acyltransferase-beta inhibitor CT32228 in chronic myelogenous leukemia sensitive and resistant to imatinib. *Clin Cancer Res* 12:6540-6546.
121. Douvas, M. G., K. N. Hogan, Y. Ji, D. Hollenback, L. Bonham, J. W. Singer, and B. S. Mitchell. 2006. Effect of lysophosphatidic acid acyltransferase-beta inhibition in acute leukemia. *Leuk Res* 30:1027-1036.
122. Thiam, A. R., R. V. Farese, Jr., and T. C. Walther. The biophysics and cell biology of lipid droplets. *Nat Rev Mol Cell Biol* 14:775-786.
123. Szymanski, K. M., D. Binns, R. Bartz, N. V. Grishin, W. P. Li, A. K. Agarwal, A. Garg, R. G. Anderson, and J. M. Goodman. 2007. The lipodystrophy protein seipin is found at endoplasmic reticulum lipid droplet junctions and is important for droplet morphology. *Proceedings of the National Academy of Sciences of the United States of America* 104:20890-20895.
124. Lundin, C., R. Nordstrom, K. Wagner, C. Windpassinger, H. Andersson, G. von Heijne, and I. Nilsson. 2006. Membrane topology of the human seipin protein. *FEBS Lett* 580:2281-2284.
125. Magre, J., M. Delepine, E. Khallouf, T. Gedde-Dahl, Jr., L. Van Maldergem, E. Sobel, J. Papp, M. Meier, A. Megarbane, A. Bachy, A. Verloes, F. H. d'Abronzo, E. Seemanova, R. Assan, N. Baudic, C. Bourut, P. Czernichow, F. Huet, F. Grigorescu, M. de Kerdanet, D. Lacombe, P. Labrune, M. Lanza, H. Loret, F. Matsuda, J. Navarro, A. Nivelon-Chevalier, M. Polak, J. J. Robert, P. Tric, N. Tubiana-Rufi, C. Vigouroux, J. Weissenbach, S. Savasta, J. A. Maassen, O. Trygstad, P. Bogalho, P. Freitas, J. L. Medina, F. Bonnicci, B. I. Joffe, G. Loyson, V. R. Panz, F. J. Raal, S. O'Rahilly, T. Stephenson, C. R. Kahn, M. Lathrop, and J. Capeau. 2001.

Identification of the gene altered in Berardinelli-Seip congenital lipodystrophy on chromosome 11q13. *Nature genetics* 28:365-370.

126. Chen, W., V. K. Yechoor, B. H. Chang, M. V. Li, K. L. March, and L. Chan. 2009. The human lipodystrophy gene product Berardinelli-Seip congenital lipodystrophy 2/seipin plays a key role in adipocyte differentiation. *Endocrinology* 150:4552-4561.
127. Boutet, E., H. El Mourabit, M. Prot, M. Nemani, E. Khallouf, O. Colard, M. Maurice, A. M. Durand-Schneider, Y. Chretien, S. Gres, C. Wolf, J. S. Saulnier-Blache, J. Capeau, and J. Magre. 2009. Seipin deficiency alters fatty acid Delta9 desaturation and lipid droplet formation in Berardinelli-Seip congenital lipodystrophy. *Biochimie* 91:796-803.
128. Skinner, J. R., L. A. Harris, T. M. Shew, N. A. Abumrad, and N. E. Wolins. 2013. Perilipin 1 moves between the fat droplet and the endoplasmic reticulum. *Adipocyte* 2:80-86.
129. Tsuboyama-Kasaoka, N., M. Takahashi, K. Tanemura, H. J. Kim, T. Tange, H. Okuyama, M. Kasai, S. Ikemoto, and O. Ezaki. 2000. Conjugated linoleic acid supplementation reduces adipose tissue by apoptosis and develops lipodystrophy in mice. *Diabetes* 49:1534-1542.
130. Giordano, A., I. Murano, E. Mondini, J. Perugini, A. Smorlesi, I. Severi, R. Barazzoni, P. E. Scherer, and S. Cinti. Obese adipocytes show ultrastructural features of stressed cells and die of pyroptosis. *Journal of lipid research* 54:2423-2436.
131. Herrero, L., H. Shapiro, A. Nayer, J. Lee, and S. E. Shoelson. Inflammation and adipose tissue macrophages in lipodystrophic mice. *Proc Natl Acad Sci U S A* 107:240-245.